Emergent Phenomena From Dynamic Network Models: Mathematical Analysis of EEG From People With IGE

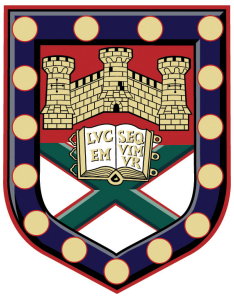

Submitted by Wessel Woldman to the University of Exeter
as a thesis for the degree of
Doctor of Philosophy in Mathematics
In June 2016

I certify that all material in this thesis which is not my own work has been identified and that no material has previously been submitted and approved for the award of a degree by this or any other University.

Signature: _____

Abstract

In this thesis mathematical techniques and models are applied to electroencephalographic (EEG) recordings to study mechanisms of idiopathic generalised epilepsy (IGE). First, we compare network structures derived from resting-state EEG from people with IGE, their unaffected relatives, and healthy controls. Next, these static networks are combined with a dynamical model describing the activity of a cortical region as a population of phase-oscillators. We then examine the potential of the differences found in the static networks and the emergent properties of the dynamic network as individual biomarkers of IGE. The emphasis of this approach is on discerning the potential of these markers at the level of an individual subject rather than their ability to identify differences at a group level. Finally, we extend a dynamic model of seizure onset to investigate how epileptiform discharges vary over the course of the day in ambulatory EEG recordings from people with IGE. By perturbing the dynamics describing the excitability of the system, we demonstrate the model can reproduce discharge distributions on an individual level which are shown to express a circadian tone. The emphasis of the model approach is on understanding how changes in excitability within brain regions, modulated by sleep, metabolism, endocrine axes, or anti-epileptic drugs (AEDs), can drive the emergence of epileptiform activity in large-scale brain networks.

Our results demonstrate that studying EEG recordings from people with IGE can lead to new mechanistic insight on the idiopathic nature of IGE, and may eventually lead to clinical applications. We show that biomarkers derived from dynamic network models perform significantly better as classifiers than biomarkers based on

static network properties. Hence, our results provide additional evidence that the interplay between the dynamics of specific brain regions, and the network topology governing the interactions between these regions, is crucial in the generation of emergent epileptiform activity. Pathological activity may emerge due to abnormalities in either of those factors, or a combination of both, and hence it is essential to develop new techniques to characterise this interplay theoretically and to validate predictions experimentally.

Acknowledgements

I am grateful to several people who have dedicated a lot of time and energy during my research described in this thesis. First of all, my supervisor, John Terry, has supported me tremendously, by giving me great advice, support and encouragement over the course of my PhD project. Working and learning under his guidance has been exciting, insightful and stimulating, and I thoroughly enjoyed our meetings and discussions. I would also like to thank my second supervisor, Peter Ashwin, who has been a valuable source of knowledge and ideas over the course of my PhD, especially with respect to dynamical systems and nonlinear dynamics. Furthermore, under their supervision I was able to engage with people with epilepsy, GPs, neurologists, and EEG-tech companies during a commercialisation-project, which was incredibly stimulating and insightful.

The research described in this thesis critically depends on the crucial efforts from all clinical collaborators, such as the data-collection and preprocessing. I would like to thank my clinical mentor, Mark Richardson, for his support over the last couple of years, and his research-lab at King's College in general. Additionally, I have learned a great deal about epileptiform discharges from a clinical perspective from Udaya Seneviratne and Mark Cook, for which I am grateful.

I would also like to thank Oscar Benjamin for his help early on in this project; Helmut Schmidt and George Petkov for double-checking codes and methods used in producing this thesis; and Marc Goodfellow, Jamie Walker, Dean Freestone, and Sid Visser for engaging discussions concerning my research.

Finally, I would like to thank my friends and family for their support during my PhD, especially anyone that came to visit me here in Exeter. In particular, I am grateful for the unconditional love and support from my sister Mirthe, my brother Martijn, my mother Willemijn, and my father Tieme. And even though perhaps 90% of the content of this thesis will likely appear completely foreign to you (your own words), Christina, your loving support was crucial in realising it.

Author's declarations

I declare that the work in this dissertation was carried out in accordance with the requirements of the University's Regulations and Code of Practice for Research Degree Programmes and that it has not been submitted for any other academic award. Except where indicated by specific reference in the text, the work is the candidates own work. Work done in collaboration with, or with the assistance of, others, is indicated as such (summarised in a footnote on the first page of every chapter). Any views expressed in the dissertation are those of the author.

List of abbreviations

- **AED:** anti-epileptic drugs
- **BNI:** brain network ictogenicity
- **CAE:** childhood absence epilepsy
- **DTI :** diffusion tensor imaging
- **ECoG:** electrocorticography
- **ED:** epileptiform discharge
- **EM:** Euler-Maruyama
- **EEG:** electroencephalogram
- **GSW:** generalised spike-wave
- **HP:** Hopf-bifurcation point
- **IED:** interictal epileptiform discharge
- **IGE:** idiopathic generalised epilepsy
- **JAE:** juvenile absence epilepsy
- **JME:** juvenile myoclonic epilepsy
- **LFP:** local field potential
- **LP:** limit point
- **LOO:** leave-one out cross-validation
- **MEG:** magnetoencephalography
- **MRI:** magnetic resonance imaging
- **PLF:** phase-locking factor
- **SDE:** stochastic differential equation
- **SVM:** support vector machine
- **TMS:** transcranial magnetic stimulation

Contents

List of Figures

List of Tables

Chapter 1

Introduction

1.1 Introduction

Epilepsy is a serious neurological condition characterised by an increased predisposition to seizures. In this regard, epilepsy should not be understood as a single disorder but rather as a collection of conditions manifesting from underlying brain abnormalities, as seizures can affect sensory (i.e., somatosensory, auditory, visual, olfactory), motor, and autonomic function; consciousness; emotional state; memory; cognition (i.e., problems with perception, attention, emotion, memory, speech) or behaviour [21]. This wide variety of behavioural manifestations is presumed to result from the involvement of a number of large-scale brain networks in the generation of seizures. As a result of the myriad of combinations that lead to seizures and ultimately result in a diagnosis of epilepsy, precise definitions for both "epilepsy" and "seizures" have proved challenging. Practically, a diagnosis of epilepsy typically involves a detailed case history of the subject combined with the observation of epileptiform activity in EEG recordings. If the electrical activity consistently appears discretely localised to a confined area, the epilepsy is likely to be classified as focal, whereas pathological activity involving bilateral networks is usually characterised as generalised.

The general question that forms the basis of this thesis is the following: what can be learned about epilepsy, and generalised epilepsy in particular, from recordings of scalp EEG when seizures are not present? Even in very severe cases of epilepsy, for the majority of time the electrical activity of the brain, as observed with scalp EEG, is apparently normal. Given that seizures

emerge out of this apparently normal background activity, of particular interest is the possibility that there may exist markers of epilepsy that defy standard clinical analyses but might be detectable using advanced mathematical and computational techniques. Therefore the motivation of this thesis is to develop advanced mathematical and computational techniques that enable us to interrogate these routinely acquired clinical EEG recordings and gain a greater understanding of the mechanistic basis for the emergence of seizures. To pursue this we combine methods for inferring networks from EEG recordings, with dynamic models of the activity within brain regions and interrogate clinical human EEG with mathematical techniques and models in order to discern whether there are features present within those patterns of activity that are in fact characteristic of generalised epilepsy. This will lead to deeper insight in the mechanisms underlying the emergence of epileptiform activity, and may consequently form the foundation of decision support tools aiding clinicians in cases of diagnostic uncertainty.

Our approach is highly collaborative: through our collaborators at the Institute of Psychiatry at King's College London and the St. Vincent's Hospital at the University of Melbourne, we gained access to three databases of recordings. The first database consists of 20 seconds of resting-state scalp EEG from 35 subjects with IGE, 42 unaffected first-degree relatives, and 40 normal controls. The second database consists of 20 seconds of resting-state scalp EEG from 30 drug-naive subjects with IGE and 38 normal controls. The third database consist of detailed distributions of epileptiform discharges from 107 subjects with IGE recorded from 24-hour ambulatory scalp EEG. Alongside these EEG recordings, there was additional meta data with details on the age, gender, type of epilepsy, and treatment history of each subject.

1.2 Overview

The structure of the thesis is as follows: the second chapter introduces epilepsy as a complex, multi-scale, dynamical disorder and provides an extensive overview of mathematical and computational approaches that have been used to describe and understand the processes and mechanisms underlying epilepsy and seizures. It will become clear that the current understanding of epilepsy is

transitioning towards one that recognises the importance of the relationship between local dynamics (i.e., the activity of a cortical region) and the global network structure (anatomical, functional) in emergent epileptiform activity. Traditionally, structure was mainly understood in anatomical terms in this context, but it is becoming increasingly clear that epilepsy and seizures cannot be understood simply through physical abnormalities, especially for the generalised epilepsies. Instead, the evidence suggests it is essential to take into account how pathological activity can spread over a network of interacting regions (functional connectivity) to give rise to the emergence of epileptiform activity. In this setting, pathological activity can emerge due to network structure, individual dynamic of brain regions, or a combination of the two.

This is starkly illustrated in chapter 3, where we interrogate recordings of resting-state scalp EEG from subjects with IGE, unaffected first-degree relatives, and normal controls. Graph theory is used to describe brain network topology for each subject, which allows us to summarise the properties of the networks and compare them at the group-level. Our findings suggest brain network topology differs between subjects with IGE and normal controls, and that some of these graph measures show abnormalities for both the subjects with IGE as well as their unaffected relatives who do not have epilepsy. This suggests abnormal brain network topology is an essential component of IGE, though not in itself sufficient to cause epilepsy.

In the fourth chapter, we combine the results from chapter 3 with an additional set of features derived from resting-state EEG that have been shown to be different between people with epilepsy and normal controls. Crucially, the static networks are now integrated into a dynamic description of the cortex, since emergent properties of these dynamic network models have been shown to differ between people with IGE and controls. We aim to examine the potential of these properties as individual biomarkers of epilepsy on a subject-specific basis. The features will be derived from the resting-state activity of drug-naive subjects with IGE and normal controls, and their performance examined using standard classification techniques. Finally, the potential of combinations of these markers will be analysed by using support vector machines (SVM).

In the fifth chapter an existing phenomenological model describing seizure-

onset arising from bistable cortical regions is extended to include dynamic excitability, replacing static, constant levels of excitability in the original formulation of this dynamic network model. The use of this time-dependent excitability is found to enable the replication of distributions of epileptiform discharges recorded on EEG from a large cohort of people with IGE. These results are in line with the increasingly accepted hypothesis that abnormal activity of the epileptic brain crucially depends on the specific dynamics describing the activity of individual brain regions, combined with the network structure governing the interactions between these regions.

The sixth and final chapter discusses the implications of the results presented in the thesis with respect to mathematical, computational and experimental neuroscience, as well as to their potential clinical impact. Additionally, we will discuss how future research directions could provide a deeper understanding of the key features responsible for the emergence of epileptiform activity, and consequently help us to find ways to characterise those at risk of epileptiform activity.

Chapter 2

Computational modelling and analysis in epilepsy [1]

2.1 Introduction

As pointed out in the introduction, precise definitions of "epilepsy" and "seizures" and consequently diagnosis of epilepsy as a seizure-disorder have proved challenging. In an attempt to provide consensus on the usage of the terms *epileptic seizure* and *epilepsy* amongst physicians, people with epilepsy, and researchers, the International League Against Epilepsy (ILAE) and the International Bureau for Epilepsy (IBE) defined an epileptic seizure as

> a transient occurrence of signs and/or symptoms due to abnormal excessive or synchronous neuronal activity in the brain

and epilepsy as

> a disorder of the brain characterised by an enduring predisposition to generate seizures and by the neurobiological, cognitive, psychological, and social consequences of this condition [66].

However, very recently a new definition of epilepsy was proposed by the same team, in an attempt to clarify some anomalies created by their earlier definition

[1] The work presented in this chapter has been reported in the following publication: Woldman W, Terry JR. (2015) Multilevel Computational Modelling in Epilepsy: Classical Studies and Recent Advances, Bhattacharya BS, Chowdhury F (eds), Validating Neuro-Computational Models of Neurological and Psychiatric Disorders, New York, Springer, 161-188.

[65]. In this new framework, a person is considered to have epilepsy if they meet one of the following conditions:

1. they have experienced at least two unprovoked (or reflex) seizures separated by a time-span of more than 24 hours,

2. they have experienced at least one unprovoked (or reflex) seizure and have a probability of further seizures similar to the general recurrence risk for people with epilepsy (at least 60%),

3. they have been diagnosed with an epilepsy syndrome.

This revised definition was developed mainly for clinical use, and the authors recognise that other groups such as researchers might prefer to use the older definition, or devise a new definition individually.

Epilepsy has a global prevalence of around 1% (roughly 50 million people worldwide) and, despite a common misconception as a condition that is relatively easily treated with medication, has a high mortality rate [159]. Indeed, people with epilepsy fall into three groups: those who enter remission spontaneously, those whose seizures are effectively controlled through the use of anti-epileptic drugs (AEDs), and those whose seizures cannot be controlled using standard therapeutic interventions. About $5 - 10\%$ of all people will suffer a single seizure before the age of 80, with a 40% to 50% probability of experiencing a second seizure if the first encounter remains untreated [20]. Much current research aims to find ways to predict and control seizures, as there currently is no structural way of predicting whether a particular AED will be effective [94, 186]. For those people with epilepsy who are unresponsive to AEDs, surgical treatment might provide an optional solution to affect the frequency and severity of the seizures [247].

A critical advancement in the understanding of brain structure and function has resulted from the development of the electroencephalogram (EEG) by Berger in the 1920s [23]. The EEG is a measure of the aggregated electrical activity, predominately from cortical pyramidal neurons, although these may be modulated by inhibitory interneurons, as well as neurons from deeper brain areas. This results in characteristic patterns of activity, that correlate strongly

with the state of arousal of the subject [151]. EEG is used clinically, alongside a study of psychological and behavioural symptoms, to determine the initiation and termination of seizures in people with epilepsy.

EEG is also extensively used for the purpose of clinical diagnosis of epilepsy. It is standard practice to record a routine EEG in the process of diagnosing a subject, with the purpose of recording patterns of activity characteristic of epilepsy, such as a seizure or so-called epileptiform discharges. These are brief, paroxysmal electrographic events distinct from ordinary, healthy patterns of activity and background activity and in the case there is no corresponding clinical event, they are classified as interictal epileptiform events or discharges (IEDs). However, the presence of epileptiform abnormalities in the EEG does not necessarily indicate the subject has epilepsy, as non-epileptic individuals can show similar abnormalities on the EEG; EEG has sensitivity-levels in the range of $(25 - 56\%)$ and specificity of $(78 - 98\%)$ [202]. The golden standard for diagnosing a subject epilepsy is a combination of a seizure history with a positive EEG (i.e. the presence of IEDs or an actual seizure), but misdiagnosis remains a serious issue [18, 222].

Seizures fall into two main categories: generalised and focal. The Commission on Classification and Terminology of the ILAE recently proposed a framework for classifying seizures [22]. It is assumed that focal seizures consistently originate in networks located in one particular hemisphere, whereas generalised seizures engage bilateral networks. Generalised seizures are then further distinguished into tonic-clonic, absence, myoclonic, tonic, and atonic seizures. In turn, these may be further extended on the basis of the underlying cause, which can be either genetic, structural/metabolic, or unknown. This has resulted due to older categorisation (e.g. idiopathic, symptomatic, and cryptogenic) being considered insufficient and problematic from a clinical perspective. It should be noted however, that the current framework of existing classifications is prone to future reinterpretation due to advances in clinical and computational neuroscience, using imaging techniques such as positron emission tomography (PET) scans, magnetoencephalography (MEG), functional magnetic resonance imaging (fMRI), and diffusion tensor imaging (DTI). An extensive overview on the many applications of EEG and its importance on

studying seizures in particular can be found in the book of Niedermeyer and Lopes da Silva [151]. Whilst the majority of cases of epilepsy have no known cause, a set of features including the age of onset, typical seizure types, seizure frequency, and patterns observed in the EEG, generally allow clinicians to describe specific epilepsy syndromes.

Much current research conceptualises epilepsy as a complex, nonlinear, and dynamical disease which naturally promotes the use of mathematical and computational models to study the condition. For example, the dynamics of EEG during seizures is presumed to reflect patterns of hypersynchronous electrical activity of neuronal networks, which are thought to be mediated by a disruption to the dynamic balance between excitation and inhibition leading to hyperexcitable networks [134]. It is generally thought that developing integrated approaches to bridge the many spatial and temporal scales of brain activity (see Figure 2.1) could lead to prediction and control of seizures. The neuronal systems and processes involved in epilepsy implicate dynamic mechanisms from the sub-cellular level (ion channels, neurotransmitters), to the cellular level (individual neurons connected through axons and dendritic trees), up to the level of networks of neurons (specific modules, nuclei), and finally cortical areas and hemispheres. The shortest timescale at the microlevel are the spike-trains of individual neurons, comprises brief spikes and bursts in the order of several milliseconds. At the macroscale an EEG recording of a spike-wave discharge (SWD) will typically show a spike of average activity in the $20-30$ Hz range and a slower wave component at $2-4$ Hz, and the generation of SWDs has been strongly linked to interactions between the cortex and the thalamus. Individual seizures will typically initiate and terminate within seconds or minutes. The onset of a seizure is generally believed to be related to specific changes in the macroscopic brain activity prior to the seizure. Circadian factors, such as the level of stress [9, 107], and the lack of sleep can play a crucial role in the frequency and severity of seizures over days. Finally, seizure frequency varies over the time course of months and years, as people with epilepsy might grow out of their condition (in particular in juvenile and childhood types of epilepsy).

Juvenile absence epilepsy (JAE) and childhood absence epilepsy (CAE)

are part of a larger group called genetic or idiopathic generalised epilepsy (IGE), which is a particularly interesting type of epilepsy as they are generally considered to have an underlying genetic cause. Although absence seizures are very common in IGE, they are not a necessary and sufficient condition. An overview of the concepts and classifications relevant to IGE, can be found in a review by Mattson [133]. By combining computational, human, and animal experimental studies there is now a clearer understanding of the pathophysiology of absence seizures and the associated SWDs. Absence seizures are usually seen in children and adolescents and are characterised by impairments in consciousness. Particular strains of genetically epileptic rats (WAG-Rij or GAERS) or animals treated with $GABA_A$-antagonists in the feline generalised penicillin model of epilepsy (FGPE) can reproduce patterns of activity similar to SWDs, as well as display behavioural symptoms resembling absence seizures and response to medication [26, 40, 166]. These experimental and animal models are crucially important in identifying the different spatial brain structures involved in absence seizures. Further, they provide a testing environment for investigating the influence of new types of medication and other treatments of epilepsy and seizures.

Although the generation of SWDs and absence seizures are not clearly understood physiologically, the spike component of the SWD is generally associated with simultaneous firing of cortical neurons, whereas the slower wave component is thought to be mediated by slow $K+$ currents [56]. A large body of experimental results point to a critical role of the interplay between the thalamus and cortex in the generation of absence seizures and SWDs, and there are many modelling attempts investigating probable causes, such as excessive corticothalamic feedback or inhibitory rebound potentials. A detailed overview of these type of models and how they relate to activity patterns during sleep, can be found in the work of Destexhe and Sejnowski [57].

The purpose of this chapter is to provide an overview of established and influential computational models of generalised and focal epilepsies, alongside a presentation of more recent approaches, that attempt to integrate either computational and experimental, or computational and clinical work respectively. Given that seizures and epileptiform activity in general, arises from the

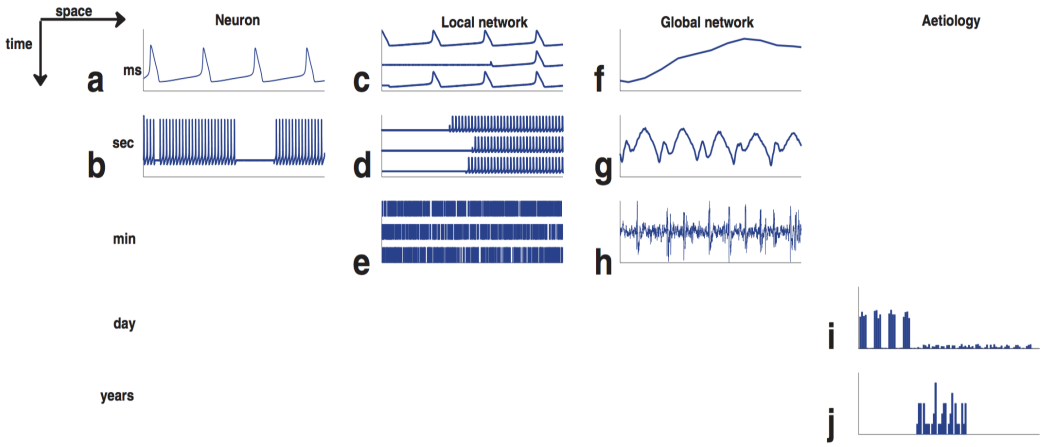

Figure 2.1: Spatial and temporal scales in epilepsy. (**a-b**) Consider the activity of a single neuron generating a spike-train. (**c-e**) Consider a network of coupled neurons. The generated spike-trains show corresponding episodes of firing, introducing the notion of synchronicity. (**f-g**) Consider a single channel of EEG from a person with absence epilepsy displaying SWD characteristic of absence seizure EEG. (**h**) The seizure activity arises from healthy background activity, generating seizures lasting for several seconds. (**i**) Schematic histogram counting the number of SWDs in bins over 24 hours. (**j**) Schematic representation of absence epilepsy seizures over 20 years where the person grows out of the condition.

same structures that govern normal brain function, the many scales relevant in modelling neural activity more generally are first introduced.

2.2 Multilevel computational models of neural activity

When building a mathematical or computational model of neural activity it is important to consider the constituent building blocks required. As described in the introduction, it is presumed (due to the nature of behavioural manifestations associated with seizures) that a malfunction of dynamical interactions between large-scale brain regions plays a critical role. Unpicking this statement suggests that seizures may be thought of as an emergent property, dependent upon the dynamics within a brain region and the connectivity between regions. In this context, the term brain connectivity may refer to many different things, including anatomical links (structural connectivity), statistical dependencies (functional connectivity), or causal interactions (effective connectivity) across

different scales (from synapses to whole brain areas). Whilst ultimately large-scale neural activity arises from interactions between neural populations at many levels of description, the challenge of building and analysing fully multi-scale computational models means that the focus is instead often constrained to a single scale of description that is typically governed by the availability of data. However, it is worth considering what are the fundamental building blocks of neural activity across multiple spatial scales, and how might function at one level inform and constrain function at another?

At the very highest level one might consider behaviour to be an emergent property of the interactions between macroscopic brain regions, including the cerebral cortex, hippocampus and subcortical nuclei such as the thalamus and basal ganglia. Brain regions are then typically subdivided into smaller functional compartments. For example, the cortex consists of around 10^5 to 10^6 cortical columns which on their turn consists of around $50 - 100$ smaller minicolumns (see Table 2.1) [145, 205, 229]. This combinatorial explosion in connectivity is what makes a fully multiscale model of the brain difficult to develop. Further, complexity theory teaches us that even if such a model could be developed it may be of limited value. Across complex networks the emergent dynamics of the network are not typically predictable from a study of the component parts. Further, how far should our reduction process continue? For example, beyond the single neuron level there are several smaller scales of description such as cell biophysics or the molecular biology of gene regulation.

Structure	**Thickness**	**Neurons/synapse**	**Scale**	**Data**
Cortex	2-4 mm	$10^{11}/10^{14}$	Global	EEG/fMRI
Cortical column	200-1000 µm	$10^4 - 10^8$	Meso	LFPs
Minicolumn	20-40 µm	$100 - 200/10^4$	Micro	Single-unit

Table 2.1: Details of the different levels organisation spanning the cortex: from the cortex as a whole to a cortical column to a minicolumn. The number of neurons and synapses are estimates, as the actual numbers depend on the specific location and area of the structure under study. The last column indicates the imaging modalities that record activity at the relevant scale.

Most established and commonly used computational models and ap-

proaches span roughly three distinct spatial scales of description. At the microscale, properties of individual neurons and their dendritic and synaptic connections are considered. At the mesoscale, properties of networks of circuits consisting of larger numbers of neurons, such as cortical columns are considered. It is at the mesoscale where one typically starts to approximate statistical properties of the population, rather than studying the properties and behavior of all the individual neurons. Finally, at the macroscale, the brain is considered at the level of specific brain regions (grey matter), connected by fibre pathways (white matter). This chapter will provide a brief overview of how different modelling approaches operate across these scales, before describing their specific contributions to the understanding of seizures in terms of neural dysfunction at these different scales of description. For an alternative, more illustrative, summary of these challenges, see the recent review by Tejeda and colleagues [217], which compares the possible advantages and disadvantages of using specific type of models (i.e., deterministic, stochastic, phenomenological, physiological).

2.2.1 Microscale

At the microscale, anatomical and physiological studies have revealed many of the main characteristics and interconnections of cortical microcircuits. Fundamentally, a neuron consists of three main parts: the cell body, the axon, and the dendritic tree. Information comes into the neuron through the dendritic tree, where it is integrated at the cell body and the transformed signal is eventually sent as output through the axon. The dynamical behaviour of neurons is closely related to the evolution of the potential difference between the inside and the outside of the cell. The dynamics of the membrane potential depend on the electrophysiological properties of the neuron, such as the specific ion currents and conductances, and the overall connectivity-structure including the synaptic inputs. More specifically, it is mediated by the inflow and outflow of ionic currents across the membrane caused by the ion-pumps and ion-channels within the membrane. Neurotransmitters are responsible for opening and closing the ion channels by binding to the receptors on the cell membrane and thereby increase (depolarise) or decrease (hyperpolarise) the

membrane potential. For example, GABA is mainly an inhibitory neurotransmitter but can have an excitatory effect on the developing brain [16], whereas glutamate is the main excitatory neurotransmitter in the brain. When a neuron receives sufficiently strong input through its synapses, the spiking-threshold is exceeded and the membrane potential undergoes a very fast transient change of the membrane voltage called a spike or action potential. Action potentials propagate via the axon to other neurons, which then on their turn can be excited if their synaptic inputs are sufficiently strong. Spikes are the main means of communication between neurons and spike-trains and specific spike-timings are generally considered as the basic building blocks for encoding and transmitting information [48, 113]. It is important to point out that information flow is not constant or instantaneous as conductances cause transmission delays, thereby further complicating the dynamical complexity of the system, even at this small spatial scale. This complexity is confounded by the many different types of neurons, characterised by different ionic properties and neurotransmitters [176].

Within a mathematical framework, a neuron is often characterised as an excitable, non-linear, dynamical system arising as the result of being close to a bifurcation from resting-state to spiking activity. One can study neural excitability in a deterministic setting through a separation of time-scales, with typically a slow recovery variable and a fast voltage variable. The resting-state of a neuron corresponds to a stable equilibrium, and large enough inputs can push the system into a stable period orbit, corresponding to periodic spiking activity. The intrinsic properties of the neuron, such as the number and type of currents, their conductances, the number of ion-channels and their kinetics, affect the location, the shape, and the period of the stable limit cycle. Transitions between resting and spiking states can occur in different dynamical settings as the equilibrium and limit cycle might coexist (bistable setting) or one of the states might disappear due to external inputs (bifurcation setting).

The Hodgkin-Huxley model of the squid giant axon is one of the most widely utilised and accepted descriptions of neurons with voltage-sensitive currents [93]. Using patch-clamp techniques, three main currents in the squid axon were determined: a voltage-gated K^+-current, a Na^+-current, and an

Ohmic leak current. The Hodgkin-Huxley equations model the dynamics of the membrane potential by describing the evolution of the activation variables with Markovian kinetics, assuming that the proportion of open channels is dependent on the number of activation gates and inactivation gates and the probability of an activation gate being open or closed. The evolution of the activation variables of the voltage-gated channels depends in turn on the voltage-sensitive steady-state activation function and a time constant, which are determined using voltage-clamps. Positive and negative feedback loops in the model can lead to the generation of an action potential as the system might be perturbed from its attractor. To illustrate this, assume that an external current causes a slight depolarisation in the cell-membrane. Consequently the sodium-conductance will increase, thereby depolarising the cell even further. After a short time-period, the slower potassium-channels activate, resulting in an increase in the potassium-conductance, causing the cell to repolarise and eventually hyperpolarise.

Although the structure of the squid giant axon is somewhat simplistic in comparison to cortical neurons, the Hodgkin-Huxley equations form the basis for many deterministic conductance-based models. As experimental techniques have advanced, new details of the mechanisms governing ion channels have emerged, such as spike frequency adaptation or synaptic depression, and these insights can be incorporated into new conductance-based models thereby providing a closing agreement between model output and experimental data (such as single-unit recordings). One famous extension of the Hodgkin-Huxley equations is the Connor-Stevens model which takes into account an additional transient current within the framework (a K^+-conductance) [42]. As an alternative, rather than increasing the complexity of the system, some researchers have sought to reduce the model to its most critical parts. For example, by using a fast-slow decomposition, lower-dimensional models such as the FitzHugh-Nagumo model or the Morris-Lecar equations are derived [67, 143]. These reductions allow mathematical treatment such as phase-plane analysis, bifurcation analysis, and fast slow-analysis while still capturing the essential dynamic properties of the full Hodgkin-Huxley equations. As such, conductance-based neurons provide a successful mechanistic understanding of crucial phenomena

such as neuronal excitability and spike-generation [99].

Although morphological studies have revealed much insight in the detailed structure of neurons and inspired detailed compartmental models using cable theory (see [30] for example), most simple models characterise a neuron as a single compartment or point corresponding to the cell-body. In these point-models, current flows strictly inside and outside of the cell, not between different regions within the cell. One of the earliest and simplest model of a neuron is the leaky integrate-and-fire neuron, a simple resistance-capicitator circuit with an Ohmic leakage [1]. By restoring the membrane potential of a neuron to a resetting-value after a specified threshold is reached, the model is able to mimic the generation of action potentials. Although integrate-and-fire models are piece-wise continuous and the spikes are not resultant from any realistic biological dynamics or kinetics, their reduced formulation makes them particularly suitable for mathematical analysis and for proving several theorems. As such, they allow a particular simple setting that includes spikes, excitability, refractory periods, and the difference between excitation and inhibition. This balance between excitation and inhibition has been a crucial dynamical concept in the study of neural activity, especially in relation to synchronisation of networks, and as such often provides a direct relation to the modelling of seizures [227].

An alternative approach for modelling microscale neuronal activity is to focus exclusively on the firing rate properties of neurons [63]. Firing rate models are built on the assumption that, on average, the input from a presynaptic neuron is proportional to its firing rate, and that the total synaptic input is obtained by summing the contributions of all the presynaptic neurons. These approaches specify a relationship between the firing rate and the input a neuron receives from other neurons in the network, or external or sensory inputs (such as an applied current). Note that firing rate models explicitly include the interactions between neurons, whereas the previously discussed conductance-based models were mainly studied in isolation without specified input-relationships. These approaches naturally extend the scale from an individual neuron to the level of networks of interacting neurons [233].

2.2.2 Mesoscale

Computational models of single neurons are often used to describe the underlying dynamics of realistic neuronal networks consisting of interconnected neurons. By coupling neurons together into larger ensembles or (sub)populations, networks of variable size are constructed as sets of coupled differential equations. Simulating these networks then gives the evolution of the state-variables of every individual neuron and reveals the emergent spatiotemporal patterns at the network level. Networks at the microscale are in the order of micrometers, whereas at the mesoscopic scale larger networks of cortical (mini)columns operate at the scale of hundreds of micrometers. The mesoscale is a relevant level of observation in the context of integration of information from the microscale towards whole brain areas, as it extends the level from single neurons to interacting local neural groups. Multi-unit recordings or local field potentials (LFPs), measuring summated dendritic current, can reveal activity of the brain at the mesoscopic level [229]. As shown in the work of Destexhe, networks of single compartment models are used to calculate field potentials, thereby relating both experimental data as well as models from the microscale to the mesoscale [57]. However, it should be noted that due to Kirchhoff's law the sum of all currents in a single compartment equals 0, computing a field potential is non-trivial, and typically carried out by using the membrane potential as a proxy for the external current.

At this level of description, one can consider different levels and types of connectivity or coupling. First there is the level of neuronal connections, where coupling will either have an increasing (excitatory) of decreasing (inhibitory) effect on the membrane potential of the receiving neuron. Further, there might be a hierarchal structure within the overall network, as information might flow from one area to another in a feedback (top-down) or feedforward (bottom-up) structure within the network [229]. Once the type of neuronal coupling (i.e., strength, delay, periodicity) is established and the connectivity-structure described (i.e., all-to-all, sparse connectivity, specific areas), the output of the simulated network can be used to study the collective behaviour of the network as well as the individual neuronal responses.

Current detailed, biophysical modelling attempts typically incorporate

more biophysical details into multi-compartmental models using specified software (i.e., NEST, Genesis, Neuron) with the computational power of supercomputers. A particularly striking example of this is the Blue Brain Project [128] and its sequel, the Human Brain Project. It should be highlighted that these large-scale simulations and models limit a global understanding of the dynamical behaviour of the underlying model, in the sense that one typically cannot decide whether the observed simulation displays converged activity or whether there are any other possible attractors within the system. Additionally, given the large numbers of physiological parameters and the fact that it is often notoriously hard to establish reliable estimates for them, a thorough understanding of the dynamical behaviour of these models may require a thorough sensitivity-analysis, as the model might critically depend on the exact settings of the parameters. An interesting future avenue of work here would be to develop uncertainty quantification techniques (see for example [155]), which have proved popular in large-scale climate models, for quantifying uncertainty associated with parameters of these large-scale simulations.

Networks of interacting neurons can exhibit collective behaviour that is not intrinsic to the individual activity patterns, such as synchronisation. Synchronisation is a crucially important concept in the computational modelling of the brain and seizures. For example, synchronisation within large-scale networks of interacting neurons causes the emergence of oscillatory activity in the thalamocortical system, such as the alpha and gamma rhythms [32]. The existence of distinct oscillatory frequencies in LFPs and EEG suggest that the brain, despite its dynamical complexity, produces patterns and trajectories that could be projected onto much lower-dimensional subspaces and studied accordingly. This approach, often termed mean-field approximations, form the basis for lumped models that typically operate at both the meso- and macroscale, by describing the evolution of neural activity with collective variables, such as the proportions of active neurons at a given time in a population, the mean membrane potential, or average firing rate. Simulating networks of thousands of individual conductance-based neurons at such a larger scale is computationally expensive because of the many dimensions, and furthermore, the large number of neurons makes it impracticable to study the influence of

each element individually. Lumped approaches offer an alternative for modelling neuronal networks by coupling large collections of individual neurons, by characterising the activity of the neuronal populations in an aggregated manner. An important example of this approach is the Kuramoto-model, which describes the behaviour of large groups of neurons as near identical phase-coupled oscillators [117]. Here, the action potential of the neuron is considered to reflect a periodic oscillation and focus on the study of the phase of this oscillation rather that the membrane potential directly. In the case of weak coupling, the amplitudes of the oscillations remain approximately constant, such that interactions can be described by focusing on the phase alone. Synchronisation within this framework typically relates to phase-locking (or coherency), and then often studied in the thermodynamic limit (e.g. the network-size growing to infinity). Mathematical analysis of the order-parameter can then reveal that the dynamics of the network of oscillators can be described by studying its statistical properties [99] and treating the network as a field.

Another motivation for considering mean-field activity of neural populations results from the nature of experimental data recorded at the mesoscale. As LFPs predominately reflect the summated dendritic current at a scale of around 1 milimetre, they highlight the common action of local networks of neurons rather than the activity of individual neurons [229]. Another popular approach for describing neural population activity is based on a mean-field approximation of the ensemble density function. The ensemble-approach is explained in detail in a review by Deco and others [50], and is based around methods from statistical mechanics to formulate a probability density function that captures the distribution of all neuronal states of a population. Instead of following the evolution of thousands of individual neurons, the probability density function describes the time-dependent average activity level of the whole ensemble. By using appropriate assumptions, the stationary solutions of the probability density function might be analysed in a generic setting. However, one can simplify the probability density approach by relating the evolution of the density to a single variable, instead of a collection. It is this specific mean-field assumption which forms the basis of neural mass models [68]. A neural mass model treats large-scale activity as a point process, and as

such can equally reflect that activity of neuronal ensembles or EEG-sources. This comes at the cost of throwing away higher-order moments, such that interacting populations can only influence each other through their expected population rate. Despite this limitation, this simplification of the dynamics of the neuronal populations allows one to study interacting subpopulations with small computation times. A particular popular neural mass formulation is the Jansen-Rit model [101] which forms the basis of many of the epilepsy models that are considered later.

2.2.3 Macroscale

We now consider models at the macroscale of millimetres, where very large numbers of neurons and neuronal populations form distinct brain regions which are interconnected by inter-regional pathways. It is the brain activity arising from macroscopic populations that is observed directly from EEG or MEG recordings. The activity patterns recorded by EEG are widely regarded as the summation of interactions of large populations of cortical pyramidal neurons, which due to their dendritic organisation align perpendicularly to the surface of the cortex [153]. Whilst EEG reflects the extracellular output of pyramidal cells, these are generated as a consequence of receiving both excitatory and inhibitory postsynaptic potentials.

One approach to study the emergent rhythms of these large-scale brain regions are neural field models. Neural field models are effectively extensions of neural mass models describing the average or coarse-grained activity of populations of interacting neurons by treating the cortex as a continuous excitable medium. Consequently, the spatially extended sheet is modelled as a function of space and time, and the macroscopic ensemble dynamics are described by a set of partial differential equations or integro-differential equations. Using fundamental methods from statistical mechanics, Wilson and Cowan developed the basis of neural field models by extending the earlier work of Beurle by including both excitation, inhibition, and a refractory period within their approach [243, 244]. A review by Destexhe and Sejnowski shows how the Wilson-Cowan equations have been used to include more sophisticated and realistic mechanisms such as bursting, adaptation, and synaptic depression, and how

their work predicted neural oscillations and stimulus-evoked responses [58]. Naturally, neural field models have been used to model the generation of EEG rhythms, and a key feature of neural field models in the context of seizures is related to the functional significance of the macroscopic variables in relation to EEG-recordings, making it easier to intuitively relate the computational model to the observed data.

The terminology of mean-field approaches can be somewhat confusing in the overall context of neural fields, as neural field modelling is not necessarily confined to only mean-field activity, but can often result from other assumptions and approximations, such as the probability density approach or from an integro-differential approach [50]. Neural field models have been extensively used to study a wide variety of topics including memory storage, pattern-formation, and travelling waves [5, 29, 43, 46], where they are typically formulated as a PDE, with the assumption of some underlying Green's function describing the connectivity kernel [103]. Alternatively, many mean-field approaches are defined as a set of integro-differential equations describing the coarse-grained activity of a population of neurons, where particular choices of the integral kernel describe the synaptic connectivity structure of the cortex. Common examples of these connectivity structures include short-range (local) excitation and long-range (lateral) inhibition (so-called Mexican hat), long-range excitatory to excitatory connections and short-range inhibitory to inhibitory connectivity (the inverse Mexican hat), and global excitation [68, 103, 153]. The choice of weight function enables specific dynamical patterns to emerge such as oscillatory behaviour, travelling waves, or bumps [29]. For example, Liley et al. [124] and Robinson et al. [182] include all main types of connectivity at the local scale (e-e, e-i, i-e, i-i) but only long-range excitatory connections that interact with both the excitatory and the inhibitory populations. Liley further includes high-order neurotransmitter kinetics and synaptic reversal potential to describe the excitatory and inhibitory cortico-to-cortical interactions more accurately, finding alpha oscillations to be crucially dependent on the local inhibitory-inhibitory interactions [124]. Furthermore, these models show how different biophysical assumptions regarding the dendritic and axonal structure and dynamics affect the nature of the equations,

as the voltage-equations might be either first-order (Liley) or second-order (Robinson) depending on whether the population response has (in)finite rise times affecting the propagation of the response through the cortical sheet. In summary, these modelling choices and assumptions on anatomical and physiological properties have a critical influence in determining the overall dynamical repertoire of the models as well as the suitability of analytical tools.

Currently, there is great interest in understanding the relationship between biophysically detailed spiking models at one scale, and neural field models at the other. In relating different levels of description, the question arises how microscopic properties of individual neurons relate to mesoscopic local networks or the macroscopic behaviour of large-scale networks and brain areas. Given the wide variety of different model approaches (see Table 2.2), how do these models relate to each other, i.e., how they complement or differ, and how we can describe the complex dynamical distributed activity of the brain aided by these modelling approaches? This is a particularly complex task because of the range of spatial scales (from micrometers to centimetres) as well as the variety in temporal scales, with dynamical changes taking place at the range of milliseconds to years within the brain. Under some very specific constraints, the relationship can be inferred [185], but this relationship is neither unique, nor true in generality [50]. Indeed, as highlighted by Bressloff, there is currently no structural multi-scale analysis of conductance based neural networks that allows a rigorous derivation of neural field equations [29]. An alternative approach is to include higher-order moments beyond the first order mean-field approximation, for example including the variance of activity [64]. Very recently, work by Visser and colleagues has focussed on the addition of delays into the framework of neural fields. These authors argue that conduction delays are likely to critically effect the synchronising effects of brain networks and should therefore be incorporated [225, 232]. A more detailed overview of the development and application of both neural mass and neural field models, can be found in a review by Coombes [44].

Type	Model class	Model	References
Neuronal	Conductance-based	Connor-Stevens	[42]
		FitzHugh-Nagumo	[67]
		Hodgkin-Huxley	[93]
		Morris-Lecar	[143]
	Phase-models	Izhikevich	[68]
		Kuramoto	[117]
	Phenomenological	Firing-rate	[63]
		Integrate-and-fire	[1]
Neural field	Phenomenological	Amari	[5]
		Wilson-Cowan	[243, 244]
Neural mass	Physiological	Jansen-Rit	[101]

Table 2.2: Summary of classical neurocomputational models: model types include neuronal (network), neural mass, and neural field models, with the following model classes: physiological (i.e. conductance-based) and phenomenological (i.e. phase-models).

2.3 The application of multilevel models in epilepsy

Given that epilepsy is a pathological condition whose hypothesised causes have been characterised both experimentally and clinically across a wide range of spatial and temporal scales, computational modelling approaches to epilepsy have grown rapidly (see for example [237] for a review of articles predating 2005). Computational models provide an additional tool with which to interrogate experimental and clinical data, and when appropriately utilised, enable a reiterative cycle whereby models can be used to identify underlying candidate mechanisms from data recordings, which may then in turn be tested through new experiments. It is hoped that this understanding may ultimately lead to new techniques for seizure prediction, treatment and control [142, 188, 189, 238]. Further, the textbook "Computational neuroscience in epilepsy" edited by Soltesz and Staley [204], provides a structural overview of some aligned approaches to computational study seizures and epilepsy and demonstrates the critical advances that the pursuit of a multidisciplinary ap-

proach to the problem can enable.

There are further excellent reviews that focus on the overall process of multilevel computer modelling in epilepsy; discussing the basic mathematical concepts (e.g. attractors, nonlinearity, stability), underlying multiscale models (e.g. deterministic versus stochastic, microscopic versus lumped), as well as their application to various types of epilepsy, including both focal and generalised epilepsies [120, 126, 139, 209]. In a further recent review, Badawy and colleagues [9] present a summary of experimental and modelling evidence for dynamic changes of excitability within epileptic brain networks both during (ictal) as well as away from (interictal) seizures. They discuss how the underlying physiology influences the balance between inhibition and excitation in the interictal state before the onset and evolution of a seizure, highlighting several candidate mechanisms, including changes in blood sugar levels and hormones, that could change the level of cortical excitability of these epileptic brain networks over time (see also [179]). From these publications, a specific selection of what could be considered to be the key publications (Table 2.3) is highlighted, which have strongly influenced the current modelling approaches (Table 2.4) that are the focus of the remainder of this chapter.

One approach to studying epilepsy considers the hypothesis that seizures could be the result of the structural failure of mechanisms within the brain that are reflected by scale-invariant power laws [45]. If the brain follows such power laws, this means that dynamical changes and characteristic behaviour can be found at every spatial and temporal scale within the brain. Furthermore, systems that operate near a critical state often follow a power law distribution, leading to the notion of self-organised criticality as a potential mechanism relevant to epilepsy [17, 160]. Some studies discuss the possibility that the dynamics emerging from an observance to power law distributions might interfere with neural computation, thereby disrupting the healthy network activity and forcing the brain in a state of hyperexcitability [138, 246].

Extending these concepts from a dynamical systems perspective, Lopes da Silva and colleagues [125] highlight two fundamental mathematical mechanisms that could lead to the generation of a seizure as reflected in electrophysiological data recordings: the bifurcation and the noise-induced transition

in a multistable system. Both scenarios are shown to give rise to the abrupt transition from background activity to seizure dynamics. Perhaps the most well characterised of these is the spike-wave discharge (SWD), where a low-amplitude signal transitions near instantaneously into a high amplitude, approximately 3Hz signal, each oscillation consisting of a sharp spike and a slow wave. In the bifurcation setting, a smooth change in an underlying system parameter or parameters, leads to a sudden transition in the system dynamics. Alternatively, in a multistable setting there are several stable attractors, and the initial conditions and noisy inputs are determining factors for understanding the dynamical behaviour of the system. For example, one could consider the healthy interictal state as well as a synchronised seizure-state as stable attractors that co-exist. In normal subjects, the basin of attraction of the seizure-state may be considered to be vanishingly small. On the other hand, in people with epilepsy, the basin of attraction of the seizure state has positive measure and thus an appropriate perturbation may lead the dynamics into the seizure regime.

These types of ideas have formed the basis of a number of physiological studies of SWDs at both the micro- and macro-scales of spatial description. Many of these studies have explored in detail the role of the neocortex in generating SWDs, especially in conjunction with thalamic networks. Motivated by experimental evidence, a compartmental microscopic model is presented in the work of Destexhe which provides a detailed approach for understanding the mechanisms underlying SWDs [53, 55]. The authors summarised in vivo evidence regarding the behaviour of individual neurons and brain regions obtained from the feline generalised penicillin model. The networks consists of thalamocortical projection cells (TC), local inhibitory cortical interneurons (IN), reticular projection cells (RE), and corticothalamic projection cells (CT). It is shown that $GABA_B$-mediated inhibition plays a crucial role within the model, and SWDs are initiated and terminated by slow time-scale currents in the TC cells while the cells are quiescent between SWDs [54]. During these periods of rest, several TC cells will slowly lose stability thereby causing an initial burst of activity that will then further recruit the rest of the network, eventually causing a SWD at the macroscale. Similar experimental and com-

putational models focussing on the cellular and network structures underlying SWDS are discussed in reviews by Blumenfeld and McCormick [26, 134].

Building on these fundamental ideas, a mean-field model introduced by Robinson and colleagues distinguishes the short timescale dynamics associated with the oscillatory phase of the SWD from the longer timescales implicated in the initiation and termination of SWDs at the macroscale [28, 181]. The model describes the averaged activity of three homogeneously synchronised populations of TC, RE and cortical cells and is thus closely related to the microscale neural work model of Destexhe. Seizure-onset results from a dynamical bifurcation of short timescale dynamics, as the change from the inter-ictal to the ictal state appears due to a change of parameters. Bifurcation analysis of this model demonstrates how an increase in the cortical input into the TC population can lead to spike-and-wave dynamics. This model was extended to explicitly account for the slow $GABA_B$-mediated inhibition of the TC population by RE neurons [131, 184] and this slow inhibitory process was also shown to be capable of leading to a transition to SWDs. These two studies highlight two critical mechanisms necessary for the transition to SWDs. First, a variation in the dynamic balance between excitation and inhibition within the TC nucleus of the thalamus. Second, a separation of time-scales resulting in a slow-fast system [183]. In the work of Robinson and colleagues [181], the time-delay within the cortico-thalamic loop gives rise to a separation of scales, whereas in the work of Marten et al. the separation is caused by the difference mechanisms of action of GABAergic inhibition [131]. A critical difference between the two models is the ability of the Marten et al model to generate poly-spike and wave complexes, which are typically observed in the EEG of people with absence epilepsy. Using this model, the same authors developed a multi-objective evolutionary algorithm to fit parameters of the model from clinical EEG recordings [148], from which they hypothesise that the resulting path through parameter space of the generative model may provide a mechanistic characterisation of different types of epilepsy syndrome.

A possible limitation of these studies is that they only considered space-clamped solutions, justifying this assumption by the observation that the abnormal dynamics associated with SWD occur near simultaneously across the

entire cortex. However, there is a growing body of experimental evidence for the involvement of large-scale networks in the generation of SWDs. For example the classical work of Meeren and colleagues demonstrated that SWDs in the WAG/Rij genetic model originate in a specific region of neocortex - the somatosensory cortex - before spreading to other cortical regions [135]. Similarly, Buszáki and colleagues investigated the genesis of SWDs in Fischer-344 rats, and proposed the discharges might be the result of rhythmic cell populations in the thalamus [33]. A historic review of the different paradigms on the genesis of generalised absence seizures can be found in [136].

Motivated by this, Taylor and colleagues consider a spatially extended neural field model, based upon the Wilson-Cowan model with two inhibitory populations and observe that spike and wave oscillations can generate and propagate in the model [216]. Once more, the presence of two inhibitory timescales being critical to generating the activity. Whilst this study was one of the first to consider spatial-extent in the context of generalised epilepsy, it might be considered somewhat limited, as the spatial-extent is homogenous, whereas the human cortex is fundamentally heterogeneous. To address this, Goodfellow and colleagues extend the Jansen-Rit neural mass model to incorporate spatial heterogeneity [80–82]. They demonstrate that epileptic activity could arise transiently as a consequence of connectivity structure of the tissue. These intermittent transitions between background and spike-wave like activity provide a third candidate mechanism for generating seizure-like activity in brain networks. By introducing a discrete-time map, the authors further present a mathematical analysis of the role of heterogeneity. They study both spontaneous and stimulation-induced activity patterns, and relate these findings to clinically recorded rhythms. In their most recent work, they demonstrate the fundamental mechanisms by which intermittent transitions can arise through a reduction of their detailed neural mass model to a phenomenological set of equations, that might be considered as a normal form of the more detailed model [79].

The use of these reduced approaches (often referred to as phenomenological models) provides the opportunity to study (often analytically) the fundamental mechanisms that may contribute to seizures. Typically these studies

consider a bistable mechanisms rather than the bifurcation mechanisms considered thus far. For example, recent work by Kalitzin and colleagues, and Benjamin and colleagues [19, 111] describe the bistability using a subcritical Hopf bifurcation, permitting a bistable regime in which noise governs the transitions between the interictal and ictal stages. This phenomenological approach provides an alternative framework for exploring the role of heterogeneity, whereby interactions between internal node dynamics and the macroscale network structure can lead to transitions to seizures, either emerging from a single brain region or as a consequence of the network in general. This model has recently been appropriated in the context of surgical resection in people with temporal lobe epilepsy by Hutchings and colleagues [96].

A recent study by Jirsa et al. presents a structural taxonomy of seizures and derives a 5-dimensional model (the "epileptor") containing the necessary elements for describing invariant seizure activity and temporal features including spike-wave discharges, fast oscillations, and a slower permittivity variable [105]. This model can be understood as a normal form for the bifurcation mechanisms underlying seizure generation and seizure termination, by a saddle-node bifurcation and a homoclinic bifurcation respectively. Predictions based on the models were supported experimentally by several experimental findings, including a baseline shift at seizure-onset (due to the saddle-node bifurcation) and logarithmic scaling of interspike intervals at offset (due to the homoclinic bifurcation).

Building on this theme, Richardson [179] presents experimental and clinical evidence suggesting that multi-frequency oscillations may play an important role in the generation of seizures, and that these oscillations may emerge from a particular brain region - the classical concept of a "seizure onset zone" - or from properties of the network structure more generally. This alternative concept for the emergence of rhythms is well described in the work of Buszáki [32], yet its potential application to epilepsy has only very recently been considered. In this setting, Terry and colleagues demonstrated how the interplay between excitability, network structure, and noise can generate emergent dynamics reflecting both generalised and focal seizures [218]. Intriguingly, the study demonstrates settings where the emergent dynamics of both seizure types

can result from either a single brain region (the classical concept of "seizure onset") or from a general network perspective. Further, the influence of removing an edge from the network is studied in detail, revealing an interesting explanation of experimental results (where loss of white matter has been associated with the generation of seizures [35]) in that the system becomes less stable (and thus more prone to transitions to seizures) as connections are removed. This may at first seem counterintuitive, in that the spread of seizure activity across the whole cortex might be felt to occur most rapidly if all regions of the cortex are strongly connected.

The role of disrupted networks in focal epilepsies has also received much recent attention. For example, a recent study by Wendling and colleagues, describes an approach for combining computational modelling with multiscale experimentally recorded data (specifically in the hippocampus (both in vitro and in vivo)) and clinical MTLE data [240]. The study reveals mechanisms underlying oscillatory activity from inter-ictal spikes to high-frequency oscillations and seizures, including lumped-parameter approach as well as a detailed microscopic model of coupled networks of hippocampal CA1 and CA3 cells. In line with this, the role of the gap junctions, the electrical coupling between neurons, should be considered as a possible key player in the generation of (focal) seizures, as reported by Traub and Volman [219, 234]. Jiruska and colleagues discuss evidence suggesting excessive synchronisation of large neuronal populations could lead to hypersynchronous states during seizures [106]. The authors describe how seizures can result from dynamical changes in the synchronisation patterns during the ictal and interictal stages, both at the microlevel as well as the macrolevel. For example, desynchronisation is often observed before the onset of the seizure whereas high levels of synchronisation are typically observed when the seizure terminates. The onset of seizures is often related to a characteristic area of brain networks, and this concept of seizure onset zones is particularly relevant in relation to focal epilepsy, where the use of electrical stimulation has attracted recent interest [72, 221]. Further, Anderson describes how the prediction of focal seizures might be complicated by the various different mechanisms that could deregulate the healthy background state by using a detailed neocortical model [7]. In a related approach,

the work of Blenkinsop is focussed on the time evolution of macroscopic epileptic rhythms in focal-onset epilepsy, by using a neural mass model based on the work by Wendling [25, 239]. These neural mass models are an extension of the standard Jansen-Rit model, incorporating additional inhibitory populations, and describe the relationship between commonly observed wave-forms in clinical intracranial EEG recordings. The bifurcation routes from background to seizure activity of these models have been characterised in the work of Grimbert and Faugeras [85], and recently, van Drongelen and Visser described an integrational approach to relate microscopic detailed models to meso- and macroscopic models [224, 231].

To understand the differences between a singular pathological region or a pathological dynamical network disrupting normal neural activity, Richardson argues that combining connectomics with brain dynamics is necessary to provide further insight into the relationship between individual node dynamics and the collective behaviour of the network [180]. The relationship between structure and dynamics and the emergence of function has generated much recent interest across the field of biology more generally, particularly to study the role of complex interactions on the global behaviour of networks [27]. Specific to epilepsy, there have been several studies based on data from people with epilepsy that aim to find differences within these recorded time-series between people with epilepsy and healthy subjects. By using graph theory, signal analysis, and time-series analysis, these approaches aim to derive a graph (a specific set of nodes and edges) which is then typically characterised by a collection of measures such as the small world index (SWI) or the characteristic path length. Determining structural, effective, or functional connectivity between different regions is usually based on regression technique or Bayesian methods. With the development of several useful toolboxes, one can easily use a wide variety of network-derivation techniques such as cross-correlation, Granger causality, dynamic causal modelling (DCM), transfer entropy, the directed transfer function (DTF) and partial directed coherences to derive an (un)directed, (un)weighted graph, and then analyse the graph properties by using the Brain Connectivity Toolbox [13, 36, 75, 187, 196]. Within this context, one can study the resting-state connectivity structure as well as how

networks change dynamically over time, analysing how the graph properties evolve during seizures or just before the seizure-onset [121, 122]. One study explores the significant differences in functional connectivity structures in IGE in resting-state activity [127], while an additional study reveals how networks become more orderly during absence seizures [173]. These and other studies are reviewed in more detail by Engel and colleagues [62].

2.4 Clinical applications

Much of the focus on the use of computational models of seizures (and epilepsy more generally) is in their ultimate application in the clinic. A method that could reliably identify whether a person with epilepsy was in remission, or had responded to medication would revolutionise the clinical management of the condition. Consequently, much research has focussed on the identification of features in neural activity that can differentiate people with epilepsy and normal controls. For example, Wendling and colleagues provide a spatial analysis of iEEG in case of partial epilepsy by using non-linear regression analysis [241], whereas Freeman conducts a similar spatial analysis of electrocorticograms (ECoG) to find optimal conditions for analysing the frequency content of the recorded signals [69]. Additionally, computational models are developed to describe and reproduce the recorded signals, thereby providing the possibility of discerning the mechanisms underlying the observed dynamical phenomena. Wang and colleagues describe how epileptic EEG recordings can typically be categorised as one of four dominant wave forms (fast oscillations, large slow waves, fast spiking, spike waves) [236]. By focussing on the interplay between excitation and inhibition, they formulate a minimal model that reproduces the essential wave forms, thereby inferring a set of necessary interacting processes underlying epileptic neural activity. Jirsa presents a neural field framework for describing EEG and MEG patterns in the context of electrical stimulation [104], whereas David and Friston use a neural mass formulation to focus on the coupling structure and propagation delays underlying these EEG and MEG signals [47]. Dynamic causal modelling differs from the bivariate or multivariate regression techniques in the sense that DCM is a Bayesian method, constructing a generative model describing the propagation

of neural activity through brain networks, estimating the causal interactions using Bayesian inference techniques. As such, DCM may be thought of as an alternative formulation to many of the dynamical systems approaches to studying seizures and epilepsy considered in earlier sections. DCM has been used both in the context of neural mass modelling more generally [141] and has been applied to EEG/fMRI data from people with epilepsy as a result of brain tumour near the hypothalamus [146].

Computational models may also have a critical role to play in informing surgical resection that is used as a treatment strategy for medically intractable epilepsies. Understanding the different candidate mechanisms of seizure-onset may be critically important in informing suitable treatment. A particular treatment option (for example removal of a specific brain region) may not be effective if the underlying mechanism is a disruption within the overall network structure. Furthermore, seizures onset in people with intractable epilepsy may well have different, or even multiple, underlying dynamic mechanisms and hence require different treatment.

2.5 Current developments

Whilst the main focus of our chapter has been to review relevant computational approaches for studying seizures and epilepsy, a few remarks on the current direction of the field will conclude this chapter. As experimental techniques (particularly methods for recording neural activity at very small spatial scales and optogenetic methods for manipulating specific neural populations) evolve, we can expect that physiological parameters and functions within models of microlevel activity will significantly advance. For example, one could envisage that computational models will have a critical role to play in advancing our understanding of so-called "microseizures" [208]. Further, by incorporating more details of the actual dynamical processes at the genetic, molecular and cellular level, these models may ultimately enable the genetic contribution to a wide variety of epilepsy syndromes to be identified. Additionally, as we move towards exascale computing, very detailed models (such as promoted within the Human Brain Project) may enable the multiscale interrelationships within the brain to be described, and consequently the identification of mechanisms

by which their disruptions lead to neurological disease.

At the macroscale, further work to delineate the contribution of network structure and dynamics in the emergence of seizure activity may result in new methods for distinguishing people with epilepsy from controls, or to classify people with epilepsy according to their likely response to available anti-epilepsy drugs (AEDs). A pragmatic approach to achieving this could be based on a combination of computational models and anatomical or functional networks derived from people with epilepsy and trying to identify how the internal brain dynamics as well as the brain connectivity structure are modulated by AEDs over time. Databases of longitudinal EEG recordings could be utilised to inform the estimation of parameters of computational models before and after treatment, and changes in these parameters may determine whether people with epilepsy have appropriately responded to treatment. In this regard, we might think of seizures as emerging from either normal dynamics with abnormal connectivity, or abnormal dynamics with normal connectivity, or maybe even a combination of the two.

Seizure type	Model type	Main findings	Ref.
Generalised	Field	Enflurane and isoflurane induce epileptiform activity	[123]
		Focal/absence seizures caused by physiological parameter-changes	[181]
Focal	Neuronal	Weak excitatory synapses generate seizure-like activity	[224]
		Gap junctions could underlie fast population oscillations	[219]
Absence	Neuronal	Thalamocortical network mechanisms generate SWDs	[26]
		GABA-receptors in thalamocortical circuits generate SWDs	[53, 54]
		Cortical LTS cells important in genesis of SWDs	[55]
		SWDs caused by dynamical bifurcations in bistable framework	[211]
	Phenomenological	Noise governs transitions to seizure-state in bistable framework	[212]
Tonic-clonic	Field	Bifurcation-analysis reveals difference between absence and tonic-clonic seizures	[28]
Astrocytes	Neuronal	Intracellular oscillation patterns in epileptic astrocytes	[12]

Table 2.3: Classical papers in computational modelling of epilepsy: seizures are classified as focal, generalised, absence (spike-wave discharge), tonic-clonic, or astrocytes. Note that all these references appeared in the time period 1998-2006.

Seizure type	Model type	Main findings	Ref.
Generalised	Neuronal	Inhibitory synapses crucial in generating seizures	[87]
		Failure of adaptive self-organised criticality causes seizures	[138]
		Control of seizures through depolarising periodic stimulation	[163]
		Computational improvements in multi-scale epilepsy modelling	[169]
		Slow depression mechanism enforces seizure termination	[230]
		Addition of gap junctions suppresses seizure-like activity	[234]
		Changes in balance of conductances explain seizures	[251]
	Mass	General framework for generating seizure-like patterns	[70–72]
Focal	Neuronal	Conditions on prediction of focal seizures	[7]
	Mass	Importance of balance between excitatory and inhibitory feedback	[140]
	Phenomenological	Synchronisation of LFP causes afterdischarges	[110]
Absence	Neuronal	Non-ictal phases in bistable model affect likelihood of seizures	[111]
	Phase	Abnormal white fibre connections facilitate generation of SWD	[249]
	Mass	SWD result from intermittency caused by spatial heterogeneities	[79–82]
	Field	SWD caused by bifurcation as well as bistability	[130, 131]
		Genetic algorithm reveals clinical differences between seizures	[148]
	Phenomenological	Network structure influences escape times in bistable model	[19]
		Bistable model describes seizure-onset	[112]
NCSE/SWD	Field	Phase-locking delta-oscillations stochastic precursor SWD	[92]

Table 2.4: Recent papers in computational modelling of epilepsy: seizures were classified as focal, generalised, absence, or non-convulsive status epilepticus/spike wave discharge (NCSE/SWD). Note that all publications appeared in the time period 2009-2014

Chapter 3

Network-analysis of resting-state EEG from families with IGE [1]

3.1 Introduction

Idiopathic generalised epilepsy (IGE) comprises a group of clinical syndromes accounting for $15-20\%$ of all epilepsies [100]. Although the classification scheme for the epilepsies is evolving, the concept of IGE remains popular, consisting of a set of epilepsy disorders characterised by specific well-recognised generalised seizure types. Although IGE may very rarely be a monogenic disorder in a few families, typically it has a complex inheritance suggesting susceptibility is associated with multiple genes [91, 164].

Generalised spike-wave (GSW) observed in EEG is a hallmark of IGE, and reflects abnormal hypersynchronous electrical activity within brain networks. There is at present much interest concerning the structural and functional nature of brain networks in which seizures arise and how these factors give rise to specific seizure types or epilepsy syndromes [178]. The complexity of the brain makes it challenging to study and compare time-series from subjects, but a well-developed approach to characterising complex networks,

[1] The work presented in this chapter has been reported in the following publication: Chowdhury FA, Woldman W, FitzGerald TH, Elwes RD, Nashef L, Terry JR, Richardson MP. (2014) Revealing a brain network endophenotype in families with idiopathic generalised epilepsy, PLoS One, volume 9, no. 10, DOI:10.1371/journal.pone.0110136. For this publication the contributions were as follows: Performed the experiments: FAC. Analysed the data: FAC WW THBF RDCE JRT. Contributed reagents/materials/analysis tools: RDCE LN JRT. Wrote the paper: FAC WW THBF RDCE LN JRT MPR. For the chapter, all scripts underlying the analysis were written and carried out by WW, and adjustments to the text were made throughout by WW.

graph theory, has recently had a substantial impact on the investigation of data relating to brain networks [31]. Graph theory enables local and global characteristics of network connectivity to be computed and compared between subjects. Brain networks can be inferred from EEG by examining the patterns of association between EEG signals (correlation, synchronisation), based on the ability of EEG to capture information about multiple brain sources of activity. It is assumed that neuronal activity in distributed brain networks is reflected in multiple sources of independent activity detectable in scalp EEG, and that examining interactions between the signals obtained by different EEG electrodes is a reasonable proxy for examining interactions between the underlying sources which constitute the brain network. Graph theory can be used to summarise structural topological features of brain networks; these structural properties may have a key influence on the dynamics which the network can generate [178]. Abnormality of brain dynamics is evident in epilepsy as the paroxysmal occurrence of seizures, therefore it is logical to propose that these abnormal dynamics may be dependent on abnormal network topology. The aim of this study is to use graph theory applied to EEG to explore the hypothesis that abnormal properties of brain networks are a component of the inherited phenotype in IGE.

Investigations of the complex genetics of brain disorders have in several instances made important progress through investigating endophenotypes; heritable traits with a simpler genetic basis than the full disorder, which may be present in family members who do not have the disease [83]. In this regard, measures of network topology have been suggested as a candidate approach for identifying potential endophenotypes, by quantifying the genetic risk for a specific neurological condition [31]. Some basic EEG-derived network metrics obtained using graph theory, particularly clustering coefficient and average path length, show high heritability in healthy subjects, especially in the alpha frequency band [199, 200]. Studies of the maturation of brain networks in children suggest that normal development is characterised by a gradual alteration of the balance between the strength of local connectivity, presumably reflecting cortical localisation of function, and the strength of long-range connections which presumably reflects the functional integration between lo-

calised regions required for normal brain function [174]. Given that IGE may often have onset in childhood and remit with maturation, it is hypothesised that brain networks in people with IGE and their relatives will show altered network properties compared to healthy controls, and that this may have a basis in aberrant development. For this purpose eyes-closed resting-state EEG recordings were used, which has been recommended as the standard baseline approach for EEG studies that do not require visual inputs [15].

Interpretation of EEG in a clinical setting typically uses five broad frequency bands defined according to prominent features visible to an expert observer. A recent literature has sought to establish the frequency bands in which EEG oscillatory activity is maximally independent, hypothesising that such maximally-independent bands may represent different neurobiological generators, and may be optimally sensitive to differences between subjects or experimental manipulations. Although the conventional clinical EEG frequency bands relate to qualitative features seen in the EEG, it is not necessarily the case that these conventional bands optimally reflect the underlying generators. Furthermore, given that brain network features in the alpha band may show evidence of heritability, and that anti-epileptic drug treatment may alter peak alpha frequency [199, 200, 220], there is a particularly focus on the alpha range through dividing into sub-bands. Here, the frequency bands are defined by Spectral Factor Analysis (SFA) in two independent datasets of resting EEG activity, in which these bands were shown to be extremely robust to a range of methods used to determine the bands, artefact rejection schemes and scalp electrode positions [197].

3.2 Materials and methods

3.2.1 Recruitment and selection of participants

Subjects with IGE were identified from five hospitals in London and outlying regions, and were a consecutive series that met the inclusion and exclusion criteria and were able to participate. Inclusion criteria for people with IGE were age $>$ 18 years old, a diagnosis of IGE, and $\geq$ 2 family members with epilepsy according to self-report. Twenty-eight families were recruited; in 16 families the reported presence of epilepsy in more than one family member was

confirmed from history and investigation; in the other 12 families, the reportedly affected family members were not available for assessment. In addition to the affected probands (the first affected family member seeking medical care for a genetic disorder), clinically unaffected first degree relatives were recruited from the 28 families. These unaffected relatives were interviewed in detail by a neurologist (FAC) and had no evidence of symptomatic seizures from detailed history. Furthermore, in addition to the EEG study carried out as part of this investigation, all unaffected relatives underwent diagnostic MRI which was in all cases normal. Healthy participants with no personal or family history of neurological or psychiatric diseases were recruited via a local research participant database. Participants were excluded if they had any other neuropsychiatric condition or a full scale IQ (FSIQ) < 70. Ethical approval was obtained from King's College Hospital Research Ethics Committee (08/H0808/157). Written informed consent was obtained from all participants. The neuropsychometric findings in this cohort of people with IGE, relatives and controls were reported in [38].

3.2.2 EEG acquisition

Conventional 10-20 scalp EEG was collected using a NicoletOne system (Viasys Healthcare, San Diego, California, USA), 19 channels, sampling rate 256 Hz, bandpass filtered 0.3-70 Hz. EEG was carried out using the same system in the same recording room, undertaken by the same EEG technologist using conventional measurement techniques to determine electrode positions. Collection of subjects from the different groups was interleaved over the duration of the study. Ten minutes of awake EEG in all participants and 40 minutes of sleep was obtained where possible. Where specific consent was obtained, hyperventilation and photic stimulation were carried out. In this chapter only awake EEG was examined. The EEGs were reviewed independently by two expert reviewers. The following features were noted: presence of GSW; focal abnormalities including spikes, sharp waves and slow waves; response to photic stimulation; and normal variants.

3.2.3 Quantitative EEG analysis

EEG data was referenced to the channel average. A single 20 second epoch was selected which included continuous dominant background rhythm with eyes closed, without any artefacts, epileptiform abnormalities or patterns indicating drowsiness or arousal. Epoch selection for analysis was carried out by one EEG expert who was blinded to subject group. These EEG epochs were used for all the subsequent analysis methods described below. The analysis used 5 frequency bands defined from previous literature applying SFA to resting EEG: 1-5 Hz, 6-9 Hz, 10-11 Hz, 12-19 Hz and 21-70 Hz [197]. Normalised power spectra were computed and showed no significant statistical differences at the group-level (see figure 3.1). Although different from the conventional clinical EEG frequency bands, the frequency bands used here were shown to be extremely robust to a range of methods used to identify the maximally independent bands, artefact rejection schemes and scalp electrode positions [197]. Analyses were performed using a combination of the EEGlab toolbox, the Brain Connectivity Toolbox [187], in addition to custom Matlab (Mathworks, Natick, Massachusetts, USA) scripts for band-pass filtering the EEG data to optimise the rectangular drop-off at the boundary between frequency bands [52].

3.2.4 Construction of weighted undirected networks

Networks were constructed from resting-state EEG recordings by applying the Hilbert transform to the band-pass filtered EEG to generate instantaneous estimates for the phase and amplitude. The Hilbert transform is one of the most common approaches to derive information about the phase of a time-series, by transforming the signal $x(t)$ to an analytical signal:

$$\rho(t) = x(t) + ix_H(t) = A(t)e^{i\phi(t)} \tag{3.1}$$

$$x_H(t) = \frac{1}{\pi}\text{P.V.}\int_{-\infty}^{\infty}\frac{x(t')}{t-t'}dt' \tag{3.2}$$

with P.V. the Cauchy principal value. The original signal $x(t)$ is transformed into the frequency domain to find estimates for the instantaneous phase $\phi(t)$

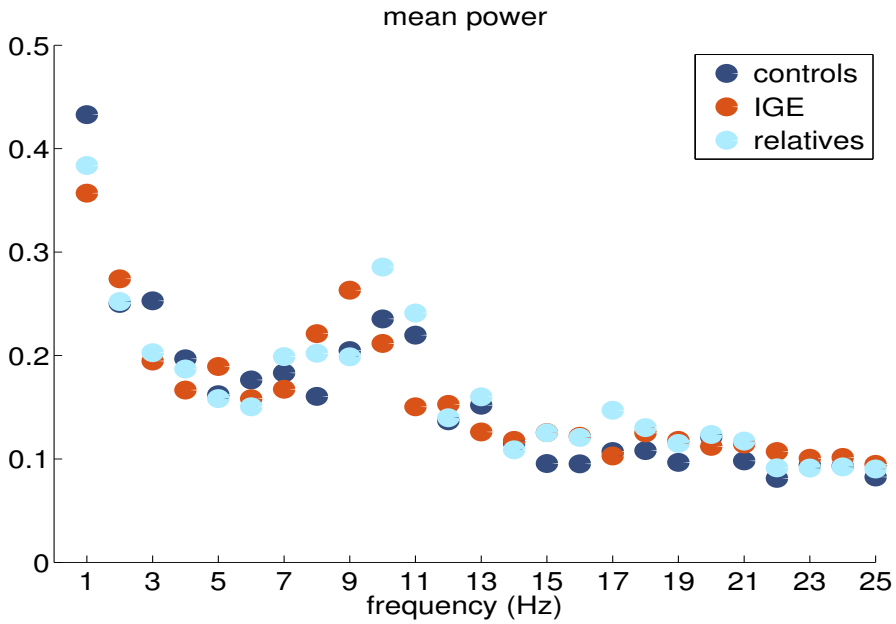

Figure 3.1: Normalised average power spectra. For channel C3, the average normalised power spectra were computed for normal controls (dark blue, $n = 40$), subjects with IGE (orange, $n = 35$), and first-degree relatives of people with IGE (light blue, $n = 42$). Standard errors were less than 0.007 for any cohort at any frequency.

and amplitude $A(t)$ of $x(t)$ (with f a chosen narrow frequency-band):

$$\hat{x}(f,t) = A(t)e^{\mathrm{i}(ft+\phi_x(t))} \tag{3.3}$$

By separating the amplitude and phase of a signal, the Hilbert transform reveals fundamental information about the temporal evolution of the data [223, 229].

As the recordings were collected using a standard 10-20 set-up with 19 electrodes, the network consists of 19 nodes and the connectivity between these nodes (edge-strength), was determined by calculating the phase-locking factor (PLF) [118, 215]. Given two signals (recorded from two different electrodes), X and Y, with corresponding digitally sampled signals x_i, y_i with $1 \leq i \leq N$, the discrete Hilbert transform of both signals leads to complex coefficients x_i^H, y_i^H with $1 \leq i \leq N$ and estimates for the amplitude and phase (ϕ_x, ϕ_y). The PLF

between the two signals X and Y is defined by:

$$\mathrm{PLF}(t) = \frac{1}{N}\left|\sum_{n=1}^{N} \exp\left(i(\phi_x(t) - \phi_y(t))\right)\right| \tag{3.4}$$

The edge strength between the two nodes is found by taking the mean over all the samples. Using this procedure, every 20 second epoch from each individual leads to 5 different weighted, undirected networks. It should be pointed out that these brain networks are functional networks, as opposed to anatomical or effective networks. In functional networks, connectivity is typically defined by statistical correlations between the sources of activity.

The networks were analysed by computing a set of characteristic graph measures, which capture specific local or global properties of the network structures at hand, such as functional integration and segregation. The following graph metrics were selected: mean degree, mean degree variance, clustering coefficient (local segregation), and characteristic path-length (global integration). The mean degree (MD) and mean degree variance (DV) summarise the degree distribution, by indicating whether the network contains nodes with approximately equal degrees or whether they vary over a broader range, and thereby provide fundamental insight in the network's architecture. The clustering coefficient C captures the tendency of a network to form local clusters in the network, whereas the characteristic path length L measures how well the nodes of the network are interconnected [187, 206].

The clustering coefficient and characteristic path length are sensitive to changes in network degree distribution [206, 207]. In order to control for this, these measures were normalised by using surrogate networks: $\hat{\mathrm{CC}} = CC/CC_{\mathrm{surr}}$ and $\hat{\mathrm{PL}} = PL/PL_{\mathrm{surr}}$ where CC_{surr} and PL_{surr} are the mean clustering coefficient and characteristic path length of a distribution of 500 surrogate random networks [206, 207]. $\hat{\mathrm{CC}}$ and $\hat{\mathrm{PL}}$ were computed for each subject for each frequency band network. All network topology analyses were carried out using the Brain Connectivity Toolbox [187], and customised where needed.
'

3.2.5 Statistical testing

To explore differences in the proportions of each group showing qualitative EEG abnormalities a Fisher's exact test was used with significance threshold of $p = 0.05$ two-tailed, Bonferroni-corrected for three between-group comparisons. Prior to testing, all quantitative measures were tested for normality and a non-normal distribution was observed. Thus a non-parametric Kruskal-Wallis test was used to examine for effects in each measure across the three groups and five frequency bands; results were declared significant at $p < 0.05$ two-tailed, Bonferroni corrected for five frequency bands. Where the Kruskall-Wallis test was significant, an additional Mann-Whitney test was used to compare between pairs of groups for each frequency band. Results were declared significant when $p < 0.05$ after Bonferroni correction for three between-group comparisons.

3.3 Results

The study included 117 participants: 40 normal controls (20 female, mean age 30.7 years), 35 people with IGE (21 female, mean age 34.4 years), and 42 unaffected first-degree relatives of people with IGE (19 female, mean age 36.0 years). The age and gender distributions of the groups were not significantly different (all $p > 0.05$ uncorrected). Clinical details of the people with IGE who participated in the study are presented in Table C.1 in the Appendix. Thirteen subjects with IGE and 8 relatives refused photic stimulation because of the risk of provoking a seizure.

3.3.1 Qualitative analysis

People with IGE were more likely to have generalised epileptiform discharges compared with relatives and controls (17/35 people with IGE, 2/42 relatives, 0/40 controls; chi-squared with Fisher's exact test, one-sided $p < 0.0001$ Bonferroni corrected in both instances), but there was no significant difference in the proportion of relatives with generalised epileptiform discharges compared with normal controls ($p = 0.27$ uncorrected). There were no significant differences between any pair of groups in the proportions of subjects with focal discharges, positive photoparoxysmal response or normal variants.

3.3.2 Graph theoretical metrics

Mean degree (MD) differed between the groups only in the 6-9 Hz band (Kruskall-Wallis $p = 0.0064$, Bonferroni corrected for five frequency bands), see table 3.1 and figure 3.2. Subsequent comparison of group pairs revealed that MD was higher in the people with IGE than normal controls (Mann-Whitney $p = 0.0008$, Bonferroni corrected for three between-group comparisons); in relatives, MD was higher than healthy controls and lower than people with IGE but did not differ significantly from either group. Degree distribution variance (DV) showed a difference between the three groups only in the 6-9 Hz band ($p = 0.0005$, Bonferroni corrected for five frequency bands). Examining paired comparisons between groups, DV was higher in people with IGE and relatives than in normals in this band ($p = 0.0005$ and $p = 0.0009$ respectively, Bonferroni corrected). Clustering coefficient ($\hat{C}C$) differed between the three groups only in the 6-9Hz band ($p = 0.0018$, Bonferroni corrected). $\hat{C}C$ was greater in the people with IGE and relatives than in normal controls ($p = 0.0025$ and $p = 0.0013$ respectively, both Bonferroni corrected). There were no differences between groups for $\hat{P}L$. There were no other significant differences or trends between groups in any other frequency band, comparing controls, people with IGE and relatives. In particular, there were no differences between epilepsy and relative groups in any frequency band for any measure.

3.4 Discussion

These findings suggest brain network topology differs between people with IGE and normal controls, and that some of these network measures show similar deviations in people with epilepsy and in unaffected relatives who do not have epilepsy. This suggests brain network topology may be an inherited endophenotype of IGE, present in unaffected relatives who do not have epilepsy, as well as in affected people with epilepsy. These results suggests that abnormal brain network topology may be an endophenotype of IGE, though not in itself sufficient to cause epilepsy. Although it is conceivable that EEG network features in the people with IGE may differ from normal subjects as a result of anti-epileptic drug treatment, the unaffected relatives were not taking medication. In conclusion, brain network topology may be a component of an inherited

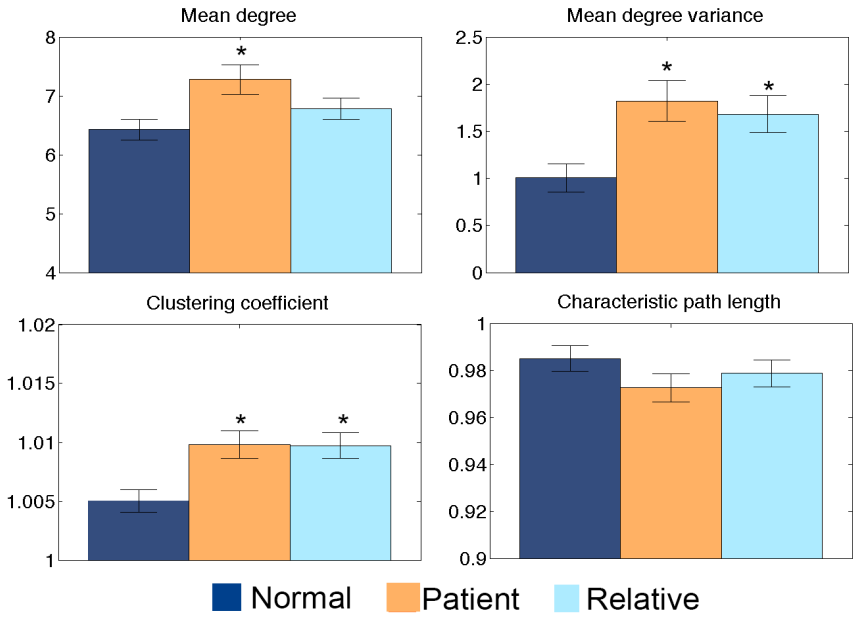

Figure 3.2: Graph measure comparison between people with IGE, their relatives, and healthy controls. An abnormal EEG network topology is an endophenotype of IGE, present in people with IGE and first-degree relatives. Group means +/- standard error of the mean are shown for: (A) mean degree MD, (B) mean degree variance DV, (C) clustering coefficient $\hat{C}C$, and characteristic path length $\hat{P}L$, in the 6-9Hz band. Normal controls (dark blue), subjects with IGE (orange), and first-degree relatives of people with IGE (light blue). * = $p < 0.05$ Bonferroni corrected compared with normal controls.

endophenotype of IGE, and not dependent on medication effects.

A small study examined interictal MEG in five adults with absence epilepsy and five matched controls [37]. Using coherence as the measure of interaction between channels, the authors found that average node strength, clustering coefficient, and global efficiency were all greater in people with IGE than normal controls; these findings would be in keeping with the results described here. A group of 26 adults with IGE characterised by generalised tonic-clonic seizures was compared with 26 normal controls using fMRI and DTI [250]. The brain was parcellated into a large number of nodes, and connectivity between all pairs of nodes estimated from both datasets. The results were somewhat inconsistent between methods, but a decrease in small world-

Measure	Comparison	1-5Hz	6-9Hz	10-11Hz	12-19Hz	21-70Hz
MD	all groups	0.9513	**0.0064**	0.9321	0.5501	0.5435
MD	C vs IGE		**0.0008**			
MD	C vs R		0.0514			
MD	R vs IGE		0.0718			
DV	all groups	0.8795	**0.0005**	0.8533	0.6280	0.2206
DV	C vs IGE		**0.0005**			
DV	C vs R		**0.0009**			
DV	R vs IGE		0.5947			
$\hat{C}C$	all groups	0.9003	**0.0018**	0.7291	0.5370	0.1315
$\hat{C}C$	C vs IGE		**0.0025**			
$\hat{C}C$	C vs R		**0.0013**			
$\hat{C}C$	R vs IGE		0.8780			
$\hat{P}L$	all groups	0.5920	0.0814	0.4343	0.3798	0.8177
$\hat{P}L$	C vs IGE					
$\hat{P}L$	C vs R					
$\hat{P}L$	R vs IGE					

Table 3.1: Graph measure comparison between people with IGE, their relatives, and healthy controls. Summary of effects found comparing three groups: C: normal controls, IGE: people with IGE, R: their first-degree relatives. Bold-faced indicates Bonferroni corrected values: individual comparison between two groups were only carried out if the correct Bonferroni value was significant at the group level.

ness and a decrease in clustering coefficient were found comparing people with IGE with normals. A further study also used DTI to compare brain networks in 18 children with childhood absence epilepsy with 18 matched normal controls [248]. This study found that the network connection strength, clustering coefficient, local efficiency and global efficiency were decreased in the people with IGE, and the characteristic path length increased. Although some of these findings are contradictory to the results described here and those of [37], at the current time, it is extremely difficult to reconcile results found with MRI

methods with those found using EEG/MEG.

Animal models of childhood absence epilepsy (CAE) show abnormalities in a complex brain network comprising a combination of a focal cortical region which drives the onset of generalised seizure discharges in thalamocortical networks, and an abnormality of anterior transcallosal pathways; this transcallosal abnormality has also been found in human juvenile myoclonic epilepsy (JME), hence there is a justification to propose that large-scale brain network abnormalities are a feature of IGE [35, 136, 158]. A large study of recent-onset IGE demonstrated $34-49\%$ failed to achieve 12-month remission with first-line anti-epileptic drugs, indicating an urgent need for better treatment based on improved mechanistic understanding of IGE [129]. This improved understanding is likely to emerge from detailed phenotyping, genotyping, and the development of explanatory models. It seems likely that seizures emerge in large-scale brain networks through the interaction between brain network structure and the dynamics of the brain regions which constitute the network nodes [218]. The likelihood that seizures will emerge from a specific brain network is captured by the term brain network ictogenicity (BNI). In this study, it is shown that one contributor to brain network ictogenicity - network structure - is abnormal in subjects IGE compared with healthy controls, and that a similar abnormality is observed in the unaffected relatives of the subjects with IGE. These findings contribute to a more detailed phenotype of IGE and have implications for future genetic studies.

The fundamental aim of this study was to identify a brain network endophenotype of IGE. An endophenotype is a heritable trait which is a component of a disorder or associated with high liability to develop the disorder. An endophenotype may be present in family members who do not have the disease, hence increasing the power of genetic studies, and its inheritance is likely to be simpler than the full disorder [83]. This concept has been extensively exploited in other common brain disorders with complex inheritance, such as schizophrenia [4]. Given the universal availability of EEG, and that GSW is a cardinal feature of IGE, EEG is an obvious place to look for an IGE endophenotype. It has been shown that 0.5% of unaffected adults and 1.8% of unaffected children under 16 years may show GSW [77, 84]. Unaffected first-

degree relatives of subjects with IGE show a much higher prevalence of GSW: $8-40\%$ of unaffected siblings under 16 years had GSW when awake and up to 72% when asleep; but only $6-9\%$ of unaffected siblings over 16 years had GSW [51, 61, 61, 102]. Therefore GSW may be an endophenotype of limited usefulness in adults, since, if IGE is explained by complex inheritance, at least 50% of first-degree relatives of subjects with IGE should share one or more genes contributing to the IGE phenotype.

Conventional expert EEG review of the subjects revealed GSW in 49% of people with IGE, 5% of relatives and zero controls; these findings are expected, and suggest that the cohort is unexceptional. Finding GSW in some "unaffected" relatives might suggest the possibility that some relatives in fact have unsuspected epilepsy. Although this is possible, detailed assessment of the relatives did not reveal any evidence of symptomatic seizures in any of the unaffected relatives group; post hoc exclusion of the two relatives with GSW does not alter the effects found.

Measures of EEG network topology differed between groups, revealing strong similarities between brain networks of people with IGE and first degree relatives. For networks inferred from EEG band-pass filtered in the 6-9Hz band, both the mean degree and mean degree variance was lower in normals than either people with IGE or relatives. This indicates that the variability in the number of connections per network node is greater in people with IGE and relatives, revealing the existence of a brain network endophenotype characterised by both unusually overconnected brain regions (hubs) and underconnected brain regions.

Comparison of subjects with epilepsy taking anti-epileptic drugs with unmedicated normal controls introduces the potential confound that effects found may be due to the drugs and not due to the disease, and this possibility cannot be excluded. However, as the relatives were unmedicated, the comparison of relatives with controls does not suffer this confound.

The network analyses were carried out in "sensor space" that is, networks were constructed which described the interactions between activities at the EEG electrodes, rather than the interactions between the actual brain sources generating these patterns of brain activity. The limited spatial sampling of

routine clinical EEG would not readily permit source reconstruction, but future studies should attempt to identify the origins of these network properties in the brain.

The studied networks were weighted graphs, in contrast to some studies (e.g. [177]) which have examined unweighted graphs. An unweighted graph is produced by choosing a threshold for edge weight, and assigning the value of an edge as either zero or one according to this threshold. In order to examine the generalisability of the group findings, the same statistical analysis was carried out for unweighted, binary networks, and the statistical significant differences remained (see table 3.2).

Comparison	DV	$\hat{C}C$	$\hat{P}L$
All groups	0.0005 / 0.0005	0.0018 / 0.0353	0.0814 / 0.0007
IGE vs. controls	0.0005 / 0.0009	0.0025 / 0.0218	0.0231 / 0.0015
Relatives vs. controls	0.0009 / 0.0006	0.0013 / 0.0307	0.0986 / 0.0008
IGE vs. relatives	0.5947 / 0.9307	0.8780 / 0.7050	1.6180 / 0.5061

Table 3.2: Comparison between graph measures for weighted and unweighted networks in low-alpha.. Values for weighted networks were presented first, and values for unweighted networks came after the backslash. Unweighted networks were obtained by thresholding the weighted networks, where the values below the threshold are set to 0 and the values above the threshold to 1. The threshold is chosen such that the network has a fixed mean degree ($MD = 8$ in this case). It is important to note that even though the comparison between the results showed the same statistical significances, this specific threshold was found to be the most optimal; a different choice of threshold would lead to a decrease in statistical significances. Note that another method for thresholding could have been used, i.e. using the same threshold for every network in a cohort, and this approach would lead to variable mean degrees, but the choice of this threshold would again be non-trivial.

As has been discussed in detail in [228], there are limitations to either approach. By choosing a threshold, the mean degree becomes a fixed parameter rather than a variable graph measure capturing potentially valuable information about the network structures at hand. Another practical limitation in the data is that the networks have only 19 nodes, therefore the range of possible network degree is limited; the consequence of this is that defining an unweighted network using a high threshold (or low network degree) would

have the consequence that many networks will fall apart into disconnected components and therefore could not be validly compared; whereas using a low threshold (or high network degree) would have the outcome that the networks would tend to be fully connected (i.e. every possible edge is present) therefore there would be very limited possibility to identify any difference between networks and additionally there is currently no straight-forward or structural approach for deciding the appropriate threshold. Given these considerations, using a weighted unthresholded approach might be preferable.

One could question the particular choice of graph metrics, as there are is a wide variety of other candidates that have been used in other graph theoretical analysis of brain networks [31]. As there currently is not a structural approach that can be used to decide on the choice of graph metrics that would optimally interrogate a complex network, the decision was made to use four well-established and rather fundamental metrics that reveal information about the functional integration, segregation, and the network distribution. This enabled a robust comparison between the networks from the people with IGE, their relatives, and healthy controls. Another recurrent issue concerning the analysis of EEG pertains to the choice of the reference electrode. Therefore, an identical analysis was carried out using bipolar montage, which confirmed the reported findings.

There is an inherent problem with work of this kind, which may be described as the problem of reducing bias due to common sources of EEG activity seen at more than one scalp electrode, and which encompasses both the selection of reference electrode and consideration of the effect of volume conduction in selection of the method to determine interaction between EEG time-series. The problem of common sources is well-known and does not have a single optimal solution [86, 167, 207]. An average reference electrode was used, and interactions between EEG channels were quantified by the PLF, which detects synchronisation at zero phase lag. Note that previous work shows this combination of measure and reference is able to detect real differences in synchronisation [207]. There are many different methods of deriving functional network connectivity structures from imaging data, which potentially would lead to different network structures and consequently to different outcomes

for the graph measure comparisons. However, as there currently is no proven structural method to decide on the choice of network derivation technique [168, 235], the general consensus towards analysing time-series data is to start with traditional linear approaches before using more complicated non-linear methods. However, it should be recognised that different approaches may reveal different parts of the interdependence between the recorded signals. As the phase-locking factor approach is a linear synchronisation-based approach, the results were compared to a correlation-based technique (delayed cross-correlation) [190], which showed the similar overall results.

The cohort of people with IGE could be divided in those who were able to enter seizure-remission (no seizures for at least 12 months, 19/35) and those with on-going seizures (at least one seizure during the last 12 months, 16/35). A similar graph theoretical comparison can be carried out for these two different cohorts in order to examine whether these groups show striking differences and whether the networks of the people who were able to enter seizure-remission (for example, because of successful drug treatment) were similar to those of healthy controls. The results are shown in table 3.3, and surprisingly show that several graph measures are statistically different between the networks from the healthy controls and those who entered seizure-remission, potentially indicating that the mechanism responsible for entering seizure-remission does not force the networks to behave like those of healthy controls, but instead, alter them in a different "domain". It should be pointed out that the group-size of these cohorts (19 and 16) is arguably too small to derive strong conclusions.

A crucial consideration in experimental research is whether the results are reliable and can be reproduced. An important strength of the study is the sample size of 117 subjects, and the detected effect sizes are highly significant, which is a strong defence against error. However, an important question is whether results are stable if a different epoch of EEG data were chosen from each subject. The difficulty of identifying artefact-free EEG data epochs of 20s from every subject should not be underestimated - EEG is highly prone to movement, blink and other artefacts. Furthermore, artefact-free epochs were identified by expert opinion rather than by using an approach that automat-

Comparison	MD	DV	$\hat{CC}$	$\hat{PL}$
controls vs ongoing	0.0309	0.0184	0.0295	0.5138
controls vs seizure-free	0.0003	0.0003	0.0016	0.0053
ongoing vs seizure-free	0.2083	0.2205	0.2205	0.0793
relatives vs ongoing	0.4865	0.7807	0.6763	0.9307
relatives vs seizure-free	0.0342	0.2896	0.5436	0.0462

Table 3.3: Graph measure comparison between people with IGE with ongoing seizures, people with IGE in seizure remission, first-degree relatives of people with IGE, and healthy controls: counterintuitively, graph measures extracted from networks from healthy controls were significantly different than those from seizure-free for all 4 graph measures.

ically selects potential epochs by using artefact removal tools. Hence, it was typically not possible to find more than one suitable epoch for every subject. Post hoc, the stability of the findings was examined by dividing the single epoch from each subject into two equal non-overlapping epochs of half the length (labelled as epoch 1 and epoch 2). An identical analysis was repeated for both epochs from all subjects: in the analysis of the full 20s epoch, five pairwise comparisons were reported that reached significance using Bonferroni correction; using epoch 1 for every subject, the same 5 comparisons remained significant; using the epoch 2, three of the five comparisons remained significant and two were at the level of strong trend (and were significant without Bonferroni correction). Furthermore, the comparison between people with IGE and relatives of mean degree, degree distribution variance, and clustering coefficient revealed no differences using the full 20s epoch, and also revealed no differences using either epoch 1 or epoch 2. Therefore, the findings are reproducible within two non-overlapping epochs of EEG data. Nonetheless, it should be pointed out that the reliability of the findings needs to be established in an independent dataset.

It is not yet established whether individual syndromes of IGE are entirely unrelated, with no shared aetiologic, genetic or mechanistic factors, or represent a continuum or set of overlapping disorders with important shared

pathophysiology. In this context a divergence of views between those who seek to identify individual syndromes on the basis of highly detailed phenotyping, and those who seek common aetiological and mechanistic factors across the range of common IGE syndromes. In this study, the aim was to specifically seek shared factors between families and between different IGE syndromes, hypothesising that there are likely to be shared genetic and mechanistic factors between different IGE syndromes [6, 26, 144]. It should be noted this approach has been successful in recent genetic studies, which have identified recurrent chromosomal microdeletions (deletion of a small piece of a chromosome) as the most frequent identifiable genetic factor associated with the common IGE syndromes [49, 60, 90]. For example, the most frequently identified microdeletions each accounted for people with IGE with at least three of the four common IGE syndromes included in the study here [49]: Microdeletions at 15q11.2 were identified in subjects with JME, JAE, CAE and GTCS; microdeletions at16p13.11 were found in JME, CAE and GTCS; and microdeletions at 15q13.3 were found in JAE, JME and CAE. These genetic findings strongly support the argument that a similar brain network endophenotype might be found across the range of common IGE syndromes.

In summary, it is shown here for the first time a brain network endophenotype of IGE may be present in the resting-state EEG from relatives and people with IGE. These findings have significant implications for the current mechanistic understanding of IGE, and for future phenotyping and genetics studies. Additionally, the existence of this endophenotype has ramifications for the value of network analysis of resting-state EEG in the context of diagnosis of epilepsy: as the networks from people with IGE are indistinguishable from their relatives, the network approach on its own no potential added value to the process of diagnosing epilepsy but instead should be complemented by at least a second level of description, such as a mathematical model.

Chapter 4

Mathematical biomarkers of IGE derived from resting-state EEG [1]

4.1 Introduction

Epilepsy is challenging to diagnose and misdiagnosis of epilepsy is a serious issue, associated with several negative psychological and socio-economic consequences (loss of mobility and stigma) for an individual [202]. At present, a confirmed clinical diagnosis of epilepsy relies on a reliable case history (including a detailed diary of the dates and times of suspected seizures, eye-witness accounts, and video clips of the subject undergoing suspected seizures) and a positive EEG, showing the presence of abnormalities known as epileptiform discharges. However, a positive EEG occurs in approximately 60% of cases, resulting in diagnostic uncertainty for many subjects with suspected epilepsy [202], with significant associated costs [109] resulting from additional, longer-term, EEG monitoring, repeated unplanned admissions to the hospital (emergency department, and first seizure clinics) [242]. Conventional EEG analysis has low sensitivity and specificity, and the process is expensive, inconvenient, and inefficient, particularly for people with low seizure-frequency.

[1] The work presented in this chapter is based on: Schmidt H, Woldman W, Goodfellow M, Chowdhury FA, Koutroumanidis M, Jewell S, Richardson MP, Terry JR (2016). A computational biomarker of idiopathic generalized epilepsy from resting-state EEG, Epilepsia, 10.1111/epi.13481. Conceived and designed the experiments: HS WW MG JRT MPR. Performed the experiments: FAC, MK, SJ. Analysed the data: HS WW MPR JRT. Wrote the paper: HS WW MG, FAC, MK, SJ, MPR JRT. For the chapter, all scripts underlying the analysis were written and carried out by WW, and adjustments and extensions to the text were made throughout by WW (SVM-method).

The National Institute for Clinical Excellence (NICE) guidelines for diagnosis and management of epilepsy gives an outline of the steps supporting the examination of subjects with a suspected first seizure [149, 150]. The diagnostic process commonly starts when a subject experiences an event which a GP suspects may have been a seizure. The subject is referred on to a neurologist by the GP, usually at a first-seizure clinic. Alternatively, a subject may be referred to a first-seizure clinic following admission to an emergency department. The neurologist evaluates the case history of the subject; if the neurologist concludes the event might indeed have been a seizure, he or she will arrange a routine EEG recording (20-30 minutes long). The guidelines recommend that children should have an EEG after the second suspected seizure whereas for adults an EEG should be recorded if the clinical history suggests an epileptic seizure.

The routine EEG is used by clinicians to identify the presence of interictal epileptiform discharges. These discharges are paroxysmal patterns on the EEG that serve as a marker for epilepsy, and signify an increased tendency of the brain to generate seizures. However, it is important to point out that normal EEG findings do not exclude the possibility of epilepsy, due to its limited sensitivity of about $30-50\%$ in the interictal period [226]. These discharges are a signature of abnormal (typically increased) synchronisation of neuronal populations. The common types include (poly)spikes, sharp waves, and spike-and-wave discharges [226]. Similar to seizures, epileptiform discharges can appear either focal or generalised. Since focal epileptiform discharges might be confined to a relatively small area of the cortex (the so-called epileptogenic zone) or occur in a sulcus, scalp electrodes often fail to record several focal discharges recorded by simultaneous intracranial EEG [214].

If the first routine EEG returns negative (i.e. no abnormalities), it is likely a second EEG will be arranged, which commonly will last longer (60-90 minutes) and may include activation methods such as photic stimulation and hyperventilation or may be recorded when the subject is sleep deprived. If the second EEG is negative as well, the neurologist might decide to use ambulatory EEG or long term video-EEG. Eventually, a sufficiently convincing history and/or a positive EEG will lead to a clinical diagnosis of epilepsy. In cases of

diagnostic uncertainty, an electrocardiogram (ECG) is commonly performed since the symptoms of cardiac arrhythmias and vasovagal syncope are often mistaken for seizures [201]. Neuroimaging modalities such as MRI and CT scans might support a diagnosis of epilepsy by revealing abnormalities causing epileptic seizures (e.g. a lesion), but are of limited value to epilepsies with a strong genetic component (such as IGE and benign rolandic epilepsy), as these are not associated with structural abnormalities [149].

The presence of epileptiform abnormalities in an EEG recording does not necessarily indicate a subject has epilepsy, since people without a seizure history can show similar abnormalities on EEG recordings [3]. Incidence rates of epileptiform abnormalities recorded from subjects without epilepsy vary across studies, and depend on the age of the subject, their health status (e.g. other neurological conditions), and whether epileptiform discharges occurred during a routine EEG recording or after activation methods or sleep deprivation [203]. Epileptiform discharges observed in healthy children are often hypothesised to reflect a predisposition for developing clinical seizures at a later age, but longitudinal studies have shown most epileptiform discharges disappear spontaneously during childhood [156, 203].

Due to the fact that this diagnostic process is time-consuming, potentially unspecific, and additionally may be affected by variability in the interpretation of EEG recordings [222], there is great interest in developing new biomarkers of epilepsy [76, 245]. A biomarker is defined as a "characteristic that is objectively measured and evaluated as an indicator of normal biological processes, pathogenic processes or pharmacological responses to a therapeutic intervention" [147], and might indicate the development of epilepsy. The development of new biomarkers for epilepsy is particularly relevant as it holds the potential to improve the accuracy of the current process of diagnosing epilepsy, as well as make it faster and less invasive. Recently proposed biomarkers for epilepsy include high-frequency oscillations (HFO) characteristic of epileptogenic zones [252] and reduced relaxation times of amygdala T2 weighted images characteristic of the development of temporal lobe epilepsy in children with febrile status epilepticus [39].

The specificity and sensitivity of a biomarker in principle determine its

value with respect to diagnosis and prognosis of epilepsy, by summarising the performance of a classification test on a cohort of subjects including subjects with epilepsy (positives) and subjects that do not have epilepsy (negatives). However, other considerations such as the time associated with observing the marker as well as the medical discomfort and risk in acquiring the biomarker, play a critical role in determining its ultimate clinical use. Specifically, a further consideration is the context within which the biomarker is being utilised. For example, a biomarker with 100% specificity would allow a GP to prevent referring people without epilepsy on to a neurologist, whereas a biomarker with 100% sensitivity would allow a neurologist to confirm a diagnosis with complete certainty. Additionally, the implications of false positives and false negatives depend on the specific clinical context, since a false positive by a GP can be correctly characterised as a true negative by a neurologist.

Recently, interrogation of eyes-closed resting-state activity on scalp EEG has revealed properties of the EEG vary significantly between cohorts of people with epilepsy and healthy controls. These properties include the mean degree of functional networks in the low-alpha band (discussed in chapter 3), the peak of the alpha frequency in the power-spectrum [119], and the ability of inferred functional network structures to synchronise within the setting of a dynamic network model [191]. In order to examine the potential of these measures as a biomarker, their performance needs to be tested at the level of individual subjects, as there might be substantial overlap between the cohorts, due to the variance from the means in the cohorts (i.e. statistically significant differences between two cohorts does not necessarily equate to predictive power for individuals from these cohorts).

In a study by Larsson and Kostov [119], peaks in alpha frequency from eyes-closed resting-state activity were compared between a group of 18 subjects with epilepsy (10 with focal epilepsy, 8 with generalised epilepsy) and 10 non-epileptic subjects. EEG was recorded using 25 channels with a 10-20 system, and consisted of 20 minutes of eyes closed background activity. 10 second artefact free segments were selected at the start of the recording, after hyperventilation, and at the end of the recording. Mean alpha frequency was computed for a variety of scalp locations (F3, F4, T5, T6, O1, O2) and com-

pared amongst the groups, revealing significant differences between the two cohorts for all segments in the frontal and occipital channels.

Schmidt and colleagues, study the ability of functional networks inferred from resting-state EEG to synchronise within a phenomenological model description of the brain [191]. From each segment of eyes-closed resting-state EEG a functional network topology is derived, which is then used to define the interactions between networks of phase oscillators of Kuramoto type [117]. In this model setting, the seizure-generating capability of each region (channel) within this model is evaluated computationally as the mean level of emergent epileptiform activity across the global network. Networks from 35 people with IGE were significantly more likely to generate computational seizures than the networks derived from 40 healthy controls, in both the theta (3-6 Hz) and low-alpha (6-9 Hz) bands [191].

This chapter examines the performance of these candidate biomarkers with respect to a cohort of drug-naive subjects with IGE and healthy controls. First, a description of the process of collecting and preprocessing the clinical data is given, after which the computation of the candidate biomarkers is discussed. Then the performance of the biomarkers is compared by using leave-one-out cross-validation, and the concluding results discussed with respect to potential clinical use.

4.2 Methods

4.2.1 Subjects and data

Standard eyes-closed resting-state EEG was studied from 38 healthy controls and 30 people with IGE aged between 16 and 59. The individuals with IGE were drug-naive and recruited through clinics at St Thomas's Hospital (London). A diagnosis of epilepsy was confirmed in each case by an experienced epilepsy specialist through observation of typical generalised spike-wave (GSW) activity on EEG either spontaneously or following hyperventilation or photic stimulation. For 10 of these people the diagnosis was confirmed following an initial routine EEG. For the remaining 20, diagnosis occurred following sleep-deprived or longer-term EEG monitoring (including sleep). Similar healthy control EEG was collected at King's College Hospital (London)

EEG department. Controls gave written informed consent and data collection was approved by King's College Hospital Research Ethics Committee (08/H0808/157). Under UK law, patient data collected during normal clinical routine and anonymised before research use may be used for research without additional consent; this procedure was reviewed and approved for this project by St Thomas's Hospital and King's College Hospital's Research and Development Directors.

4.2.2 Pre-processing

A trained clinical EEG technician identified a 20-second long, GSW and artifact free, segments of eyes-closed resting-state EEG activity from the initial stage of the recordings from each participant. These data were band-pass filtered using a Butterworth filter between 0.5 and 70Hz, and band-stop filtered between 48 and 52Hz to remove power-line artifacts. Since signal amplitude may vary between individuals due to different anatomical features (such as the size and shape of the cranium) the data were normalised by dividing the power spectrum in each channel by the total power in the spectrum averaged across all channels. Normalisation of the power in this fashion preserves relative differences in power between channels.

4.2.3 Biomarker 1: alpha peak frequency

The first candidate biomarker corresponds to the peak in alpha frequency which was shown to be significantly lower in people with epilepsy than in people without epilepsy in [119]. For each segment of resting-state EEG from the maximal peak between 8 Hz and 13 Hz is determined, and defined as the alpha frequency for that subject. Using this method, peaks are computed for the 38 subjects with IGE as well as the 30 healthy controls.

4.2.4 Biomarker 2: mean degree of functional networks

The second candidate biomarker corresponds to the mean-degree of the inferred functional networks, which is elevated in people with IGE, as previously described in chapter 3. EEG segments were band-pass filtered in the low alpha band (6-9Hz) [197], and functional networks inferred using the Phase-Locking Factor [215]. Note that there were also significant differences between subjects

with IGE and healthy controls for the mean degree variance and the clustering coefficient, however, the relatives were also statistically different from the healthy controls for these measures. This is the reason why we do not consider them as independent candidate biomarkers, since it is highly undesirable to have a decision support tool that would classify asymptomatic relatives as subjects with IGE.

4.2.5 Biomarker 3 & 4: Kuramoto-model

4.2.5.1 Mathematical Model

The third candidate biomarker is derived in the context of phenomenological model of the brain using Kuramoto oscillators [117, 191]. The Kuramoto model is a standard model for studying synchronisation with applications in physics, chemistry, and biology, and has been used in the field of computational neuroscience to model cortical (micro)columns and areas [99, 191]. Schmidt and colleagues show in [191] that networks derived from resting-state EEG from people with IGE were significantly more likely to generate computational seizures than the networks derived from healthy controls. The homogeneous Kuramoto model describes the evolution of N identically coupled phase oscillators:

$$\frac{d}{dt}\left(\theta_j\right) = \omega_j + \frac{K}{N}\sum_{k=1}^{N}\sin(\theta_k - \theta_j) \text{ for } j = 1, ..., N \tag{4.1}$$

with phase θ, natural frequency ω drawn from distribution $g(\omega)$, and coupling strength K between oscillators. The collective behaviour of the population is usually studied by calculating the order parameter, which measures the average amount of synchronisation amongst oscillators. The coupling strength K crucially determines the emergent activity of the population of oscillators: if the coupling strength is below a certain threshold, the oscillators are incoherently moving along the circle, whereas strong enough coupling enables synchronisation into a coherent state, see figures 4.1 and 4.2. In order to

quantify synchronisation, it is common to compute the order parameters r, ψ:

$$re^{\mathrm{i}\psi} = \frac{1}{N}\sum_{j=1}^{N} e^{i\theta_j} \tag{4.2}$$

where r between 0 (incoherent) and 1 (coherent, fully synchronised), and ψ the average phase of the population of phase-oscillators between 0 and 2π.

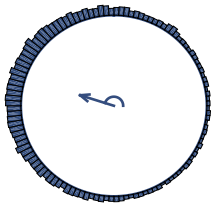

Figure 4.1: Population of Kuramoto oscillators. Snapshot of a simulation (at $t = 120$) for a network of 10000 Kuramoto oscillators with $K = 1.15$ described by equation 4.1. Movements of the oscillators along the circle is driven by their natural frequency ω and the contributions received from the other oscillators in the network through the coupling. Bars correspond to histogram bins, counting the number of oscillators on that segment of the unit circle (phase density). The magnitude of the order parameter (length of the arrow starting in the origin, defined by equation 4.2) is a measure for the average amount of synchrony in the population of oscillators (the magnitude of the order parameter is 0 for the incoherent case and 1 in the synchronised, coherent state), and the associated angle represents the average phase of the population. Simulations were carried out using a forward Euler scheme with $\mathrm{dt} = 10^{-3}$, and natural frequencies drawn from a Gaussian distribution with mean 0.5, and oscillators were initially evenly spread around the unit circle.

Now instead of a single population of oscillators, consider a network of P populations ($c = 1, 2, ..., P$), where each population c contains N_c Kuramoto oscillators [14, 132, 198]. The natural frequencies of the oscillators in population c are drawn from the distribution $g_c(\omega)$. With N the total number of oscillators in the entire network of populations, define $\eta_c = N_c/N$. The coupling between population c and γ is defined by $K_{c\gamma} \in \mathbb{C}$. The evolution of the

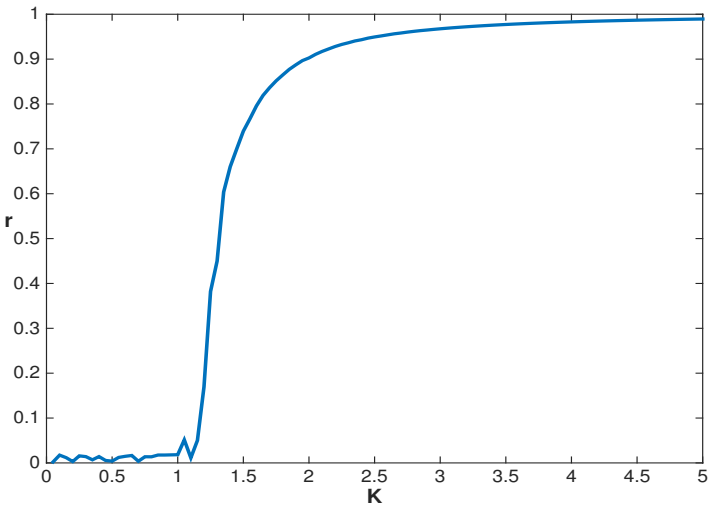

Figure 4.2: Order parameter versus coupling strength. Simulations with a network of 10000 Kuramoto oscillators (equation 4.1) where the coupling-parameter K increases from 0 to 5 with steps of 0.05: initially the population of oscillators is incoherent ($r = 0$) but as the coupling strength K increases, the system eventually synchronises into the coherent state $r = 1$. The order parameter (equation 4.2) is determined at the end of each run, which lasts 150 seconds. At $K \approx 1.1$ the system starts transitioning towards the fully synchronised state. Simulations were carried out using a forward Euler scheme with dt $= 10^{-3}$, and natural frequencies drawn from a Gaussian distribution with mean 0.5, and oscillators were initially evenly spread around the unit circle.

phase of the j-th oscillator from population c is given by:

$$\frac{d}{dt}\left(\theta_j^c\right) = \omega_j^c + \sum_{\gamma=1}^{P} \eta_\gamma \frac{K_{c\gamma}}{N_\gamma} \sum_{k=1}^{N_\gamma} \sin(\theta_k^\gamma - \theta_j^c) \tag{4.3}$$

In this modular network, synchronisation may emerge locally within a single population as well as across the global network. Figure (4.3) illustrates this in the simple case of a network consisting of 3 populations. In [191], Schmidt and colleagues proposed this modular Kuramoto model as a phenomenological model of EEG: the activity generated by cortical columns corresponds to the time-series of a single channel, and interactions between different cortical regions are reflected in the emergent patterns of activity recorded by all channels. In this context, the non-synchronised, incoherent state in the Ku-

ramoto model corresponds to healthy background activity observed on EEG, whereas emergency synchronous activity across the global network is taken as a proxy for epileptiform activity.

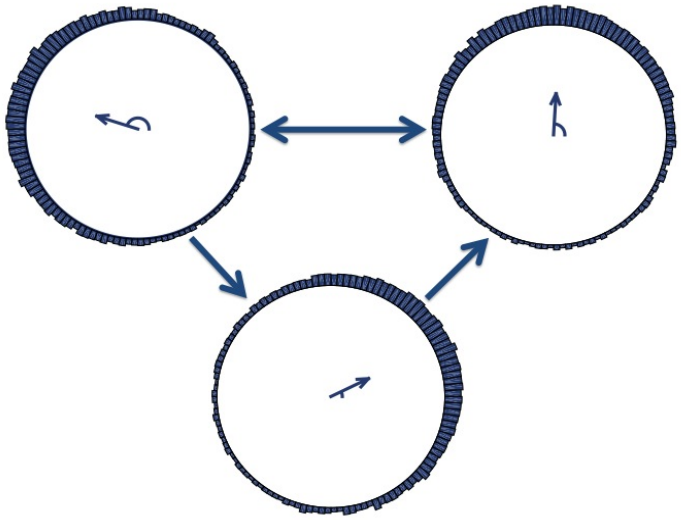

Figure 4.3: Modular network of 3 populations of Kuramoto oscillators. Simulation results for a modular network of 3 populations with each 10000 Kuramoto oscillators (equation 4.3) with moderate coupling ($K = 1.2$). Simulations were carried out using a forward Euler scheme with time-step dt $= 10^{-3}$, $\eta = 0.5$; for each population the natural frequencies were drawn from Gaussian distributions with mean 0.5, and oscillators in each population were spread evenly the unit circle at $t = 0$.

In line with the results by Schmidt in [191], phase-lags between channels are obtained in order to derive directed, functional network structures:

$$\tau_{i,j} = \text{argmax}\left(e^{\mathrm{i}(x_i(t_n) - y_j(t_n))}\right) \tag{4.4}$$

The direction of functional connections is determined by positive values for $\tau_{i,j}$, indicating a causal relationship between i and j in the sense that i causes j. Note that τ is not symmetric: $\tau_{i,j} > 0$ implies $\tau_{j,i} < 0$. In the singular case of $\tau_{i,j} = \tau_{j,i} = 0$ the connection is removed and if $\tau_{i,j} \leq 0$ it follows that $PLF_{i,j} = 0$.

4.2.5.2 Biomarker 3: effect of local synchronisation

Using linear algebra and stability analysis (see appendix A for a detailed derivation, equation A.1-A.41), a set of criteria can be derived under which the infinite-dimensional set of equations reduces to a finite set of nonlinear equations which can be solved analytically. Solutions to these equations are then used to calculate local and global order parameters, which measure the synchrony within individual regions and the global network respectively. The first Kuramoto-based biomarker is acquired by quantifying the change in emergent synchrony of the global network after setting a single node of the network (corresponding to an EEG channel) into the coherent, synchronised state. In other words, the biomarker follows by computing the resulting average level of synchronisation, which is given by the amplitude of the numerical time series, across the global network; giving a value between 0 and 1.

Consequently, this biomarker is a function of the particular channel as well as the model parameters, which can be optimised during the classification procedure and corresponds to the ability of functional networks inferred from resting-state EEG to synchronise in a phenomenological representation of the brain. The seizure-generating capability of each region (channel) within this model is evaluated computationally as the mean level of emergent epileptiform activity across the global network. The strategy is to find the channel which maximally discriminates the networks from people with IGE from the networks from healthy controls (i.e. finding a channel that when set in the pathological seizure-state leads to many emergent seizures in the simulations from the network models from people with IGE, but significantly fewer seizures in the network models from healthy controls). In [191] it was shown that on average the effect of local synchronisation in networks from people with IGE lead to significant higher levels of hypersynchronisation than in the networks derived from the healthy controls, in the theta ($3-6$-Hz) and low-alpha ($6-9$-Hz) band.

4.2.5.3 Biomarker 4: global synchronisation-parameter

The fourth biomarker is also derived from the context of the modular Kuramoto-network, but is found by computing the critical value of the global coupling

strength for which the derived network structure is driven into the fully coherent, synchronised state. In [191] it was shown that on average this value is lower for subjects with IGE than for healthy controls in the theta and low-alpha band, which suggests that the networks derived from subjects with IGE are easier to hypersynchronise (because they need less overall global coupling to be driven into the synchronised state). Details for the exact derivation of this biomarker can be found in appendix A.

4.2.6 Biomarker evaluation

Performance of the candidate biomarkers is evaluated using leave-one-out cross-validation [24], in which the recordings from all subjects are pooled, the data from one subject is successively left aside and the remaining data used as the training set. In each case thresholds are determined to give the maximal sensitivity for 100% specificity and the maximal specificity for 100% sensitivity on the training set. In turn, these thresholds are applied to classify the test subject as follows: if the value of local coupling is on the IGE side of both thresholds, then the individual is classified as unequivocally epilepsy. The individual is classified as unequivocally normal if their value is on the control side of both thresholds. If their value lies between these thresholds the individual is classified as uncertain. A graphical representation of this approach is shown in Figure (4.4). Since each outcome is discrete and non-normal, the Friedman test is used (non-parametric repeated measures ANOVA) to assess the relative performance of the biomarkers [74].

After examining the individual and independent merit of the candidate biomarkers, a support vector machine (SVM) approach is used in order to discern the potential diagnostic power of combinations of the markers. A support vector machine aims to achieve maximum separation between the training set from people with IGE and the training set from the healthy control subjects, by means of constructing a maximally separating hyperplane between the two training sets [24, 88]. Consequently, SVM methods differ from the earlier described method in the sense that is may not be possible find a hyperplane that leads to 100% sensitivity or 100% specificity for the specific training sets. However, in cases of non-separable training sets, the SVM method is guaran-

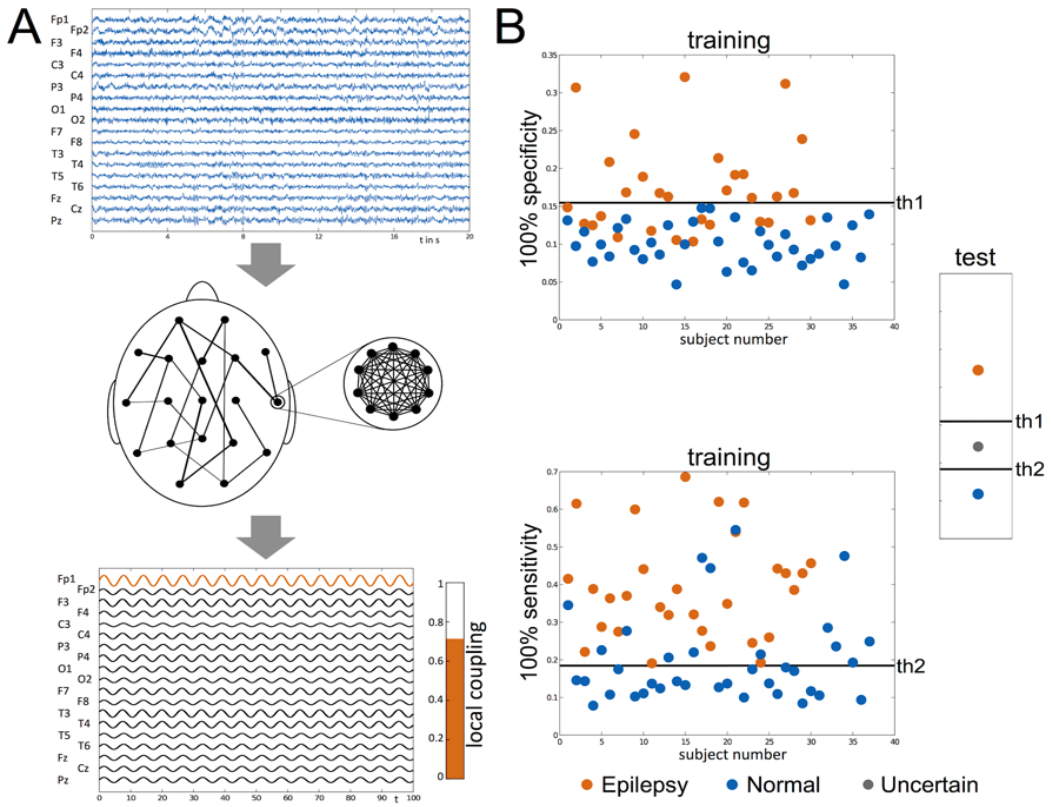

Figure 4.4: Acquisition and testing of the Kuramoto-biomarker. (A) The local Kuramoto-biomarker is acquired by inferring global (between-channel) networks from resting state EEG, and incorporating them into the Kuramoto model for coupled oscillators. The modular model is a phenomenological representation of the brain and can be used to generate in silico seizures (corresponding to the coherent, synchronised state), which is achieved by setting one node of the network (relating to a particular EEG channel) into the synchronised state. The biomarker is quantified by computing the average level of synchronisation, which is given by the amplitude of the time series, across the entire network; thus giving a value between 0 and 1. (B) To devise an unbiased test of this biomarker, leave-one-out cross-validation is used, in which one subject is left aside as test subject and all other subjects form the training set on which parameters are optimised. An optimised set of parameters is determined and a threshold for the biomarker (th_1) that yields the highest level of sensitivity at 100% specificity (top panel) and another optimised set of parameters and threshold (th_2) that yields the highest level of specificity at 100% sensitivity (bottom panel). These thresholds and parameters are applied to the single test subject, where the classification outcome can be unequivocally epilepsy or unequivocally normal if there is consensus when using both thresholds, or uncertain if there is no consensus.

teed to minimise the error made in separating these according to a predefined criterium. For the same reason, non-linear methods have been incorporated in the framework of SVM, in particular by using a "kernel trick" that could transform linearly separable data into a linearly separable data set in a higher dimension. The leave-one-out method was implemented for SVM by using the inbuilt "fitcsvm" function from the Statistics Toolbox in Matlab (Mathworks, Natick, Massachusetts, USA). Note that for an SVM-method, we include the mean degree variance and clustering coefficient, which were shown to be statistically different between people with IGE and healthy controls as well as asymptomatic relatives and the controls, since they might provide discriminatory power when they are combined with other biomarkers (necessary but not sufficient).

4.3 Results

Biomarker 1 (alpha peak frequency of the EEG power spectrum) resulted in 0% sensitivity (given 100% specificity) and 44.7% specificity (given 100% sensitivity). It classified no people with IGE as having epilepsy, 29/30 were classified as uncertain, and 1 subject was misclassified. Of the 38 healthy controls, 17/38 were correctly classified, 20/38 received an uncertain classification and 1 subject was misclassified.

Biomarker 2 (mean degree) resulted in 3.3% sensitivity (given 100% specificity) and 15.8% specificity (given 100% sensitivity). It classified one person with IGE as having epilepsy, 28/30 were classified as uncertain, and one was misclassified. Of the 38 healthy controls, 6/38 were correctly classified, 31/38 received an uncertain classification and 1 subject was misclassified.

Biomarker 3 (effect of local synchronisation) resulted in 56.7% sensitivity (given 100% specificity in the training set) and 65.8% specificity (given 100% sensitivity in the training set). Specifically, 17/30 people with IGE were classified as unequivocally having epilepsy, 10/30 received an uncertain classification, and 3/30 were misclassified. Of the 38 healthy controls, 25/38 were correctly classified and 13/38 received an uncertain classification.

Biomarker 4 (global synchronisation-parameter) resulted in 0% sensitivity (given 100% specificity in the training set) and 34.2% specificity (given

100% sensitivity in the training set). Specifically, 0/30 people with IGE were classified as unequivocally having epilepsy, 29/30 received an uncertain classification, and 1/30 was misclassified. Of the 38 healthy controls, 13/38 were correctly classified, 24/38 received an uncertain classification, and 1 subject was misclassified.

In conclusion, successive optimisation of the channel location and value of the local coupling constant give the highest levels of sensitivity and specificity. In contrast, the alpha peak frequency of the EEG power spectrum, the mean degree of the inferred functional networks, and the global coupling-strength needed to synchronise the modular Kuramoto-network have much lower diagnostic power. Performance of the Kuramoto-biomarkers in the theta-band was: 3.33% sensitivity given 100% specificity and 2.63% specificity given 100% sensitivity for the the global Kuramoto-biomarker, and 80% sensitivity given 100% specificity and 0% specificity given 100% sensitivity for the the local Kuramoto-biomarker.

A Friedman test confirms that the classification results of the local Kuramoto-biomarker are statistically significant for people with IGE (chi-squared = 37.58, $p < 0.001$) and controls (chi-squared = 47.65, $p < 0.001$) in comparison to the other potential biomarkers. Using pairwise comparison, we show that the local Kuramoto-biomarker performs consistently better than either peak in alpha power (IGE: chi-squared = 14.22, $p < 0.001$; controls: chi-squared = 25.14, $p < 0.001$), mean degree (IGE: chi-squared = 13.24, $p < 0.001$; controls: chi-squared = 19.17, $p < 0.001$), or the global Kuramoto-biomarker (IGE: chi-squared = 14.22, $p < 0.001$; controls: chi-squared = 14.00, $p < 0.001$).

The SVM method leads to 53.3% sensitivity and 86.8% specificity using leave-one-out cross-validation with a linear kernel, and 60% sensitivity and 76.3% specificity with a radial basis function. Note that the SVM method aims to find a 5-dimensional separating hyperplane since we consider 6 features: the peak in alpha frequency, and the mean degree, mean degree variance, clustering coefficient and the global and local Kuramoto biomarkers in the low-alpha band.

4.4 Discussion

Using only a 20s segment of eyes closed resting-state EEG for each subject, the local Kuramoto-biomarker achieved nearly 60% sensitivity given 100% specificity in the training set and 60% specificity given 100% sensitivity in the training set. Performance of the biomarkers was assessed in this manner since an ideal screening test to use in a non-specialist setting needs 100% sensitivity to catch every case, but some false-positives are tolerable; whereas a decision support tool in a specialist setting needs 100% specificity to avoid misdiagnosis, but less than perfect sensitivity can be compensated by further evaluation from a specialised neurologist. Furthermore, as the subjects currently classified as uncertain might be correctly classified at a later stage (for example by a new EEG), the reported levels of sensitivity and specificity are conservative estimates of the biomarker as a decision support tool. As only 3 subjects with IGE were misclassified, the misdiagnosis rate is 4.4%.

Support vector machines present an alternative classification method that could combine the predictive power of individual biomarkers into a higher-dimensional classifier. We could consider adding the Kuramoto-biomarkers from the theta-band but adding more features can worsen the performance of SVM methods by increasing the variance and overfitting [24]. When larger numbers of recordings would become available, it is likely that an approach that uses machine learning will outperform naive classifiers. However, given the importance of diagnostic tests, it is crucial to provide clinicians with reliable data about the diagnostic accuracy of the tests they use, and to consider how the results of the diagnostic test and the corresponding accuracy could be applied to their practice. It is therefore desirable that future studies on the diagnostic potential of the methods described in this chapter will be discussed with several clinicians, in order to determine the most optimal study design and method of analysis. For example, one could consider introducing a trade-off factor describing the relatives importance of false negatives to false positives.

In comparison to the local Kuramoto-biomarker, the peak in alpha frequency, mean degree of functional networks, and the global Kuramoto-biomarker show no potential as an independent candidate biomarker for IGE. This might be explained by the fact that both the peak in alpha frequency as well as the

mean degree were shown to discriminate between healthy controls and a cohort of people with epilepsy treated with AEDs. It is possible that part of the discriminatory power of these measures resulted from the alterations driven by anti-epileptic drug-treatment. As the goal of this chapter was to examine the potential of these features as biomarkers of epilepsy it was essential to test the biomarkers on drug-naive subjects with epilepsy for which a diagnosis still yet had to be made. Furthermore, the fact that means of cohorts are significantly different does not exclude potential overlap in the epilepsy cohort and the control cohort, so it is crucial to test a candidate biomarker on a subject-specific basis.

It is important to point out that age may play a crucial role in extending the result from the present study to larger cohorts of people with epilepsy, especially for younger infants. The developing brain is different from the adult brain, which is true for resting-state activity as well [154], meaning that epileptogenic mechanisms in the brains of young children might need a different set of biomarkers. This may also be the case for focal epilepsies, as the biomarkers evaluated in this study were only tested on the resting-state activity from people with generalised epilepsy. Examining the potential of the local Kuramoto-biomarker on other types of epilepsy would be interesting from both a clinical as well as a research perspective, because it will elucidate whether the subtle mechanisms that are being used to discriminate between people with generalised epilepsy and healthy controls also translate to cases of focal epilepsy.

The use of routinely acquired EEG data, combined with minimal computational cost for evaluating the biomarker, makes this an attractive proposition from the perspective of clinical decision support. At present, the most time-consuming part is visual identification of resting-state EEG, which in our study was performed by a trained EEG technician. Automating this process, would permit delivery of a result in real-time (potentially whilst EEG was still being collected). A critical advantage of this method is that there is no requirement to observe epileptiform discharges in EEG to make a diagnosis, since the networks are inferred using only brief segments of resting-state EEG. This yields the potential for a screening service to be offered in a non-specialist primary

care environment, a resource-poor setting, or even using non-specialist EEG carried out in the patient's home.

Chapter 5

Characterising distributions of epileptiform discharges from people with IGE [1]

5.1 Introduction

Epileptiform discharges (EDs) comprises a set of abnormal patterns of activity observed in EEG or MEG recordings that functions as the primary pathological marker indicating a subject has a predisposition to undergo or develop epileptic seizures [152]. In line with the terminology used in seizure-classification, epileptiform discharges appear focal or generalised, and the main morphologies include spikes, polyspikes, sharp waves, and spike and slow wave complexes [108]. Epileptiform discharges can occur during the quiescent interictal period between seizures (interictal epileptiform discharges or IEDs), as well as during clinical seizures. However, the distinction between interictal and ictal discharges is not entirely trivial and clear-cut, as a generalised discharge lasting at least 4 seconds is often classified as an absence seizure, but the subject need not demonstrate any clinical seizure manifestations during this epileptiform discharge. In this chapter we study the temporal aspects of epileptiform discharges on scalp EEG, such as their frequency, timing, and duration, and hence there is no emphasis on whether they are accompanied by clinical symptoms.

[1] The work presented in this chapter is currently in preparation: Woldman W, Seneviratne U, Cook MJ, D'Souza W, Terry JR. Characterising dynamic distributions of epileptiform discharges from a cohort of people with genetic generalised epilepsy. All data was collected and classified by US, MJC, and WDS. Methods were conceived by WW and JRT, all analysis carried out by WW.

The presence of epileptiform discharges is not exclusive to people with epilepsy, and consequently is not considered as sufficient evidence to conclude a subject has epilepsy, since approximately $1-5\%$ of the general population shows EDs on routine EEG recordings, and not all of these subjects have epilepsy or will go on to develop a seizure disorder [115, 157]. However, as epileptiform discharges are significantly more likely to occur in people with epilepsy, their presence greatly increases the likelihood of that subject having epilepsy. Consequently, the observation of epileptiform discharges together with a clinical history and other diagnostic results (e.g. blood tests or MRI), is often used in a clinical setting to establish or confirm a diagnosis of epilepsy [171]. Several methods are used in clinical settings in order to increase the chances of recording epileptiform activity, such as hyperventilation and photic stimulation [108]. Recording brain activity during sleep has revealed how different sleep-stages (such as non-REM and REM sleep) affect the frequency and morphology of epileptiform discharges recorded on scalp EEG [9, 59].

At the cellular level, ictal and interictal epileptiform discharges have been hypothesised to be caused by a paroxysmal depolarising shift (PDS) [78]. The rising phase of the discharge is hypothesised to arise from large-scale depolarisation leading to hypersynchronous neuronal firing [95, 114], followed by a slow wave of hyperpolarisation causing the amplitude to decrease. Abnormal hypersynchronous activity is characteristic of epilepsy in general, as seizures are typically characterised as the result of abnormally synchronised brain networks, caused by a disrupted balance between excitation and inhibition, for example, due to excess of excitation or the lack of inhibitory control [226]. The concept of excitability applies both at the level of individual neurons (their ability to fire action potentials, see [98]), as well as the network-level. At the macroscale of the brain, excitability is usually characterised as the overall ratio of excitation to inhibition [175].

Neural "hyperexcitability" refers to neurons becoming pathologically excitable, due to for example an increase in excitatory synaptic neurotransmission, a decrease in inhibitory neurotransmission, or several subthreshold excitatory processes synchronising, leading to increased potentials in postsynaptic neurons [251]. Once a network of neurons becomes hyperexcitable,

it commonly abnormally synchronises as many neurons discharge simultaneously. This hypersynchronisation of neurons is an emergent property of the network that is essential to the generation of a seizure or an epileptiform discharge. There are several physiological factors that influence cortical excitability in brain networks from people with epilepsy dynamically over time, such as changes in state of arousal (i.e. wakefulness, sleep) and changes in hormone levels [9], and these effects are often measured using transcranial magnetic resonance (TMS) [11].

Given that cortical excitability varies dynamically over time, and the occurrence of epileptiform discharges likely results from a disrupted balance between inhibition and excitation, the question arises how these dynamical changes affect the distribution of discharges for people with epilepsy. For example, is a subject more likely to undergo an epileptiform discharge during specific moments of the day or is there a roughly constant likelihood, and does the duration of the discharges correlate with the timing? In order to address these questions, the distribution of epileptiform discharges over the course of a day (24 hours) from 107 people with idiopathic generalised epilepsy (IGE) in scalp EEG recordings were studied, both individually as well as on the level of the entire cohort. A few studies have investigated the influence of circadian patterns on epileptiform discharges, but these studies suffered from relatively small sample size and heterogeneity in the type of epilepsies [116, 165]. Given the importance of cortical excitability, a phenomenological model was extended in order to include time-dependent excitability where changes in the excitability of cortical areas can lead to periods of increased discharges and seizures likelihood. This phenomenological representation of the cortex provides the basis of a dynamical network model, and reproduces subject-specific discharge distributions, and so we will show that it has the potential to provide a way to stratify subjects with IGE with respect to their individual susceptibility to undergo epileptiform discharges.

5.2 Methods

5.2.1 Subjects

The data have appeared in previous studies [192, 194, 195], and consisted of 24-hour ambulatory EEGs done in a cohort of 107 subjects diagnosed with genetic generalised epilepsy, from epilepsy clinics at two tertiary hospitals in Melbourne, Australia. The diagnosis of IGE was established using International League Against Epilepsy criteria [21, 41], based on EEG showing generalised epileptiform discharges on at least one recording session and consistent clinical features. Subjects were classified into childhood absence epilepsy (CAE), juvenile absence epilepsy (JAE), juvenile myoclonic epilepsy (JME), and generalised epilepsy with generalised tonic-clonic seizures only (GTCSO) according to ILAE criteria [21, 41]. Subjects who did not meet any of the criteria for those syndromes were classified as genetic generalised epilepsy unspecified (GGEU).

5.2.2 EEG data

EEG recordings were acquired with 32-channel ambulatory EEG system (Compumedics Ltd., Melbourne, Australia) and electrodes placed according to the international 10-20 system. Subjects were advised to have at least 8 hours of night-time sleep prior to the EEG recordings in order to increase the likelihood of capturing circadian variations in epileptiform discharges. Recordings started in the morning (between 9.00-10.00), with routine activation methods for 20 minutes. Intermittent photic stimulation was carried out followed by hyperventilation for 3 minutes, after which the subject resumed routine activities, wearing the ambulatory EEG device. EEG recordings were reviewed by an experienced EEG reader (US), and detailed analysis of the waveforms of epileptiform discharges was carried out using common average referential montage. Each epileptiform discharge was assessed including discharge type (focal, generalised fragment, generalised paroxysm), amplitude (mV), duration (s), frequency, time of occurrence, state of arousal, individual components (spike-wave, polyspike-wave, polyspike) and morphology of discharges. The EEG and clinical data were entered in an electronic database, where the data from the initial routine 20-min recording was entered separately. Each discharge was

classified as a fragment (duration < 2 s, interictal), paroxysm (duration ≥ 2, ictal) or focal. A total of 6923 epileptiform discharges were recorded on the ambulatory EEGs, consisting of 1291 generalised paroxysms, 5535 generalised fragments, and 97 focal discharges. The duration of discharges was measured from the beginning of the first spike to the end of the last wave. The sleep onset and sleep offset (waking) times for every subject was taken note of. The ambulatory EEG recordings and clinical data were entered into a custom-made electronic database.

5.2.3 Numerical model

The dynamics of networks of connected cortical regions was simulated using the phenomenological model described in detail in [19], and is based on the work of Kalitzin et al. [111]. This model has been discussed and analysed in the broader context of biological systems that display bistability [73]. For the purpose of modelling seizure-generation, the cortex is phenomenologically represented as a discrete set of cortical regions. The dynamics of a single brain region can be represented mathematically by the following stochastic differential equation (SDE):

$$\frac{dz}{dt} = (\lambda - 1 + \mathrm{i}\omega)z + 2z\,|z|^2 - z\,|z|^4 + \alpha d\mathrm{w}(t) \tag{5.1}$$

This equation describes a subcritical Hopf bifurcation with bifurcation parameter λ. The oscillation frequency is determined by ω and the level of noise is determined by α for the complex Wiener process $\mathrm{w}(t)$. The bistable system exhibits a fixed point and a limit cycle which are both locally attracting, separated by an unstable limit cycle. In the case of weak noise, the system will spend most of its time in the neighbourhood of one of the stable attractors and occasionally receive noise that is strong enough so that it can cross into the basin of attraction of the other attractor. In the next section we will add a differential equation for λ (equation 5.5) in order to ensure that when noise induces a node to transition from the stable fixed point (healthy state) to the stable limit cycle (epileptiform state), the node will undergo a bifurcation as λ will decrease past the limit point ($\lambda = 0$) into a regime where the stable fixed point is the only (stable) attractor. Having returned to the stable fixed point,

λ will return with a characteristic time-scale τ to its baseline value λ_{base}, where a future epileptiform discharge may be induced. The dynamical behaviour of the system is summarised in a bifurcation diagram in figure 5.1, and and example of a simulated trajectory in phase space (polar coordinates) is given in figure 5.2.

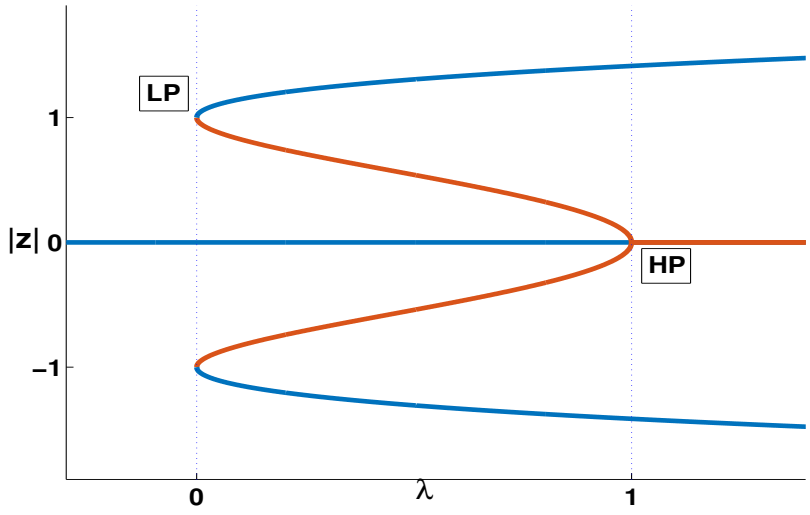

Figure 5.1: Bifurcation diagram of the deterministic part of equation 5.1 in λ. The vertical dotted lines at $\lambda = 0$ and $\lambda = 1$ mark the parameter values where a bifurcation occurs ($\lambda = 0$ is a limit point as the limit cycles (dis)appear, whereas $\lambda = 1$ is a hopf bifurcation point). The straight horizontal line represents the fixed point which exists at the origin ($|z| = 0$), which exists for all values for λ, and is a stable (dark blue) attractor when $\lambda < 1$, and unstable (red) otherwise. The two pairs of curved lines correspond to the two limit cycles in the system. The unstable limit cycle is located at $|z|^2 = 1 - \sqrt{\lambda}$ whereas the stable limit cycle corresponds to $|z|^2 = 1 + \sqrt{\lambda}$ (these correspond to steady-state solutions of the radial equation). The two limit cycles are joined by the limit point. For $\lambda \in [0, 1]$ the system is bistable as there are two coexisting stable attractors. The unstable limit cycle functions as a separatrix between the two regions of attraction. Under the influence of strong enough noise, the system can cross the unstable limit cycle, and transition from the stable fixed point to the stable limit cycle or vice versa.

Though originally a model for seizure-generation (ictogenesis), the model can be considered as the basis of a phenomenological model for the onset of epileptiform activity in general, where limit cycle activity of duration < 2 seconds corresponds to fragments and longer discharges to paroxysms. Whether

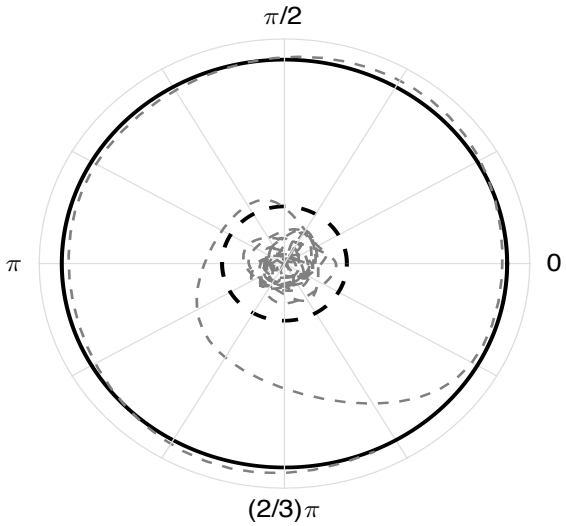

Figure 5.2: Simulated trajectory in phase space. Snapshots from an exemplar time-series (dotted grey line) of the bistable system (equation 5.1) in polar coordinates with initial condition $z = 0$ and $\lambda = 0.725$. The trajectory starts near the fixed point and eventually transitions passes the unstable limit cycle (dotted black line) that functions as a separatrix between the stable fixed point and the attracting outer limit cycle (solid black line).Simulations were carried out using an EM-scheme with dt $= 10^{-5}$, $\alpha = 0.1$; total simulation time 80 seconds, where the trajectory was plotted intermittently.

the paroxysms are accompanied with clinical seizure symptoms is outside the scope of the model, since the model provides a phenomenological description of the electrographic properties of epileptiform discharges on scalp EEG recordings only.

An alternative to additive noise would be to use activity-dependent noise. For example, the system could receive additive noise when situated in the stable fixed point but multiplicative noise when situated in the stable limit cycle [73]. However, even in this setting the emergency of epileptiform activity is driven by additive noise, which can be quantified by computing the "mean escape time" for a cortical region. This is the average time it takes for a specific region with initial condition $z(0) = 0$ to cross the unstable limit cycle that separates the two stable attractors, located at $|z|^2 = 1 - \sqrt{\lambda}$. Under conditions of small,

additive noise, Benjamin et al. [19] derived an analytical expressions for the expected escape time by using the Eyring-Kramer approach:

$$E[\tau] = \frac{\sqrt{\pi}\alpha e^{2\psi(\hat{\lambda})/\alpha^2}}{2\sqrt{2}\lambda^{1/4}(1-\sqrt{\lambda})(1-\lambda)} \tag{5.2}$$

$$\psi(\hat{\lambda}) = 1/6 - 1/2\lambda + 1/3\lambda^{3/2} \tag{5.3}$$

In figure 5.3 we compare mean escape times from numerical simulations against analytical escape times derived in [19], and also use these numerical simulations to estimate the rate of epileptiform discharges (see figure 5.4):

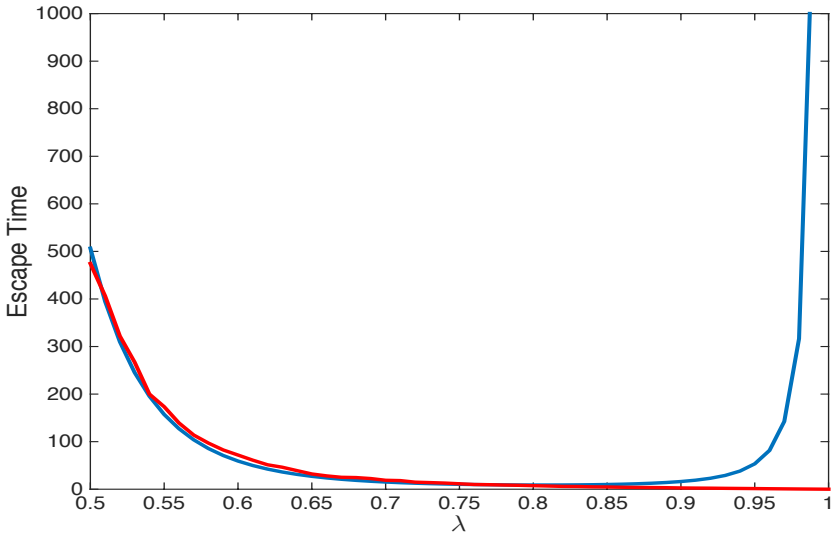

Figure 5.3: Numerical and analytical escape time against λ. Numerical escape time (in red, see equation 5.1) and analytical escape time (in blue, see equation 5.2) against λ. When λ increases from 0.5 to 1, the mean escape time decreases since the separatrix situated at $|z|^2 = 1 - \sqrt{\lambda}$ moves closer to the stable origin. λ was increased from 0.5 to 1 with step-size 0.05, and numerical mean escape times were computed by averaging the first escape times of 1000 escapes, for every value of λ. In the case of small noise, an analytical formula for the escape time was proposed and derived in [19], where the authors point out that this analytical formula is invalid in the proximity of $\lambda = 1$, as the escape time must approach 0 when the separatrix shrinks towards the fixed point.Simulations were carried out using an EM-scheme with dt $= 10^{-5}$, $\alpha = 0.1$, and the system was initially in the fixed point $z = 0$ at $t = 0$.

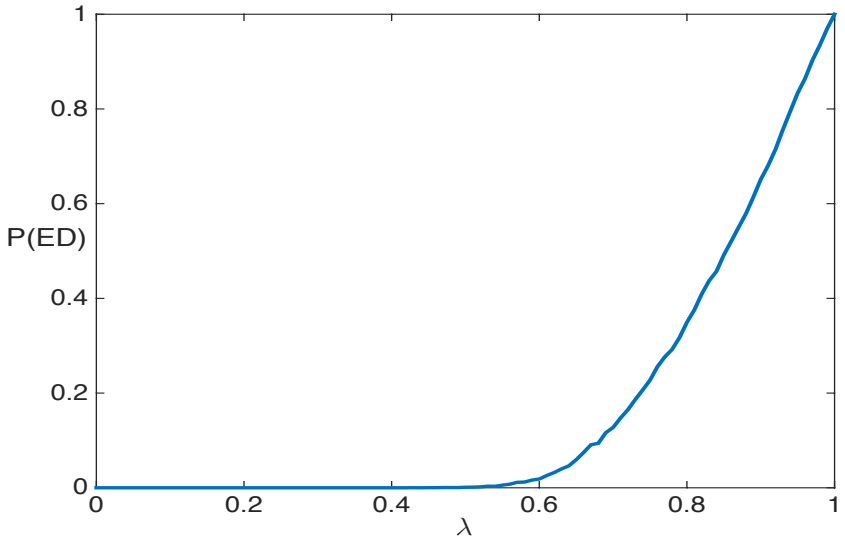

Figure 5.4: Discharge-likelihood against λ. When λ increases from 0 to 1, the discharge-likelihood in the system (equation 5.1) increases since the mean escape time decreases. λ was increased from 0 to 1 with step-size 0.01. The average time spent in the epileptiform discharge-state (time spent in the stable limit cycle, located at $|z|^2 = 1 + \sqrt{\lambda}$) was computed over the course of a 24-hour simulation for every value of λ. At $\lambda = 0$ the likelihood of being in the epileptiform state is 0 as this corresponds to the limit point, whereas if $\lambda = 1$ the origin loses stability so the system spends all its time in the attracting limit cycle. Simulations were carried out using an EM-scheme with dt $= 10^{-5}$, $\alpha = 0.1$, and total simulation time of 24 hours; the system was initially in the fixed point $z = 0$ at $t = 0$.

5.2.3.1 Network model

The model for a single region can be extended to the case of a coupled network consisting of a discrete set of N nodes (see [19]):

$$\frac{dz_j}{dt} = (\lambda_j - 1 + \mathrm{i}\omega)z_j + 2z_j\,|z_j|^2 - z_j\,|z_j|^4 + \alpha d\mathrm{w}_j(t) + \beta \sum_{k \neq j}^{N} M_{jk}(z_k - z_j) \tag{5.4}$$

where M is the adjacency matrix describing the topology of the network (that is whether a connection between node i and j exists or not), and β is the coupling strength. Each node (brain region) receives their own independent Brownian motion realisation $w_j(t)$. Connections between regions are said to

be irregular, directional, and synchronising: a connection between two cortical regions establishes a synchronising effect between regions (i.e. if a node is in a quiescent state, it will influence the connected node to become or stay quiescent whereas if the node is in the epileptiform state, it will try and influence the connected node to become or remain epileptiform). Depending on the topology of the network and the model-parameters, transitions in single nodes can lead to focal, secondary generalised, or primary generalised events at the network-level, revealing a crucial relationship between intrinsic dynamics of a single brain region and the overall connectivity structure of the network [218]. See Appendix B for a comparison of this bistable model to the previously discussed Kuramoto-model.

5.2.4 Dynamic excitability

The stable limit cycle is a stronger attractor than the stable fixed point for most values of λ, as the multiplier for the fixed point is $\lambda - 1$, whereas the eigenvalue for the stable limit cycle equals $-4(\lambda + \sqrt{\lambda})$. This means that the expected time to transition from the stable limit cycle to the fixed point may be much larger in numerical simulations of this model than those actually observed in recordings from people with epilepsy. As an epileptiform discharge commonly last in the order of seconds, λ is made time-dependent in order to obtain more realistic discharge durations:

$$\tau \frac{d\lambda_j}{dt} = \lambda_{\text{base}} - \lambda_j(t) - |z_j|^2 \tag{5.5}$$

However, note that since λ_j is now dynamic, the locations of the limit cycles now is time-dependent as well. When the system is at rest, the system converges to the value λ_{base}, where noise can drive a transition from the stable fixed point to the stable limit cycle. When this happens, λ_j will decrease past the limit-point and become negative, and thus the system will return to the stable fixed point which is the only attractor in that regime. Then λ_j will increase to the value λ_{base} governed by time-constant τ, and another discharge may occur.

This means that the intrinsic excitability of a brain region is effectively determined by the value of λ of that node. In the original studies of this

model ([111] and [19]), λ would settle to the constant λ_{base} if the system was near the stable fixed point. If noise would then tip the system towards the attracting limit cycle, the node is hypersynchronised, and λ_{base} corresponds to a hyperexcitable state. Consequently, the model in general describes the onset of a seizure assuming the cortical network is hyperexcitable but not yet hypersynchronous. In order to develop a more general model where epileptiform activity may emerge from interictal periods of background activity driven by non-hyperexcitable networks, we extend the λ-equation with an external "drive" λ_{ext}. This drive enables us to incorporate dynamic changes that may lead the system to transition into a hyperexcitable state (higher values of λ) and thus potentially hypersynchronisation (transition to limit cycle). Mathematically, this can be modelled by:

$$\tau \frac{d\lambda_j}{dt} = \lambda_{\text{base}} + \lambda_{\text{ext}}(t) - \lambda_j(t) - |z_j|^2 \tag{5.6}$$

This external drive modulates the excitability of the system; when $\lambda_{\text{ext}}(t) > 0$ it increases the excitability of the node thus making a transition to epileptiform activity more likely, whereas $\lambda_{\text{ext}}(t) < 0$ makes a transition less likely because the overall excitability is decreased (i.e. the system moves away from the hyperexcitable regime). The bifurcation diagram in figure 5.1 provides a picture of what happens to the dynamics of an individual node when the excitability is modulated: in the bistable regime ($\lambda \in [0, 1]$) the unstable limit cycles moves in closer proximity to the stable fixed point when λ increases from 0 to 1, making a transition more likely. At the network level this modulation affects the overall 'global' excitability of the network and consequently the emergent network-behaviour, since an increased likelihood of a single region becoming epileptiform will on average increase the likelihood of the entire network transitioning to the epileptiform state. A simple example of this 'driven' excitability is given in figure 5.5, where the response to a brief square pulse was plotted for different values of λ_{base}.

Figure 5.6 shows how the effect of changing the excitability of a node in a larger network depends on the interplay between the internal dynamics of the single nodes and their role in the global network. When the excitability of

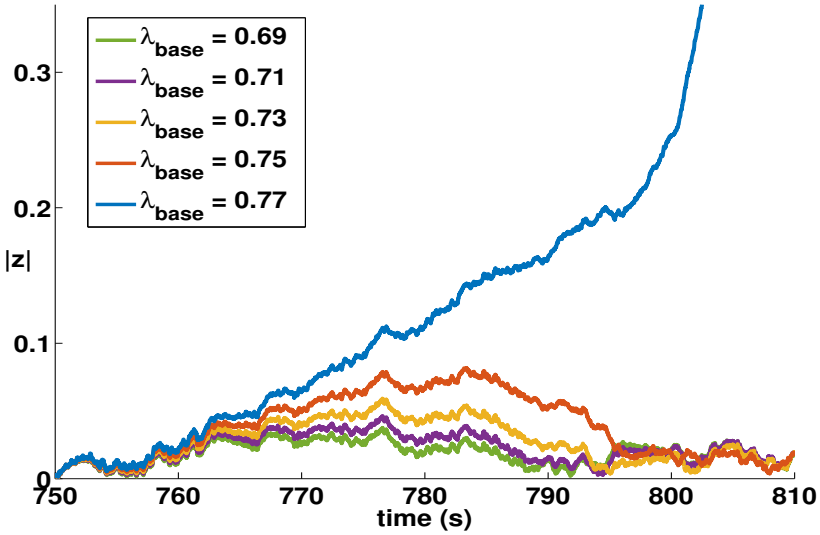

Figure 5.5: Excitability modulated by a square pulse. For a single node, the response to a brief square pulse lasting 5 seconds ($\lambda_{\text{ext}} = 15$ for $t \in [750, 755]$ and 0 otherwise) is plotted for increasing values of λ_{base} (see equation 5.1 and 5.5). The pulse effectively increases the overall excitability of the node for a brief period of time, but it depends on the inherent baseline level of excitability λ_{base} of the node whether the pulse is able to induce a transition from the stable fixed point to the stable limit cycle. Note that every run was carried out with the same noise realisation, in order to illustrate the effect of the excitability-adjustment unambiguously. If a different realisation of noise for each value of λ_{base} would be used, the results show a similar qualitative picture. Simulations were carried out using an EM-scheme with dt $= 10^{-5}$, $\tau = 10$, $\omega = 20$, $\alpha = 0.05$.

a single node is driven by a brief square pulse, whilst all the other nodes are unaffected, the global response depends on the particular affected node; only node C was able to recruit the entire network into the epileptiform state when it was driven by λ_{ext}, whereas in the other cases minor "focal" epileptiform discharges occurred localised in the affected node. This demonstrates that network structure can play a crucial role in determining whether a discharge appears generalised or focal in response to subtle alterations to the dynamics of individual nodes.

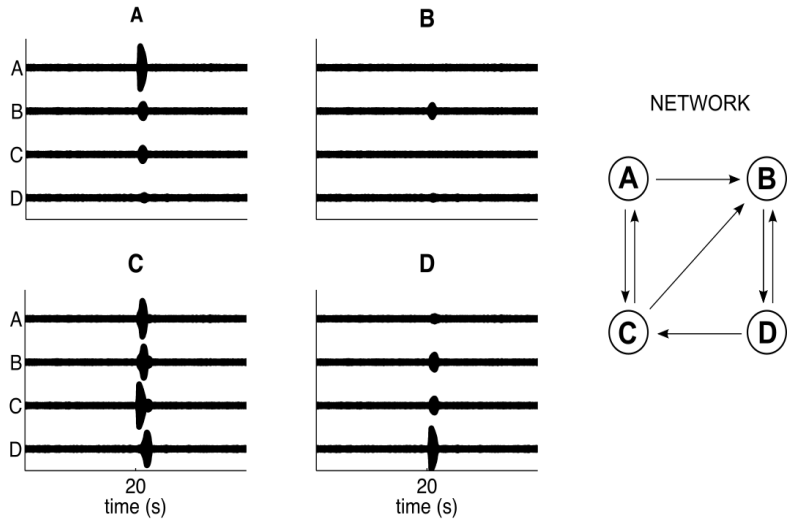

Figure 5.6: Variable effect on network behaviour of local change in excitability. The starting point was a system of four healthy regions whose network structure did not support transitions from non-epileptiform (noisy steady state) to epileptiform (large-amplitude oscillations) patterns of activity during the period of simulation (equation 5.2 and 5.5). When the excitability of a single node is driven by the brief square pulse as described in figure 5.2 (delivered at $t = 20$s), whilst the dynamics of the other nodes were held constant, the emergent behaviour depends on the specific node that is undergoing the effect of the dynamic changes in its excitability. When node A and D are driven, the brief pulse was able to induce localised focal discharges, whereas the network behaviour remained roughly unaltered under stimulation of node B. In the case of node C, the entire network was recruited into the epileptiform state. These results indicate that whilst the network structure was unaltered, different nodes propagate different types of activity across the network, revealing a subtle network-dependent effect of changes in excitability on brain networks. Simulations were carried out using an EM-scheme with dt $= 10^{-5}$; each node receives its own independent noise-realisation and was initially in $z = 0$ at $t = 0$; $\tau = 10$, $\omega = 20$, $\alpha = 0.05$, $\beta = 0.15$.

5.2.4.1 Simulations

Numerical simulations were carried out with an Euler-Maruyama scheme to find approximate solutions to the system of SDEs. The Euler-Maruyama scheme has strong convergence (referring to the expectation of the absolute difference of the analytical and numerical solution) in the order of 1/2 and weak convergence (referring to the absolute difference between the expected analytical solution and the expected numerical solution) of the order 1, as-

suming that the drift and diffusion of the SDE are Lipschitz continuous. This condition is met, since the stable limit cycle is a bounded global attractor (that is, trajectories will not extend far from the outer limit cycle located at $|z|^2 = 1 + \sqrt{\lambda}$). An appropriate time-step was determined by comparing escape times estimated from numerical simulations to analytical Kramer's rates for the case of a single node and small noise ($\alpha = 0.1$) [19] (see figure 5.3). Simulations were run for 24 hours in order to allow comparison with the 24-hour ambulatory EEG recordings, with a typical time-step of 0.00001 (for both the Euler-Maruyama scheme as well as the Brownian motion realisation). A discretised Brownian motion path was computed with independent Wiener increments: $\sqrt{dt}N(0,1)$.

5.3 Results

Figure 5.7 illustrates the total number of discharges amongst all 107 subjects with IGE plotted against circadian time ('frequency-histogram'), as well as the sum of the duration of these discharges per hour ('duration-histogram'). The maximum density of epileptiform discharges occurred in the period 23:00-07:00, with two maximum peaks at 00:00 and 6:00. In contrast, the maximum density in the duration-histogram occurs in the period 06:00-09:00, with two additional peaks at 01:00 and 14:00.

Comparison between the peaks of the frequency-histogram and the duration-histogram, implies relatively many long paroxysms took place during 07:00-09:00 and 14:00, as at these times the overall frequency-rate was moderately high whilst the sum of the durations is maximal.[1]

As there is an increased likelihood of epileptiform discharges during particular periods (i.e. early night and early morning), these histograms suggest a circadian dependency of epileptiform discharges. Histograms were then

[1]It would be natural at this point to use a statistical model to verify the presence of a circadian pattern in the discharge distributions. However, our clinical collaborators at the University of Melbourne had already submitted a paper on the circadian profile present in the distributions at the time that the collaboration started. In their work, they use a mixed effect Poisson regression analysis and verify there is a time-of-day dependency of ED-occurrence that correlates with state of arousal. Since this study is currently under revision, the decision was made to not conduct a similar analysis in this chapter. In that publication, the authors do not consider the summed duration of discharges nor present a mathematical model.

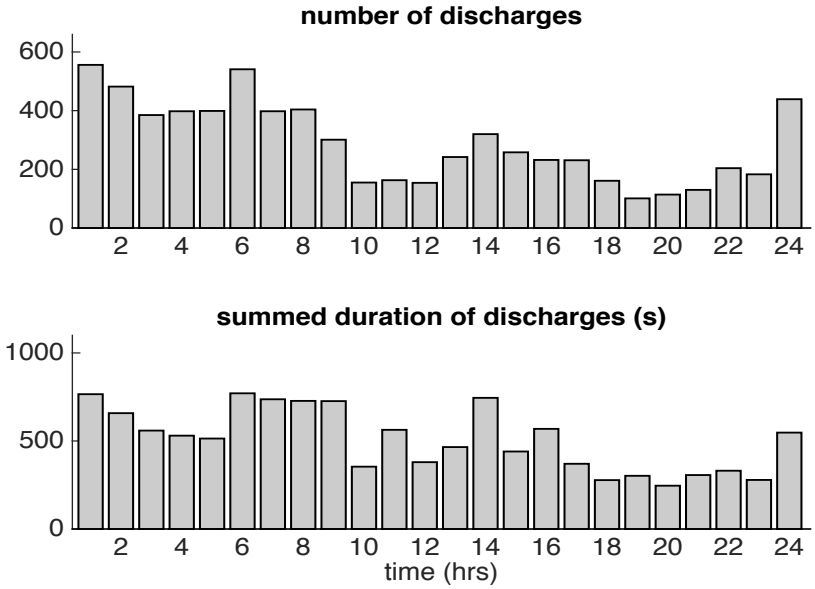

Figure 5.7: Frequency and duration histogram of epileptiform discharges. Frequency-histogram (top) illustrates the total number of epileptiform discharges from all 107 subjects with IGE against circadian time (with hour 1: 00:00-00:59 and hour 24: 23:00-23:59). Note the maximum density of epileptiform discharges occurred during 23:00-07:00, with maximum peaks at 00:00 and 06:00. Note a smaller peak (12:00-16:00) between two troughs (09:00-11:00 and 18:00-19:00). Duration histogram (bottom) illustrates the summed duration of the total number of discharges per hour from all 107 subjects with IGE. There are maximum peaks at 01:00 and 14:00, and the maximum density is during 06:00-09:00.

constructed normalised to the sleep onset and sleep offset (waking) for every subject, by which it is meant that $t = 0$ corresponded to either the moment of falling asleep (figure 5.8) or waking up (figure 5.9), respectively. Because of this normalisation, the effect of falling asleep and waking up on the distribution of discharges is studied independent of the variability of sleep onset (19:10-03:21, median 22:18) or sleep offset for each subject (04.03-12:40, median 07:34). However, the variability in sleep duration (4.2-12.7 hours, median 12.6 hours) affects all constructed histograms.

Together these histograms show that in general the likelihood of epileptiform discharges substantially increases around falling asleep, in keeping with experimental and clinical evidence that seizures and discharges are influenced

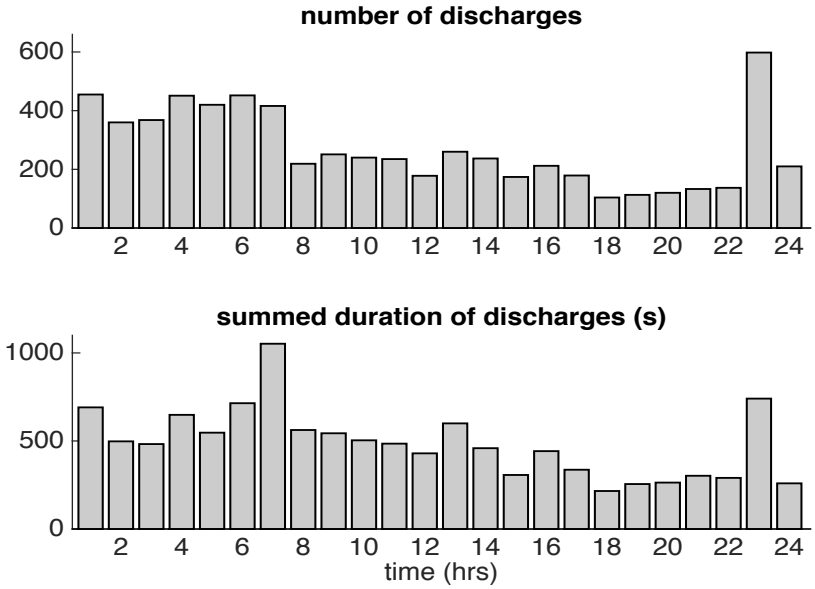

Figure 5.8: Distribution of epileptiform discharges normalised to the onset of sleep. Distribution of all discharges from all 107 subjects with IGE, with time normalised such that $t = 0$ corresponds with the onset of sleep for all subjects (i.e. all subjects fall asleep at $t = 0$). Top panel: total number of epileptiform discharges for all subjects per hour. Bottom panel: summed duration of epileptiform discharges for all subjects per hour.

by sleep-stages [9, 59]. Furthermore, the histograms reveal discharge-likelihood increases upon waking, which is not as well-studied as the effect of sleep and sleep-stage on the frequency of EDs [9]. To address the relationship between sleep on- and offset and the likelihood of epileptiform discharges, discharge distributions were examined independently for every subject. For example, roughly 40% of all subjects shows a peak in epileptiform activity around waking (figure 5.10). Furthermore, our analysis revealed that although subjects show very distinct discharge distributions correlated with sleep onset ($\approx 20\%$), sleep offset ($\approx 30\%$), or early afternoon ($\approx 10\%$), approximately 50% of the subjects have discharge distributions showing combinations of peaks or seemingly randomly distributed patterns (see figure 5.11 for characteristic examples).

A computational model was used to reproduce individual discharge distributions. The starting point for each discharge distribution was a four region network, where the baseline probability of a transition from the healthy state

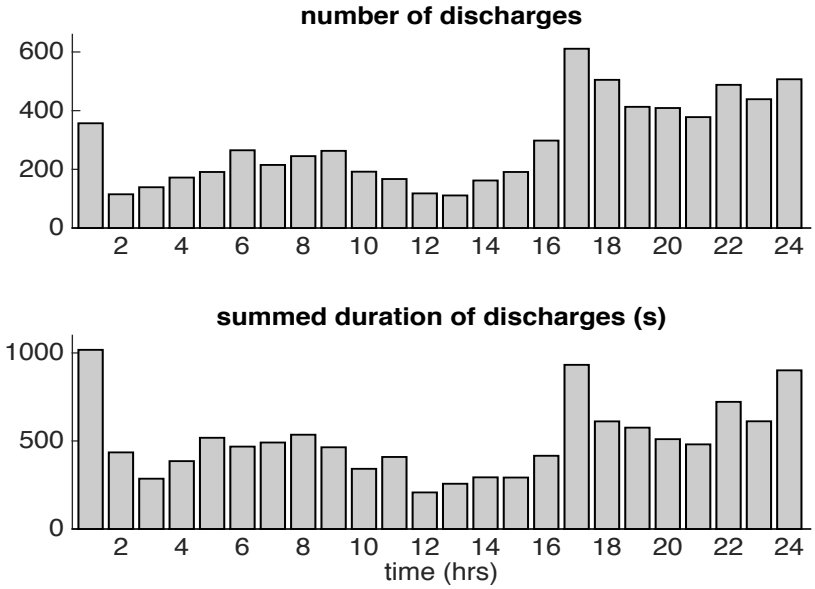

Figure 5.9: Distribution of epileptiform discharges normalised to the offset of sleep. Distribution of all discharges from all 107 subjects with IGE, with time normalised such that $t = 0$ corresponds with the offset of sleep for all subjects (i.e. all subjects wake up at $t = 0$). Top panel: total number of epileptiform discharges for all subjects per hour. Bottom panel: summed duration of epileptiform discharges for all subjects per hour.

to the epileptiform state is variable. The connectivity-strength and the individual parameters of each node were identical, although every node receives noisy input from an independent Wiener process, but with the same noise coefficient α. Of all 218 possible directed networks of four nodes, only networks without disconnected nodes were considered (no node has zero in- and out-degree). The time-dependent adjustment to the excitability $\lambda_{\text{ext}}(t)$, was modelled by combining a Wiener process with a smoothed block pulse, such that all nodes simultaneously become more excitable for a particular time-interval (or several intervals). By dynamically altering the excitability of the nodes within the networks, we found that computational discharge distributions are similar to real discharge distributions from subjects with IGE (figure 5.12). Computational histograms were based on the summed duration of discharges.

The subtle interplay between network structures and dynamical changes in excitability is considered in figure 5.13. For two particular systems of four

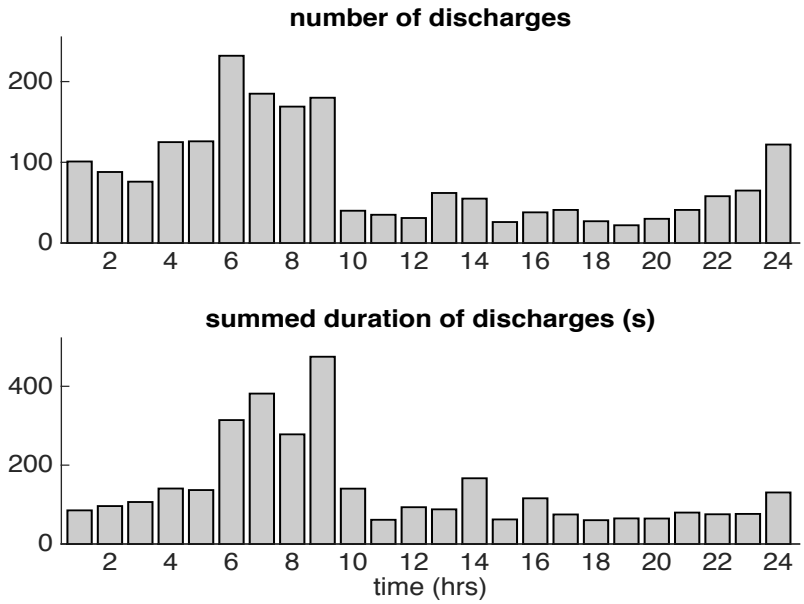

Figure 5.10: Distribution of epileptiform discharges with peak around waking. Distribution of a subset of 44 subjects with IGE (40%) showing a peak in both histograms (frequency and summed duration) around waking, with time normalised such that $t = 0$ corresponds with the offset of sleep for all subjects (i.e. all subjects wake up at $t = 0$). Top panel: total number of epileptiform discharges for all subjects per hour. Bottom panel: summed duration of epileptiform discharges for all subjects per hour. Note that several subjects of this subset also had an increased likelihood of discharges during sleep, but the peak was significantly more pronounced around waking.

brain regions with identical model-parameters, an identical excitability adjustment leads to different discharge distributions. This shows he same dynamic changes in excitability can affect network behaviour drastically different, depending on the particular network structure, suggesting there might be classes of networks that are more susceptible to the dynamical changes in excitability during the course of the day. The effect of dynamical changes of excitability on network structures can be captured by computing the Brain Network Ictogenicity (BNI), which is the likelihood that seizures emerge from the computational network model [170].

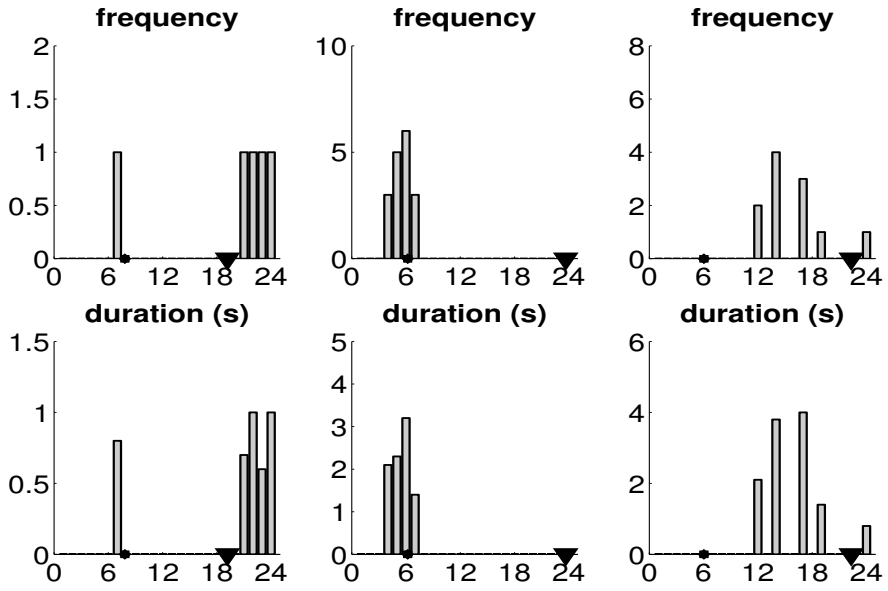

Figure 5.11: Examples of discharge distributions from subjects with IGE. Frequency and duration histogram are shown from three different subjects: discharges from subject one (left column) mainly occur during sleep, discharges from subject two (middle column) mainly occur around waking, and discharges from subject three are seemingly randomly distributed through the course of the day. Sleep onset is marked in the x-axis by black triangles, sleep offset by black circles.

5.4 Discussion

We demonstrated that there are periods of increased likelihood of epileptiform discharges during the course of the day based on a large cohort of epileptiform discharges from 107 subjects with IGE. Epileptiform discharges are more likely to occur during the early phases of sleep and around waking in the morning. Furthermore, the summed duration of epileptiform discharges increases during the early phases of sleep, waking in the morning, and in the early afternoon. Using a computational model describing the interactions between brain regions, the effect of dynamic excitability was explored with respect to the timing, frequency and duration of epileptiform discharges. Computer simulations demonstrated the effect of dynamical changes in excitability on the emergent behaviour critically depends on the network structure. Some networks remain relatively unaffected by changes in excitability that lead to an increased sus-

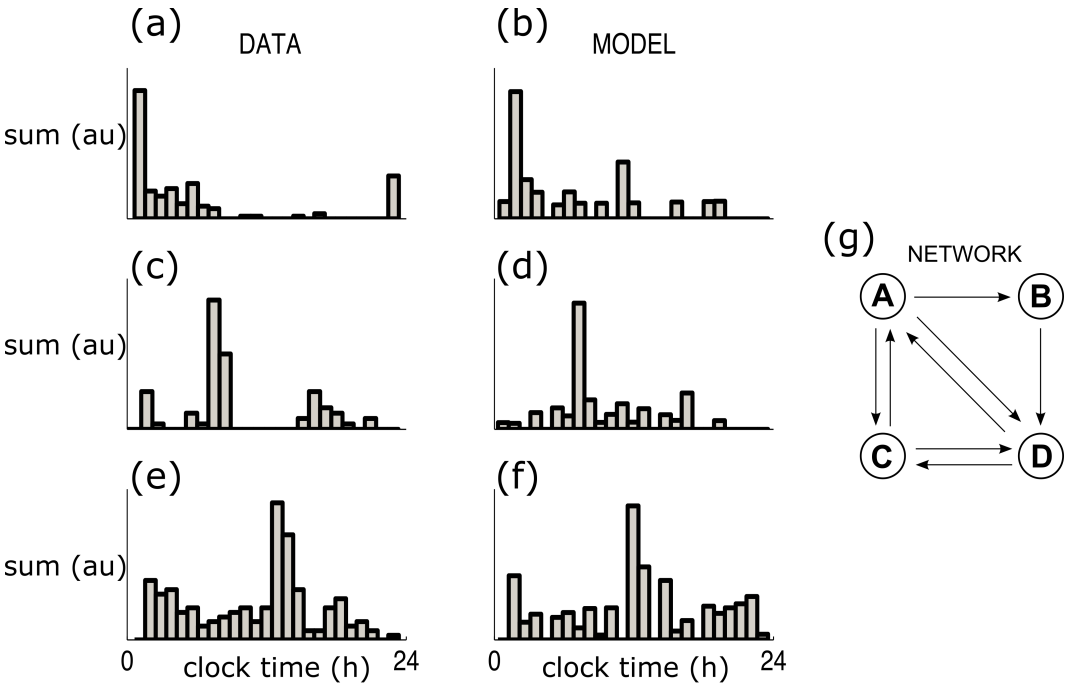

Figure 5.12: Comparison between computational discharge distributions and distributions from subjects with IGE. Histograms on the left were selected from subjects with IGE with more than 50 discharges (normalised to peak) over the course of the 24-hour ambulatory EEG-recording; computational histograms were based on a single 24-hour simulation of the computational model (equation 5.2 and 5.5) of a network consisting of four regions (panel g). Top row: patient (panel a) and computational discharge distribution (panel b) with peak at early stages of sleep. Middle row: patient (panel c) and computational discharge distribution (panel d) with peak at early morning. Bottom row: patient (panel e) and computational discharge distribution (panel f) of discharges with peak at early afternoon (14:00). Computational histograms show the duration spent in the epileptiform state (normalised to peak); note there is a linear relationship in the model between discharge frequency and durations for the computational model. As the duration-histogram is based on the time spent in the epileptiform state (in other words, it is a fraction of the total of 3600 seconds per subject) it provides an absolute measure for comparing discharge distributions, as opposed to the frequency-histogram. Simulations were carried out using an EM-scheme with $\mathrm{dt} = 10^{-4}$, $\tau = 10$, $\omega = 20$, $\alpha = 0.1$, $\beta = 0.05$, and all nodes were initially in $z = 0$ at $t = 0$, and each node receives an independent noise-realisation.

ceptibility to epileptiform discharges in other networks. These findings suggest that the interplay between network structure and the intrinsic dynamics of in-

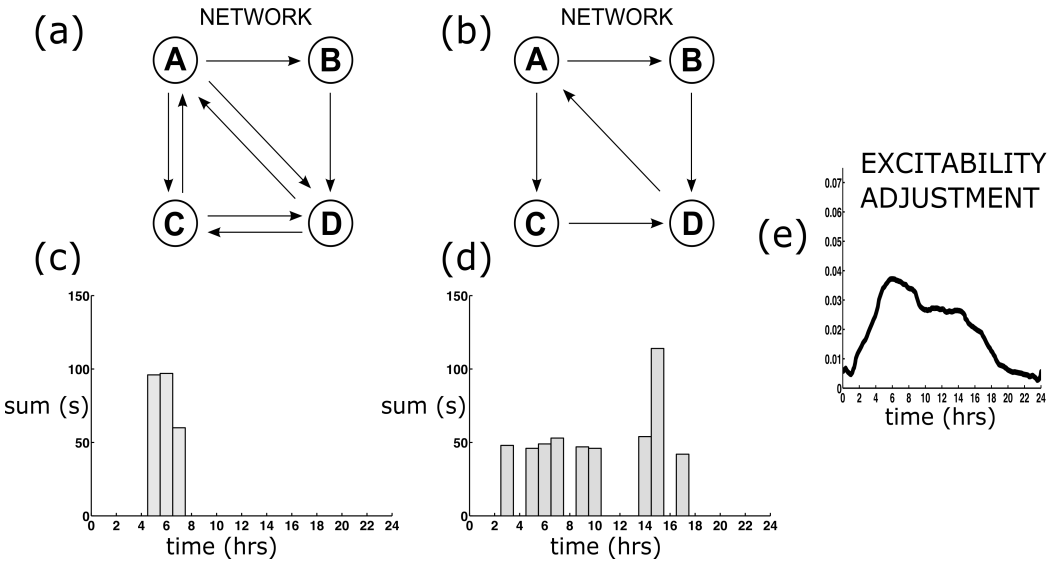

Figure 5.13: Variability in computational discharge distributions. The effect of λ_{ext} is network dependent (equation 5.2 and 5.5): two different network topologies (panel a and b) are driven by a particular adjustment in dynamic excitability λ_{ext} (panel e), and have different summed duration-histograms (panel c and d). In panel c discharges are clustered around 06:00, which is in line with the increased excitability adjustment, whereas the discharges are more dispersed throughout the day for the second network (panel d), with a peak in the early afternoon. Simulations were carried out using an EM-scheme with $\mathrm{dt} = 10^{-4}$, $\tau = 10$, $\omega = 20$, $\alpha = 0.1$, $\beta = 0.05$, and all nodes were initially in $z = 0$ at $t = 0$, and each node receives an independent noise-realisation.

teracting brain regions modulated by physiological factors crucially determine the initiation, duration and frequency of epileptiform activity.

Since EEG was recorded with scalp electrodes, it is important to address the question whether any epileptiform discharges may have been missed, that is, whether all epileptiform discharges that occurred during the 24-hour recordings were actually captured on the recordings. Indeed, for focal epilepsies it is well-known that focal discharges are often not picked up by scalp electrodes [214]. This could be due to the fact that the area in which the discharge is occurring is not large enough to generate a recognisable potential, or that that the scalp electrodes may not be sensitive enough to record epileptiform discharges occurring within a gyrus [213]. Even though only 1.4% of all the recorded epileptiform discharges appeared focal, it is not possible

to estimate how the missed epileptiform focal discharges would affect the distributions we studied. This issue could be addressed by using more invasive recording techniques such as intracranial EEG, but this is questionable in the context of generalised epilepsy (as opposed to focal epilepsy, where interictal epileptiform discharges on intracranial EEG are used to localise seizure onset during presurgical evaluation).

It is essential to emphasise that the computational model is strictly phenomenological; it includes no details of physiology processes underlying the functioning of the epileptic brain. Consequently, the model is unable to reproduce complex morphologies commonly observed in EEG recordings, nor the variability observed in discharge durations. The decision was made to use a simple network model that allows reproduction of discharge distributions, as the primary aim was to explore and illustrate how complex macroscale phenomena can arise due to dynamic changes to excitability, rather than an attempt to ascribe biophysical detail and causality at this stage. It would be highly desirable to extend the findings from the phenomenological model to a more complex physiological description, for example, using a neural mass or neural field formulation [50] with a discretised network structure inferred from ambulatory EEG-recordings [80]. Depending on the specific epochs of interest (for example, resting-state, or close or during a discharge), there are several suitable candidate methods [168] for the inference of functional networks from the EEG recordings (e.g. linear and non-linear).

It is possible that the increased likelihood of longer and more epileptiform discharges around waking could be modulated by the circadian profile of the glucocorticoid hormone cortisol. There is a strong association between stress and epilepsy, as prospective studies in patients have been shown to link to increased stress with subsequent seizures [89]; animal models show a very strong effect of cortisol on seizure exacerbation [107]. Cortisol has a variable circadian profile, and typically peaks during the early morning roughly an hour before rising. One hypothesis is that the interplay between the pattern of cortisol secretion and the brain networks upon which it acts, could mediate the effect of stress on susceptibility to epileptiform discharges. Although a recent study provides evidence for this [34], future experimental research is needed to test

this hypothesis, in order to shed light on the precise mechanisms of interactions between the brain and the stress-responsive glucocorticoid system.

In order to study the role of physiological factors such as levels of melatonin, cortisol, and insulin on increased susceptibility of brain networks to epileptiform discharges, it is essential to simultaneously record EEG and levels of these hormones. Ideally, these experiments would be combined with measures of excitability using transcranial magnetic stimulation (TMS) [10, 11, 137]. In such a setting, the observed data could be interrogated and integrated within the computational network model in order to find patient-specific relationships between the levels of hormones and emergent discharge likelihood. This has the potential to provide stratification by discerning the specific features that are responsible for increased likelihood of epileptiform discharges.

Chapter 6

Discussion

6.1 Discussion of results

The combination of mathematical analysis and modelling provides a powerful tool with which to understand mechanisms of generation and propagation of epileptiform activity. Mathematical models integrating experimental and clinical detail at diverse scales of activity have revealed the importance of many microscopic and macroscopic mechanisms in the generation of seizure-like activity, ranging from genetic and molecular mechanisms to changes in the excitability of neural populations leading to the generation of pathological oscillations.

The last few years have seen a shift in the understanding of seizure emergence, particularly with respect to the dichotomy between focal and generalised seizures and epilepsies. Focal seizures were traditionally thought of as the result of a local abnormality constrained with in a specific area of the brain (the epileptogenic region), responsible for driving the emergence of a seizure or discharge. Recent studies suggest a more subtle picture, suggesting a role for global network structures (cortical and subcortical brain structures, such as the thalamus) in emergent focal activity, rather than merely the dysfunction of a single epileptogenic region [97, 172]. This extends the concept of an epileptogenic region to "epileptogenic" networks, since network structure can play a crucial role in the way activity propagates throughout the network: the same pathological activity in a single brain region can lead to focal discharges in one network but generalised discharges in a slightly different network [218].

In this thesis we have studied the contribution of dynamic network mech-

anisms in the generation and propagation of epileptiform activity. We have used this understanding to explore the potential of a dynamic network marker as a diagnostic biomarker for seizures in people with IGE. In our approach we conceptualised epilepsy as a dynamic disorder of brain networks, where people with epilepsy have an enduring susceptibility to seizures, which occur unpredictably from otherwise healthy brain function. The overall objective was to use mathematical analysis and modelling to identify mechanisms and characteristics in resting-state activity that could be involved in the increased likelihood of epileptiform activity which is characteristic for people with epilepsy. Consequently, we aimed to gain a better understanding of the interaction between local dynamics and global network structure of the system can change over time and drive the emergence of epileptiform activity. Our work was centred around clinical recordings of scalp EEG from people with IGE, in particular segments of resting-state activity and epileptiform discharges.

6.1.1 Altered networks as an endophenotype for IGE

The main result in Chapter 3 is that altered network properties derived from resting-state EEG are an endophenotype for IGE. Networks were derived from resting-state EEG from people with IGE, their first-degree unaffected relatives, and healthy controls. This approach was motivated by combining the understanding of epilepsy as a complex network disorder spanning several temporal and spatial scales, together with the dominant hypothesis that many of the generalised epilepsies have an underlying genetic cause. Since seizures or epileptiform discharges emerge from otherwise healthy-looking background activity, static networks were derived from background EEG, which allows us to compare the functional networks (based on statistical correlations between channels) from people with IGE and their asymptomatic first-degree relatives. Crucially, this allows us to examine whether networks from people with IGE have specific characteristics in their resting-state EEG which could be responsible for the generation of epileptiform activity.

After networks were derived from the subjects, the properties of these networks were characterised by a set of graph measures (mean degree, mean degree variance, clustering coefficient, characteristic path-length), and it was

shown that the networks from the people with IGE were statistically significantly different from the networks from the healthy controls. Furthermore, the networks from the first-degree relatives differed significantly from those from the healthy controls, thus providing evidence of an endophenotype of IGE. That is, these altered networks structures in combination with other biological factors likely leads to an increased susceptibility to epileptiform activity, but are on their own not sufficient to generate seizures as the first-degree relatives also have these altered properties but have no seizure-history.

Identifying features characteristic of people with epilepsy contributes towards a deeper understanding of how pathological rhythms originate in brain networks of people with epilepsy, but not their relatives, controls, or people with non-epileptic seizures. This is particularly exciting because identification of biomarkers - features characteristic and exclusive of people with epilepsy or high seizure susceptibility - is potentially beneficial for the diagnosis of epilepsy, as well as with respect to predicting whether people with epilepsy may benefit from specific AEDs. However, one should be careful in interpreting the results with regards to the anatomical organisation of the brain since we are dealing with statistical correlations derived from scalp EEG. We therefore argue these approaches would benefit from an integrative approach where connectivity data from EEG, MEG, fMRI, and DTI is combined (preferably through simultaneous recordings).

6.1.2 Potential of computational biomarkers as a diagnostic support tool

In chapter 4 we considered a set of features derived from resting-state scalp EEG that have been shown to be significantly different for people with generalised epilepsies and normal controls. These features include the peak in alpha-frequency (lower in people with generalised epilepsy [119]), mean degree of functional networks (higher in people with IGE, shown in chapter 3), and two model-properties from a modular network of Kuramoto-oscillators (the critical value of global coupling needed to synchronise a network structure, and the effect of local synchronisation on the emergent activity of the network [191]). Since these studies examined how these properties differ at the level of

the cohort, we aimed to examine their potential as biomarkers at the level of individual subjects. Crucially, these candidate biomarkers were derived from the resting-state activity recorded from drug-naive subjects with IGE, in order to exclude any potential influence of AEDs and the control-cohort was age- and gender-matched.

We considered two strategies for developing the biomarkers using leave-one out cross-validation: one in which we found thresholds that optimised sensitivity and specificity given 100% specificity and 100% sensitivity respectively, and a support vector machine (SVM) approach that found the strongest separating hyperplane between the IGE-cohort and the control-cohort. We decided to use these two relatively straightforward methods before considering more sophisticated methods, such as Bayesian machine learning techniques. These more complicated machine learning techniques usually depend on several statistical assumptions regarding the data, and a certain amount of technical detail that renders the classification method difficult to interpret. However, if they were to have superior performance over our naive methods it is unlikely that this will hinder their contribution to clinical contexts. Given that model properties from a purely phenomenological model lead to levels of sensitivity and specificity in the same range as current clinical practice, we may expect that network models that integrate more biophysical detail derived from the EEG hold the potential to further improve accuracy rates.

6.1.3 Dynamic variation in distributions of epileptiform discharges from people with IGE

In extending the model presented in chapter 5, our original aim was to identify patterns of dynamic excitability that could underlie distributions of epileptiform discharges observed in recordings from people with IGE. One of the principal motivations was to understand how the behaviour of a bistable dynamic network model is affected by changes in the underlying network excitability, as cortical excitability is known to vary over the course of the day from experimental and clinical studies. Since the model was developed in order to develop conceptual understanding and reproduce the large-scale features of scalp EEG rather than the time-series of the EEG, we decided to use a purely phenomeno-

logical model. This phenomenological representation of the cortex captures the emergence, propagation, and termination of an epileptiform discharge arising from a noise background state with abstract dynamical concepts rather than biological detail. This enabled us to reproduce discharge distributions with simple, irregular network structures on a subject-specific basis. We could have used network inference techniques to derive network topologies from the ambulatory EEG-recordings, but we are currently unfamiliar with any approaches that would enable us to find reliable estimates of levels of dynamic cortical excitability from resting-state scalp EEG.

Our analysis of the discharge distributions indicate there are several periods during the day with increased likelihood of epileptiform discharges: there are periods of increased likelihood of epileptiform discharges during the early periods of sleeping and around waking in the morning. After locking the histograms to the onset and offset of sleep, our results suggest sleep and the secretion of cortisol (which is known to peak 20/30 minutes after waking) may play a role in making the brain networks more prone to generate epileptiform activity. By considering the summed duration of discharges we obtained an objective measure for quantifying epileptiform activity, since the fraction of time spent in the epileptiform state has an upper bound (in contrast to frequency or timing of discharges). Our results suggest that the total number of EDs occurring during sleep and around waking are similar, and that the discharges around waking are more likely to last longer.

6.2 Future research

6.2.1 Focal epilepsy

The emphasis of this thesis has been on resting-state markers of generalised epilepsies. A natural next step would be to explore the potential of these resting-state markers in people with focal epilepsy. The biomarkers derived from the dynamic network model of Kuramoto-oscillators seems a natural candidate, since it allows one to discern the influence of network topology across different scales on the emergent activity of the cortex. Of particular interest would be to explore which nodes are most involved in the generation of emergent synchronisation across the network: one could hypothesise that in silico

epileptiform activity for people with left (right) focal epilepsy would largely be driven by areas in the left (right) side of the simulated network. The clinical potential of this approach would significantly increase if it would enable similar levels of classification for focal cohorts and furthermore provide a reliable estimation of the hemisphere/areas involved in the generation of epileptiform activity.

6.2.2 Prognosis of epilepy

By applying the resting-state markers to follow-up recordings from people with epilepsy, we can monitor how the biomarkers evolve dynamically over time. Of particular interest would be to study whether any of the markers provides a way to reliably differentiate subjects that respond well to treatment versus those that do not respond well to treatment. Finding appropriate treatment for a subject with epilepsy is often a very challenging process, since many AEDs have undesirable side-effects and treatment-response is often hard to predict on a subject-specific basis [8, 193]. Given a large enough number of reliable recordings, our approach could be used as a dynamic biomarker of treatment choice by quantifying the effect of a specific AED by comparing the biomarker derived from the drug-naive recordings against follow-up recordings. Successful delivery of 6.2.1 and 6.2.2 would likely enable the creation of a decision support tool for clinicians.[1]

6.2.3 A decision support tool for epilepsy

Creating a decision support tool for the diagnosis of epilepsy ultimately depends on its ability to identify features that are exclusive to people with epilepsy. In line with this, it is important to consider that the tool will likely only be applied to recordings from people with *suspected* epilepsy. This means people who have either experienced a genuine epileptic seizure or some form of non-epileptic seizure (an event with seizure-like symptoms but that is not driven by pathological episodes of hypersynchronous neural activity).

[1] During a commercialisation program I had the opportunity to discuss the potential of the research described here to over 25 clinicians (clinical neurophysiologists, neurologists, epileptologists); though all recognised the potential application for decreasing numbers of misdiagnosis, almost all of them expressed interest in the potential of these methods as a prognostic marker.

At present, we have no understanding of the dynamic network properties of resting-state activity from people who experience non-epileptic seizures and their relationship to either healthy or epilepsy cohorts. In order to examine the actual clinical potential of these methods, it is consequently essential to test them against the resting-state activity recorded from a representative cohort of controls, which means people that came to the clinic with suspected epilepsy but turned out to not have epilepsy after further examination. This will also lead to deeper insight on the properties of brain networks derived from people that are commonly misdiagnosed, such as those with syncope and psychogenic attacks [201].

In general, the biomarkers proposed in this thesis need to be further tested for their reliability and robustness in order to discern their generalisability for epilepsy cohorts in general. For example, it is an open question whether the methods applied here would classify subjects with focal epilepsy as having epilepsy or as a normal control. Additionally, it is essential to study whether the performance of the biomarker depends on the age of the subjects. This is particularly pressing since it may be difficult to record long-enough, reliable epochs of resting-state activity from young children. Another example is to consider whether the tools are sensitive to the exact time of day of the recording, that is, whether there is a particular time during the day associated with optimal performance. In conclusion, by understanding how seizures emerge from healthy background activity from clinical recordings, we can start to understand how networks of people with epilepsy differ from the networks of people with non-epileptic seizures (e.g. syncope), and how AEDs might alter the network structures to decrease the seizure-likelihood. The main strengths of this approach from a clinical perspective result from the fact that our methods depend on resting-state activity which is relatively easy to collect (inexpensive, non-invasive), and consequently does not rely on observing epileptiform activity in clinical recordings.

6.2.4 The role of physiological factors on the emergence of epileptiform activity

A critical challenge in studying mechanisms underlying the emergence of epileptiform activity is the influence of dynamic perturbations on the behaviour of the systems under study. Given that waking has been implicated in mediating the frequency and summed duration of epileptiform discharges in people with IGE, our results suggest the circadian secretion of the stress-hormone cortisol may mediate the activity of brain networks. In fact, several recent studies have described how stress and cortisol relates to epileptic seizures and epileptiform discharges [34, 107, 114]. Future research could aim to quantify the relative roles of the circadian secretion of cortisol in increasing the likelihood of epileptiform discharges, by measuring cortical excitability from and levels of hormones directly. Excitability could be estimated using transcranial magnetic stimulation, whereas a microdialysis system could be used simultaneously with scalp EEG to investigate the interaction between endogenous secretion of cortisol and epileptiform activity. This data could then be combined with mathematical and computational approaches in order to stratify subjects quantitatively into subgroups (for example, by identifying subjects into subgroups of people with few/many discharges with low/high circadian influence of cortisol). By using a similar approach to other biological factors associated with increased epileptiform discharges such as sleep, this research builds towards a deeper understanding of the specific contributions to the emergence and propagation of epileptiform activity.

A better understanding of the interplay between the dynamics of physiological factors (such as sleep or hormone secretion) and their modulatory effect on properties of complex brain networks (such as hyperexcitability and hypersynchronisation) will provide a deeper understanding of the neural activity of people with epilepsy. In general the insights generated by these integrative approaches between clinical/experimental neuroscience and computational/mathematical neuroscience will contribute to a deeper understanding of how epileptic brains transition from background activity to epileptiform discharges and seizures, and how these states relate to each other. We will then be in a better position to identify ways of decreasing the susceptibility to

seizures and epileptiform discharges in people with epilepsy.

Chapter

Appendix

A Derivation of Kuramoto-biomarkers

The following section is organised as follows: first the standard Kuramoto model of coupled phase oscillators will be introduced for N identical phase oscillators, and then extended to a modular network. Then the system will be generalised to the case of $N \to \infty$, where the problem is reformulated in terms of a distribution function f. By using the Ott-Antonsen ansatz a system of differential equations is derived by using the continuity equation. By constraining the dynamics of this system to a particular submanifold M it is then possible to derive two uncoupled ordinary differential equations describing the order parameters of the system. Then a similar set of equations will be derived for the modular case. The Kuramoto model was originally proposed in [117], extended reviews can be found in [2, 210], and the derivation of the following section relies heavily on [14, 132, 161, 162, 198]. The homogeneous Kuramoto model describes the dynamics of N identically coupled phase oscillators:

$$\frac{d}{dt}\theta_j = \omega_j + \frac{K}{N}\sum_{k=1}^{N}\sin(\theta_k - \theta_j) \text{ for } j = 1, ..., N \tag{A.1}$$

with phase θ, natural frequency ω (from distribution $g(\omega)$), and coupling strength K. Introducing the complex order-parameter $r = \frac{1}{N}\sum_{k=1}^{N} e^{\mathrm{i}\theta_k}$ $(r \in \mathbb{C})$

results in the following equation:

$$\frac{d}{dt}\theta_j = \omega_j + \frac{K}{N}\sum_{k=1}^{N}\sin(\theta_k - \theta_j) \tag{A.2}$$

$$= \omega_j + \frac{K}{N}\sum_{k=1}^{N}\frac{1}{2\mathrm{i}}\left[e^{\mathrm{i}(\theta_k-\theta_j)} - e^{-\mathrm{i}(\theta_k-\theta_j)}\right] \tag{A.3}$$

$$= \omega_j + \frac{K}{2\mathrm{i}}\left[e^{-\mathrm{i}\theta_j}\left(\frac{1}{N}\sum_{k=1}^{N}e^{\mathrm{i}\theta_k}\right) - e^{\mathrm{i}\theta_j}\left(\frac{1}{N}\sum_{k=1}^{N}e^{-\mathrm{i}\theta_k}\right)\right] \tag{A.4}$$

$$= \omega_j + \frac{K}{2\mathrm{i}}\left[re^{-\mathrm{i}\theta_j} - \overline{r}e^{\mathrm{i}\theta_j}\right] \tag{A.5}$$

Now extend the case of a single network to a network of P populations $c = 1, 2, ..., P$, where each population c contains N_c oscillators (we will typically assume that all N_c are identical), and the natural frequencies of the oscillators in population c are drawn from the distribution $g_c(\omega)$. With N the total number of oscillators in the entire network, define $\eta_c = N_c/N$. The coupling between population c and γ is defined by $K_{c\gamma} \in \mathbb{C}$. The evolution of the phase of the j-th oscillator from population c is defined by:

$$\frac{d}{dt}\theta_j^c = \omega_j^c + \sum_{\gamma=1}^{P}\eta_\gamma\frac{K_{c\gamma}}{N_\gamma}\sum_{k=1}^{N_\gamma}\sin(\theta_k^\gamma - \theta_j^c) \text{ for } j = 1, ..., N_c, \omega_j^c \in [0, 2\pi] \tag{A.6}$$

Matrix K defines the interactions within the population of oscillators and between the populations, K_{cc} defines the local coupling in a population c, and $K_{c\gamma}$ defines the global coupling from population c to γ (note that K need not be symmetric: it need not be true that $K_{c\gamma} = K_{\gamma c}$). Entries can be complex in order to incorporate phase-lags. Note that for the purpose of biomarker discovery, we have $P = 19$. In other words, the modular network consists of 19 nodes where each node corresponds to an EEG channel.

Define complex local and global order parameters:

$$z_c(t) = \frac{1}{N_c} \sum_{k=1}^{N_c} e^{\mathrm{i}\theta_k^c(t)} \tag{A.7}$$

$$Z(t) = \sum_{c=1}^{P} \eta_c z_c(t) \tag{A.8}$$

Now equation (A.6) can be written as:

$$\frac{d}{dt}\theta_j^c = \omega_j^c + \sum_{\gamma=1}^{P} \eta_\gamma \frac{K_{c\gamma}}{N_\gamma} \sum_{k=1}^{N_\gamma} \sin(\theta_k^\gamma - \theta_j^c) \tag{A.9}$$

$$= \omega_j^c + \sum_{\gamma=1}^{P} \eta_\gamma \frac{K_{c\gamma}}{N_\gamma} \sum_{k=1}^{N_\gamma} \frac{1}{2\mathrm{i}} \left(e^{\theta_k^\gamma - \theta_j^c} - e^{-(\theta_k^\gamma - \theta_j^c)} \right) \tag{A.10}$$

$$= \omega_j^c + \frac{1}{2\mathrm{i}} \sum_{\gamma=1}^{P} \eta_\gamma K_{c\gamma} \left(z_\gamma e^{-\mathrm{i}\theta_j^c} - \overline{z}_\gamma e^{\mathrm{i}\theta_j^c} \right) \tag{A.11}$$

In the limit $N_c \to \infty$, the distribution of states of oscillators with natural frequency ω in population c at a time t is defined by the continuous distribution function $f_c(\theta, \omega, t)$, where $f_c(\theta, \omega, t) d\theta d\omega$ is a measure for the fraction of oscillators with phase θ and natural frequency ω. The evolution of an individual oscillator from community c with natural frequency ω is governed by the following equation:

$$\frac{d}{dt}\theta = \omega + \frac{1}{2\mathrm{i}} \sum_{\gamma=1}^{P} \eta_\gamma K_{c\gamma} \left(z_\gamma e^{-\mathrm{i}\theta} - \overline{z}_\gamma e^{\mathrm{i}\theta} \right) \tag{A.12}$$

$$\tag{A.13}$$

with $z_c(t)$ given by:

$$z_c(t) = \int_{-\infty}^{\infty} \int_{0}^{2\pi} f_c(\theta, \omega, t) e^{\mathrm{i}\theta} d\theta d\omega \tag{A.14}$$

note that, where appropriate, superscripts were dropped. Equation (A.12) reveals a mean-field character of interactions between the oscillators in a pop-

ulation, as the phase of an oscillator is pulled towards the collective average of the population.

In the limit $N_c \to \infty$, the continuity equation holds, meaning that the number of oscillators in every community is conserved over time:

$$\frac{\partial}{\partial t} f_c + \frac{\partial}{\partial \theta} \left\{ \left[\omega + \frac{1}{2\mathrm{i}} \sum_{\gamma=1}^{P} \eta_\gamma K_{c\gamma} \left(z_\gamma e^{-\mathrm{i}\theta} - \overline{z}_\gamma e^{\mathrm{i}\theta} \right) \right] f_c \right\} = 0 \tag{A.15}$$

The Ott-Antonsen ansatz is built around the assumption that f_c can be expressed as a Fourier series with coefficients: $\alpha_c(\omega, t)^n$:

$$f_c(\theta, \omega, t) = \frac{g_c(\omega)}{2\pi} \left\{ 1 + \sum_{n=1}^{\infty} \alpha_c^n(\omega, t) e^{\mathrm{i}n\theta} + \sum_{n=1}^{\infty} \overline{\alpha_c^n}(\omega, t) e^{-\mathrm{i}n\theta} \right\} \tag{A.16}$$

where $\alpha_c(\omega, t)$, and $|\alpha_c(\omega, t)| < 1$ in order to guarantee absolute convergence $(\alpha_c(\omega, t) : \mathbb{R} \times \mathbb{R}_{\geq 0} \mapsto \mathbb{C})$. The ansatz constrains the infinite-dimensional space of density functions f to a submanifold.

Now due to the conversation of mass (in this instance, the number of oscillators rotating on the unit circle), the continuity equation must hold. The first part of the continuity equation is:

$$\frac{\partial}{\partial t} f_c = \frac{\partial}{\partial t} \left(1 + \sum_{n=1}^{\infty} \alpha_c^n e^{\mathrm{i}n\theta} + c.c. \right) = \frac{\partial}{\partial t} \alpha_c \cdot \left(\sum_{n=1}^{\infty} n \alpha_c^{(n-1)} e^{\mathrm{i}n\theta} \right) + c.c. \tag{A.17}$$

where c.c. denotes the complex conjugate. The second part of the continuity

equation is (where dependency on θ, ω, t are omitted):

$$\frac{\partial}{\partial\theta}(f_c\frac{d}{dt}\theta) = \frac{\partial}{\partial\theta}\left\{\left(1+\sum_{n=1}^{\infty}\alpha_c^n e^{\mathrm{i}n\theta}+c.c.\right)\left(\omega-\frac{1}{2\mathrm{i}}\sum_{\gamma=1}^{P}\eta_\gamma K_{c\gamma}\overline{z}_\gamma e^{\mathrm{i}\theta}+c.c.\right)\right\} \tag{A.18}$$

$$= -\frac{1}{2}\sum_{\gamma=1}^{P}\eta_\gamma K_{c\gamma}\overline{z}_\gamma e^{\mathrm{i}\theta}+\mathrm{i}\omega\alpha_c\sum_{n=1}^{\infty}\alpha_c^{(n-1)}ne^{\mathrm{i}n\theta}+\frac{1}{2}\sum_{n=1}^{\infty}\alpha_c^n(n-1)e^{\mathrm{i}(n-1)\theta}\sum_{\gamma=1}^{P}\eta_\gamma K_{c\gamma}z_\gamma$$
$$-\frac{1}{2}\sum_{n=1}^{\infty}\alpha_c^n(n+1)e^{\mathrm{i}(n+1)\theta}\sum_{\gamma=1}^{P}\eta_\gamma K_{c\gamma}\overline{z}_\gamma+c.c. \tag{A.19}$$

$$= -\frac{1}{2}\sum_{\gamma=1}^{P}\eta_\gamma K_{c\gamma}\overline{z}_\gamma e^{\mathrm{i}\theta}+\mathrm{i}\omega\alpha_c\sum_{n=1}^{\infty}\alpha_c^{(n-1)}ne^{\mathrm{i}n\theta}+\frac{1}{2}\sum_{n=1}^{\infty}\alpha_c^{(n+1)}ne^{\mathrm{i}n\theta}\sum_{\gamma=1}^{P}\eta_\gamma K_{c\gamma}z_\gamma$$
$$-\frac{1}{2}\left(\sum_{n=1}^{\infty}\alpha_c^{(n-1)}ne^{\mathrm{i}n\theta}-e^{i\theta}\right)\sum_{\gamma=1}^{P}\eta_\gamma K_{c\gamma}\overline{z}_\gamma+c.c. \tag{A.20}$$

$$= \left(\mathrm{i}\omega\alpha_c+\frac{1}{2}\alpha_c^2\sum_{\gamma=1}^{P}\eta_\gamma K_{c\gamma}z_\gamma-\frac{1}{2}\sum_{\gamma=1}^{P}\eta_\gamma K_{c\gamma}\overline{z}_\gamma\right)\left(\sum_{n=1}^{\infty}\alpha_c^{(n-1)}ne^{\mathrm{i}n\theta}\right)+c.c. \tag{A.21}$$

The full continuity equation is now given by:

$$\left(\frac{d}{dt}\alpha_c+\mathrm{i}\omega\alpha_c+\frac{1}{2}\alpha_c^2\sum_{\gamma=1}^{P}\eta_\gamma K_{c\gamma}z_\gamma-\frac{1}{2}\sum_{\gamma=1}^{P}\eta_\gamma K_{c\gamma}\overline{z}_\gamma\right)\left(\sum_{n=1}^{\infty}\alpha_c^{(n-1)}ne^{\mathrm{i}n\theta}\right)+c.c=0 \tag{A.22}$$

and as

$$\sum_{n=1}^{\infty}\alpha_c^{(n-1)}ne^{\mathrm{i}n\theta}=\frac{1}{\alpha_c}\sum_{n=1}^{\infty}n(\alpha_c e^{\mathrm{i}\theta})^n=\frac{e^{\mathrm{i}\theta}}{(1-\alpha_c e^{\mathrm{i}\theta})^2}\neq 0 \tag{A.23}$$

it must hold that:

$$\frac{d}{dt}\alpha_c+\mathrm{i}\omega\alpha_c+\frac{1}{2}\sum_{\gamma=1}^{P}\eta_\gamma K_{c\gamma}(\alpha_c^2 z_\gamma-\overline{z}_\gamma)=0 \tag{A.24}$$

This system of equations is independent of θ, and if we assume that the fre-

quencies ω are independent and identically distributed with density $g_c(\omega)$, then the population's order parameter $z_c(t)$ is given by:

$$z_c(t) = \int_0^{2\pi}\int_{-\infty}^{\infty} f_c e^{\mathrm{i}\theta} d\omega d\theta = \int_{-\infty}^{\infty}\int_0^{2\pi} \frac{g_c(\omega)}{2\pi}\left\{1 + \sum_{n=1}^{\infty}\alpha_c^n e^{\mathrm{i}n\theta} + \sum_{n=1}^{\infty}\overline{\alpha_c}^n e^{-\mathrm{i}n\theta}\right\} e^{\mathrm{i}\theta} d\theta d\omega \tag{A.25}$$

$$= \int_{-\infty}^{\infty}\int_0^{2\pi} \frac{g_c(\omega)}{2\pi}\left\{e^{\mathrm{i}\theta} + \sum_{n=1}^{\infty}\alpha_c^n e^{\mathrm{i}(n+1)\theta} + \sum_{n=1}^{\infty}\overline{\alpha_c}^n e^{-\mathrm{i}(n-1)\theta}\right\} d\theta d\omega \tag{A.26}$$

$$= \int_{-\infty}^{\infty} \overline{\alpha_c} g_c(\omega) d\omega \tag{A.27}$$

Solutions to the system described by equations (A.24) will be constrained to an invariant manifold M: the space of functions of real variables (ω, θ) given by the Poisson kernel where $|\alpha_c(\omega, t)| < 1$ for real ω in order to guarantee convergence, and $\alpha_c(\omega, t)$ can be analytically continued from the real ω-axis into the lower half ω-plane, without any singularities and approaching zero when $\omega \to -\infty$. Take $g_c(\omega)$ as a Cauchy distribution:

$$g_c(\omega) = \frac{1}{2\pi\mathrm{i}}\left[\frac{1}{\omega - \omega_0 - \mathrm{i}\Delta} - \frac{1}{\omega - \omega_0 + \mathrm{i}\Delta}\right] \tag{A.28}$$

With contour Γ as the semicircle with infinite radius in the lower half-plane, change variables such that $\omega_0 = 0, \Delta = 1$, and use Cauchy's integral formula:

$$z_c = \int_{-\infty}^{\infty} \overline{\alpha_c}(\omega, t) g_c(\omega) d\omega \tag{A.29}$$

$$= \int_{-\infty}^{\infty} \overline{\alpha_c}(\omega, t) \frac{1}{2\pi\mathrm{i}}\left[\frac{1}{\omega - \omega_0 - \mathrm{i}\Delta} - \frac{1}{\omega - \omega_0 + \mathrm{i}\Delta}\right] d\omega \tag{A.30}$$

$$= \frac{1}{2\pi\mathrm{i}} \int_{\Gamma} \frac{\overline{\alpha_c}(\omega, t)}{\omega + \mathrm{i}} d\omega \tag{A.31}$$

$$= \overline{\alpha_c}(-\mathrm{i}, t) \tag{A.32}$$

Substituting $\omega = -\mathrm{i}$ in equation (A.24), gives (with $z_c(t) = r_c e^{-\mathrm{i}\phi_c}$):

$$0 = \frac{d}{dt}\alpha_c + \mathrm{i}\omega\alpha_c + \frac{1}{2}\sum_{\gamma=1}^{P}\eta_\gamma K_{c\gamma}(\alpha_c^2 z_\gamma - \overline{z}_\gamma) \tag{A.33}$$

$$= \frac{d}{dt}(r_c e^{-\mathrm{i}\phi_c}) + r_c e^{-\mathrm{i}\phi_c} + \frac{1}{2}\sum_{\gamma=1}^{P}\eta_\gamma K_{c\gamma}\left(r_\gamma r_c^2 e^{\mathrm{i}\phi_\gamma} e^{-2\mathrm{i}\phi_c} - r_\gamma e^{-\mathrm{i}\phi_\gamma}\right) \tag{A.34}$$

$$= e^{-\mathrm{i}\phi_c}\left(\frac{d}{dt}(r_c) - \mathrm{i}r_c\frac{d}{dt}(\phi_c) + r_c + \frac{1}{2}\sum_{\gamma=1}^{P}\eta_\gamma K_{c\gamma} r_\gamma\left(r_c^2 e^{\mathrm{i}(\phi_\gamma-\phi_c)} - e^{-\mathrm{i}(\phi_\gamma-\phi_c)}\right)\right) \tag{A.35}$$

Resulting in the following set of differential equations:

$$\frac{dr_c}{dt} = -r_c + \frac{1-r_c^2}{2}\sum_{\gamma=1}^{P}\eta_\gamma K_{c\gamma} r_\gamma \cos(\phi_\gamma - \phi_c) \tag{A.36}$$

$$\frac{d\phi_c}{dt} = \frac{r_c^2+1}{2r_c}\sum_{\gamma=1}^{P}\eta_\gamma K_{c\gamma} r_\gamma \sin(\phi_\gamma - \phi_c) \tag{A.37}$$

with $r \in \mathbb{R}_{\geq 0}$. Equations (A.36) and (A.37) constitute a set of ordinary differential equations for every community in the network. This means that although the dynamics of the distribution function f_c on manifold M are infinitely dimensional, the global dynamics of the order parameter describing the global behaviour of the large system is low dimensional.

Consider the global order parameter:

$$r_g = \left|\frac{1}{N_c P}\sum_{\gamma=1}^{P}\sum_{n=1}^{N_c} e^{\mathrm{i}\theta_n^c}\right| = \left|\frac{1}{P}\sum_{\gamma=1}^{P} r_c e^{\mathrm{i}\phi_c}\right| \tag{A.38}$$

which is a measure for the emergent synchrony within the network. By solving equations (A.36 and A.37) numerically after linearising the system (note that by assuming a rotating frame, the phase differences $\phi_c - \phi_\gamma$ converge

to 0), we find solutions for:

$$0 = -r_c + \frac{1}{2}\sum_{\gamma=1}^{P} \eta_\gamma K_{c\gamma} r_\gamma \tag{A.39}$$

Then the global order parameter is simply computed by averaging over the solutions to equation B.42 of the individual nodes of the network.

In conclusion, the local Kuramoto-biomarker is computed for a node c from a network by following the next set of steps:

1. Filter resting-state epoch (20 seconds) into low-alpha or theta band
2. Infer PLF-matrix (19-by-19 weighted, undirected network)
3. Infer phase-lags (19-by-19 weighted, directed network)
4. Use redundancy-approach to prune redundant connections (19-by-19 weighted, directed network)
5. Model each node from the network with a population of Kuramoto-oscillators
6. Let for every node in the network $N_c \to \infty$
7. Consider the Ott-Antonsen-submanifold with potential low-dimensional behaviour
8. Find the critical local coupling for node c (value that is strong enough to drive it into the coherent state)
9. Set the local coupling strength K_{cc} above this value to guarantee the node is synchronised
10. Solve equations (A.36 and A.37) for all nodes of the network
11. Quantify the effect of setting node c into the synchronised state on the global order parameter

This process is repeated for all 19 nodes (electrodes) in the network inferred from the resting-state EEG recording. The optimal node and model parameters are selected by finding the optimal combination that maximally discriminates between the cohort of people with IGE and the people with epilepsy. Consequently, it is crucial to find ways to optimise this process and reduce the associated computational effort.

The global Kuramoto-biomarker corresponds to the critical value of the global coupling ($\hat{K_g}$) that drives the global network into the coherent state. This is found by considering the linear parts of equation A.36 describing the evolution of the order parameters of the network nodes, since $\hat{K_g}$ corresponds to the point where the incoherent state r_c loses stability, and this is dominated by the linear dynamics. Consequently, we set out to find solutions for:

$$-r_c + \frac{1}{2}\sum_{\gamma=1}^{P} \eta_\gamma K_{c\gamma} r_\gamma = 0 \tag{A.40}$$

After linearisation we aim to find non-trivial solutions for the following eigenvalue problem (assuming that every node has the same local coupling, that is: K_{cc} equals some constant):

$$\mathbf{Ar} = K_g^{-1}(2 - K_{cc})\mathbf{r} \tag{A.41}$$

with global coupling parameter K_g, local coupling parameter K_{cc}, adjacency matrix $\mathbf{A}$ (network topology), and order parameter vector $\mathbf{r} = (r_1, r_2, ..., r_P)$. Consequently, it is sufficient to compute the largest eigenvalue $\lambda_{\max}$ of the adjacency matrix $\mathbf{A}$, and so we find that the critical value for global coupling is defined by: $\hat{K_g} = (2 - K_{cc})/|\lambda_{\max}|$.

B Properties of the model for epileptiform discharges

Consider the discharge-model for a network of N nodes. If we assume all-to-all coupling and only consider the deterministic part, the activity of a single node is described by:

$$\frac{dz_j}{dt} = (\lambda - 1 + \mathrm{i}\omega)z_j + 2z_j|z_j|^2 - z_j|z_j|^4 + \beta\sum_{k=1}^{N}(z_k - z_j) \tag{B.42}$$

Writing $z_j = r_j e^{\mathrm{i}\theta_j}$, and dividing by $e^{\mathrm{i}\theta_j}$:

$$r_j' + r_j \mathrm{i}\theta_j' = (\lambda - 1 + \mathrm{i}\omega)r_j + 2r_j^3 - r_j^5 + \beta\sum_{k=1}^{N}(r_k e^{\mathrm{i}(\theta_k - \theta_j)} - r_j) \tag{B.43}$$

After splitting the equation in real and imaginary parts we obtain:

$$r_j' = (\lambda - 1)r_j + 2r_j^3 - r_j^5 + \beta\sum_{k=1}^{N}(r_k\cos(\theta_k - \theta_j) - r_j) \tag{B.44}$$

$$\theta_j' = \omega + \beta\sum_{k=1}^{N}\frac{r_k}{r_j}\sin(\theta_k - \theta_j) \tag{B.45}$$

Now, if we only consider the differential equation for phase θ_j, we note that if the entire system of nodes is situated in the stable limit cycle ($r_k \approx r_j$), the equations describing the phase are essentially identically to coupled Kuramoto oscillators if we assume that every node has its own natural frequency ω_j drawn from distribution $g(\omega)$:

$$\theta_j' = \omega_j + \beta\sum_{k=1}^{N}\sin(\theta_k - \theta_j) \tag{B.46}$$

The all-to-all coupling affects the steady-state solutions to the radial equations, corresponding to the the unstable and stable limit cycle. Whereas in the case of a single-node these are located at $\sqrt{1-\sqrt{\lambda}}$ and $\sqrt{1+\sqrt{\lambda}}$ respectively, the

steady-state solutions now follow from:

$$0 = (\lambda - 1)r_j + 2r_j^3 - r_j^5 + \beta \sum_{k=1}^{N} (r_k \cos(\theta_k - \theta_j) - r_j) \tag{B.47}$$

$$= (\lambda - 1) + 2r_j^2 - r_j^4 + \beta \sum_{k=1}^{N} \left(\frac{r_k}{r_j} \cos(\theta_k - \theta_j) - 1 \right) \tag{B.48}$$

with implicit solutions:

$$\overline{r}_j^2 = 1 \pm \sqrt{\lambda + \beta \sum_{k=1}^{N} \left(\frac{r_k}{r_j} \cos(\theta_k - \theta_j) - 1 \right)} \tag{B.49}$$

The location of the separatrix of an individual node changes dynamically over time depending on contributions received through the nodes it is connected to. If we assume for simplicity that $\theta_k = \theta_j$ we consider three scenarios: in the case that $r_k > r_j$, this effect is positive, and the separatrix is transitioned closer to the stable fixed point, making a transition more likely. In the case that $r_k < r_j$, the effect is negative, thus the separatrix moves away from the stable fixed point, making a transition less likely. In the case that $r_k = r_j$ the separatrix remains fixed at its current location. The sum of all the contributions of the adjacent nodes determines the effective shift in the location of the separatrix.

C Detailed specifics of the individual subjects with epilepsy

Gender	Age	Syndrom	Onset	Type/freq	Last seizure	AEDs	EEG	MRI
M	26	GTCS	5	GTCS 1/m	2 weeks	SV 1600, T 200, L 100	GSW	Normal
M	25	GTCS	11	GTCS 3/m	3 weeks	SV 300	GSW	Normal
F	45	GTCS	2	SF	36 years	(none)	Normal	N/A
M	31	GTCS	8	GTCS 6/y	1 month	SV 2000, Z 250, LV 500, L100	GSW, Ph+	N/A
F	18	JAE	7	GTCS 1/m, Abs SF	1 week	E 250, L 600	GSW	Normal
F	20	GTCS	0.5	SF	9 years	(none)	Normal	N/A
M	49	GTCS	26	SF	1 year	(none)	GSW	Normal
F	21	JAE	10	SF	4 years	L 400, E 500	GSW	Normal
F	20	JME	13	MJ 1/w, GTCS SF	1 week	SV 1000	GSW	Normal
M	59	JME	14	SF	10 years	(none)	GSW	N/A
F	19	GTCS	15	GTCS; 4/y	3 months	LV 2000	GSW	Normal
F	28	Uncl.	20	SF	7 years	C 200	Normal	Normal
F	23	CAE	8	SF	6 years	SV 800, L 25	GSW	Normal
M	48	JME	17	SF	5 years	SV 1500, T 200, C 600	GSW, PSW	N/A
F	32	CAE	4	GTCS SF, Abs 1/w	1 weeks	(none)	GSW	N/A
M	30	Uncl.	11	SF	3 years	(none)	Normal	N/A
F	28	JME	15	SF	13 years	SV 1400	PSW	N/A
F	41	JME	11	GTCS rare, MJ 1/w	1 week	LV 1000, L 500, Z 200	GSW, PSW	N/A
M	45	CAE	3	SF	2 years	SV1400, LV 2000	GSW	N/A
M	31	Uncl.	8	SF	10 years	SV 400	Normal	Normal
M	27	Uncl.	16	SF	10 years	C 1200	Normal	N/A
F	39	GTCS	22	SF	10 years	C 200	GSW	Normal
M	28	CAE	4	SF	5 years	SV 600, LV 750, L 250	GSW	N/A
F	18	JME	15	MJ SF, GTCS 1/m	4 months	LV 1000	GSW	N/A
F	36	GTCS	21	GTCS 2/y	2 months	LV 1750	GSW, Ph+	Normal
F	43	CAE	7	SF	10 years	(none)	GSW	N/A
M	28	GTCS	8	SF	1 year	SV 400	GSW	N/A
F	53	GTCS	3	GTCS SF, Abs 1/d	1 day	(none)	GSW, Ph+	Normal
F	33	JAE	12	GTCS 3/y	4 months	T 400	GSW, Ph+	Normal
F	55	GTCS	16	SF	25 years	(none)	Normal	N/A
M	26	CAE	5	SF	8 years	(none)	GSW	N/A
F	47	JAE	11	Abs daily, GTCS SF	1 day	LV 2000	PSW	Normal
M	25	JME	14	GTCS 5/y, MJ 1/w	1 week	V	GSW	Normal
F	20	JME	15	MJ 2/m	2 weeks	L 400, LV 1500	GSW	Normal
F	21	AwEM	6	Abs 1/d, MJ 1/w	1 day	L 500	PSW	N/A

Table C.1: IGE-cohort: graph measures. AwEM: absences with eyelid myoclonia, CAE: childhood absence epilepsy, GTCS: generalised tonic clonic seizures only, JAE: juvenile absence epilepsy, JME: juvenile myoclonic epilepsy, MJ: myoclonic jerks, Abs: absences, Ph+: Photosensitivity; C: carbamazepine, E: ethosuximide, L: lamotrigine, LV: levetiracetam, SV: sodium valproate, T: topiramate, V: valproate, Z: zonisamide; GSW: generalised spike and wave, PSW: polyspike and wave; SF Seizure Free.

Gender	Age	Syndrome	EEG type	Alpha	Degree	Global	Local
F	31	GTCS	SD	U	U	U	U
M	35	JME	SD	I	U	I	I
F	32	GTCS	SD	U	U	U	U
M	41	GTCS	P	U	U	U	U
F	19	GTCS	P	U	U	U	U
F	48	LOP	SD	U	U	U	I
M	40	LOP	R	U	U	C	C
M	25	GTCS	R	U	U	U	I
M	36	GTCS	R	U	U	U	I
F	19	LOP	SD	U	U	U	I
M	57	LOP	R	U	U	U	C
M	24	GTCS	SD	U	U	U	I
M	45	GTCS	SD	U	U	U	I
M	16	JME	NS	U	U	U	U
M	18	JME	SD	I	U	I	I
F	17	JAE	R	U	U	U	U
F	18	Uncl.	SD	U	U	U	U
F	25	JAE	R	U	U	U	U
M	31	GTCS	SD	I	U	I	I
M	23	GTCS	R	U	U	U	I
M	22	GTCS	SD	U	U	U	I
F	27	ASE	R	U	U	U	I
M	20	JME	SD	U	U	U	I
M	23	JME	SD	U	C	U	C
M	32	GTCS	R	C	U	U	U
F	18	AwEM	SD	U	I	U	I
M	16	GTCS	NS	U	U	U	I
M	20	GTCS	SD	U	U	U	I
M	28	JME	SD	U	U	U	I
F	16	JAE	R	U	U	U	U

Table C.2: IGE-cohort: biomarkers. AwEM: absences with eyelid myoclonia, ASE: absence status epilepticus, GTCS: generalised tonic clonic seizures only, JAE: juvenile absence epilepsy, JME: juvenile myoclonic epilepsy, LOP: late onset photosensitive, ; R: routine EEG, SD: Sleep Deprivation, P: portable/inpatient, NS: natural sleep; C: classified as *control* I: classified as *IGE*, U: classified as *uncertain*.

Gender	Age	Alpha	Degree	Global	Local
M	30	U	U	U	U
M	22	U	C	U	C
M	24	U	U	U	C
F	29	C	U	C	C
F	26	U	U	U	U
M	30	U	U	U	C
F	30	U	U	U	C
M	28	U	U	U	U
F	31	C	U	C	C
F	19	U	C	U	C
F	46	C	U	C	C
M	25	C	U	C	C
M	20	U	U	U	C
F	18	U	U	U	C
M	26	C	U	C	C
F	30	U	U	U	U
M	23	U	U	U	U
M	22	U	U	U	U
M	23	C	U	C	C
F	30	U	U	U	C
F	28	I	U	U	U
F	37	C	U	C	C
M	20	C	U	C	C
F	28	U	U	U	U
F	28	C	C	C	C
M	52	C	U	C	C
F	27	C	U	C	C
F	27	C	C	C	C
M	45	U	U	U	C
F	38	C	U	C	C
M	25	C	U	C	C
F	49	U	U	U	U
F	41	U	U	U	U
F	39	U	I	I	U
M	37	U	C	U	U
F	24	C	C	C	C
M	51	U	U	U	U
M	26	U	U	U	C

Table C.3: Control-cohort: biomarkers. C: classified as *control* I: classified as *IGE*, U: classified as *uncertain*.

Bibliography

[1] Abbott, L.F. (1999). Lapicque's introduction of the integrate-and-fire model neuron (1907). *Brain Research Bulletin*, 50(5-6):303–304.

[2] Acebrón, J.A., Spigler, R., Matematica, D., Tre, R. , Murialdo, L.S.L. (2005). The Kuramoto model: A simple paradigm for synchronization phenomena. *Reviews of Modern Physics*, 77(January):138–182.

[3] Alarcón, G. , Valentín, A. (2012). *Introduction to epilepsy.* Cambridge University Press.

[4] Allen, A.J., Griss, M.E., Folley, B.S., Hawkins, K.A. , Pearlson, G.D. (2009). Endophenotypes in schizophrenia: A selective review. *Schizophrenia Research*, 109(1-3):24–37.

[5] Amari, S.I. (1975). Homogeneous Nets of Neuron-Like Elements. *Biological Cybernetics*, 17(4):211–220.

[6] Andermann, F. , Berkovic, S.F. (2001). Idiopathic generalized epilepsy with generalized and other seizures in adolescence. *Epilepsia*, 42(3):317–320.

[7] Anderson, W.S., Azhar, F., Kudela, P., Bergey, G.K. , Franaszczuk, P.J. (2012). Epileptic seizures from abnormal networks: Why some seizures defy predictability. *Epilepsy Research*, 99(3):202–213.

[8] Arts, W.F.M., Brouwer, O.F., Peters, A.C.B., Stroink, H., Peeters, E.A.J., Schmitz, P.I.M. et al. (2004). Course and prognosis of childhood epilepsy: 5-Year follow-up of the Dutch study of epilepsy in childhood. *Brain*, 127(8):1774–1784.

[9] Badawy, R.A.B., Freestone, D.R., Lai, A. , Cook, M.J. (2012a). Epilepsy: Ever-changing states of cortical excitability. *Neuroscience*, 222:89–99.

[10] Badawy, R.A.B., Loetscher, T., Macdonell, R.A.L. , Brodtmann, A. (2012b). Cortical excitability and neurology: Insights into the pathophysiology. *Functional Neurology*, 27(3):131–145.

[11] Badawy, R.A.B., Strigaro, G. , Cantello, R. (2014). TMS, cortical excitability and epilepsy: The clinical impact. *Epilepsy Research*, 108(2):153–161.

[12] Balázsi, G., Cornell-Bell, A., Neiman, a.B. , Moss, F. (2001). Synchronization of hyperexcitable systems with phase-repulsive coupling. *Physical Review E*, 64(4 Pt 1):041912.

[13] Barnett, L. , Seth, A.K. (2014). The MVGC multivariate Granger causality toolbox: A new approach to Granger-causal inference. *Journal of Neuroscience Methods*, 223:50–68.

[14] Barreto, E., Hunt, B., Ott, E. , So, P. (2008). Synchronization in networks of networks: The onset of coherent collective behavior in systems of interacting populations of heterogeneous oscillators. *Physical Review E*, 77:1–7.

[15] Barry, R.J., Clarke, A.R., Johnstone, S.J. , Brown, C.R. (2007). EEG differences in children between eyes-closed and eyes-open resting conditions. *Clinical Neurophysiology*, 120(10):1806–1811.

[16] Ben-Ari, Y., Gaiarsa, J., Tyzio, R. , Khazipov, R. (2007). GABA: a pioneer transmitter that excites immature neurons and generates primitive oscillations. *Physical Review E*, 87(4):1215–1284.

[17] Benayoun, M., Cowan, J.D., van Drongelen, W. , Wallace, E. (2010). Avalanches in a Stochastic Model of Spiking Neurons. *PLoS Computational Biology*, 6(7):21.

[18] Benbadis, S.R. (2007). Errors in EEGs and the misdiagnosis of epilepsy: Importance, causes, consequences, and proposed remedies. *Epilepsy and Behavior*, 11(3):257–262.

[19] Benjamin, O., Fitzgerald, T.H., Ashwin, P., Tsaneva-Atanasova, K., Chowdhury, F.A., Richardson, M.P. et al. (2012). A phenomenological model of seizure initiation suggests network structure may explain seizure frequency in idiopathic generalised epilepsy. *Journal of Mathematical Neuroscience*, 2(1):1.

[20] Berg, A.T. (2008). Risk of recurrence after a first unprovoked seizure. *Epilepsia*, 49 Suppl 1:13–18.

[21] Berg, A.T., Berkovic, S.F., Brodie, M.J., Buchhalter, J., Cross, J.H., van Emde Boas, W. et al. (2010). Revised terminology and concepts for organization of seizures and epilepsies: Report of the ILAE Commission on Classification and Terminology, 2005-2009. *Epilepsia*, 51(4):676–685.

[22] Berg, A.T. , Scheffer, I.E. (2011). New concepts in classification of the epilepsies: Entering the 21st century. *Epilepsia*, 52(6):1058–1062.

[23] Berger, H. (1929). Über das Elektrenkephalogramm des Menschen. Zweite mitteilung Ü. *Psychiatrie und Nervenkrankheiten*, 87:527–570.

[24] Bishop, C.M. (2006). *Pattern Recognition and Machine Learning*. Springer Berlin.

[25] Blenkinsop, A., Valentin, A., Richardson, M.P. , Terry, J.R. (2012). The dynamic evolution of focal-onset epilepsies - combining theoretical and clinical observations. *European Journal of Neuroscience*, 36(2):2188–2200.

[26] Blumenfeld, H. (2005). Cellular and network mechanisms of genetically-determined absence seizures. *Thalamus and Related Systems*, 3(May):181.

[27] Boccaletti, S., Latora, V., Moreno, Y., Chavez, M. , Hwang, D.U. (2006). Complex networks: Structure and dynamics. *Physics Reports*, 424(4-5):175–308.

[28] Breakspear, M., Roberts, J.A., Terry, J.R., Rodrigues, S., Mahant, N. , Robinson, P.A. (2006). A Unifying Explanation of Primary Generalized Seizures Through Nonlinear Brain Modeling and Bifurcation Analysis. *Cerebral Cortex*, 16(9):1296–1313.

[29] Bressloff, P.C. (2012). Spatiotemporal dynamics of continuum neural fields. *Journal of Physics A: Mathematical and Theoretical*, 45(3):033001.

[30] Bressloff, P.C. , Coombes, S. (1997). Physics of the Extended Neuron. *International Journal of Modern Physics B*, 11:2343–2392.

[31] Bullmore, E. , Sporns, O. (2009). Complex brain networks: graph theoretical analysis of structural and functional systems. *Nature Reviews Neuroscience*, 10(3):186–198.

[32] Buszaki, G. (2006). *Rhythms of the Brain*. University Press, Oxford.

[33] Buzsaki, G. (1991). The thalamic clock: Emergent network properties. *Neuroscience*, 41(2-3):351–364.

[34] Campen, J.S.V., Hompe, E.L., Jansen, F.E., Velis, D.N., Otte, W.M., Berg, F.V.D. et al. (2016). Cortisol fluctuations relate to interictal epileptiform discharges in stress sensitive epilepsy. *Brain*, pages 1–7.

[35] Chahboune, H., Mishra, A.M., DeSalvo, M.N., Staib, L.H., Purcaro, M., Scheinost, D. et al. (2009). DTI abnormalities in anterior corpus callosum of rats with spike-wave epilepsy. *NeuroImage*, 47(2):459–466.

[36] Chavez, M., Martinerie, J. , Le Van Quyen, M. (2003). Statistical assessment of nonlinear causality: Application to epileptic EEG signals. *Journal of Neuroscience Methods*, 124(2):113–128.

[37] Chavez, M., Valencia, M., Navarro, V., Latora, V. , Martinerie, J. (2010). Functional modularity of background activities in normal and epileptic brain networks. *Physical Review Letters*, 104(11):1–4.

[38] Chowdhury, F.A., Elwes, R.D.C., Koutroumanidis, M., Morris, R.G., Nashef, L. , Richardson, M.P. (2014). Impaired cognitive function in idiopathic generalized epilepsy and unaffected family members: An epilepsy endophenotype. *Epilepsia*, 55(6):835–840.

[39] Choy, M., Dube, C.M., Patterson, K., Barnes, X.S.R., Maras, P., Blood, A.B. et al. (2014). A Novel, Noninvasive, Predictive Epilepsy Biomarker with Clinical Potential. *The Journal of Neuroscience*, 34(26):8672–8684.

[40] Coenen, A.M.L. , van Luijtelaar, E.L.J.M. (2003). Genetic Animal Models for Absence Epilepsy: A Review of the WAG/Rij Strain of Rats. *Behavior Genetics*, 33(6):635–655.

[41] Commission on Classification and Terminology of the International League Against Epilepsy (1989). Proposal for Revised Classification of Epilepsies and Epileptic Syndromes. *Epilepsia*, 30(4):389–399.

[42] Connor, J.A. , Stevens, C.F. (1971). Prediction of repetitive firing behaviour from voltage clamp data on an isolated neurone soma. *The Journal of Physiology*, 213(1):31–53.

[43] Coombes, S. (2005). Waves, bumps, and patterns in neural field theories. *Biological Cybernetics*, 93(2):91–108.

[44] Coombes, S. (2010). Large-scale neural dynamics: Simple and complex. *NeuroImage*, 52(3):731–739.

[45] Coombes, S. , Terry, J.R. (2012). The dynamics of neurological disease: Integrating computational, experimental and clinical neuroscience. *European Journal of Neuroscience*, 36(2):2118–2120.

[46] Coombes, S., Venkov, N.A., Shiau, L., Bojak, I., Liley, D.T.J. , Laing, C.R. (2007). Modeling electrocortical activity through improved local approximations of integral neural field equations. *Physical Review E*, 76(5):1–8.

[47] David, O. , Friston, K.J. (2003). A neural mass model for MEG/EEG: coupling and neuronal dynamics. *NeuroImage*, 20(3):1743–1755.

[48] Dayan, P. , Abbott, L. (2001). *Theoretical Neuroscience: Computational and Mathematical Modeling of Neural Systems*. MIT Press, Cambridge.

[49] de Kovel, C.G.F., Trucks, H., Helbig, I., Mefford, H.C., Baker, C., Leu, C. et al. (2010). Recurrent microdeletions at 15q11.2 and 16p13.11 predispose to idiopathic generalized epilepsies. *Brain*, 133(1):23–32.

[50] Deco, G., Jirsa, V.K., Robinson, P.A., Breakspear, M. , Friston, K.J. (2008). The Dynamic Brain: From Spiking Neurons to Meural Masses and Cortical Fields. *PLoS Computational Biology*, 4(8).

[51] Degen, R., Degen, H.E. , Roth, C. (1990). Some genetic aspects of idiopathic and symptomatic absence seizures: waking and sleep EEGs in siblings. *Epilepsia*, 31(6):784–794.

[52] Delorme, A. , Makeig, S. (2004). EEGLAB: An open source toolbox for analysis of single-trial EEG dynamics including independent component analysis. *Journal of Neuroscience Methods*, 134(1):9–21.

[53] Destexhe, A. (1998). Spike-and-Wave Oscillations Based on the Properties of GABAb Receptors. *The Journal of Neuroscience*, 18(21):9099–9111.

[54] Destexhe, A. (1999). Can GABAa conductances explain the fast oscillation frequency of absence seizures in rodents? *European Journal of Neuroscience*, 11(6):2175–2181.

[55] Destexhe, A., Contreras, D. , Steriade, M. (2001). LTS cells in cerebral cortex and their role in generating spike-and-wave oscillations. *Neurocomputing*, 38-40:555–563.

[56] Destexhe, A. , Sejnowski, T. (1995). G-protein activation kinetics and spill-over of GABA may account for differences between inhibitory responses in the hippocampus and thalamus. *PNAS*, 92:9515–9519.

[57] Destexhe, A. , Sejnowski, T. (2001). *Thalamocortical Assemblies*. University Press, Oxford.

[58] Destexhe, A. , Sejnowski, T.J. (2009). The Wilson-Cowan model, 36 years later. *Physical Review E*, 101(1):1–2.

[59] Díaz-Negrillo, A. (2013). Influence of sleep and sleep deprivation on ictal and interictal epileptiform activity. *Epilepsy Research and Treatment*, 2013:492524.

[60] Dibbens, L.M., Mullen, S., Helbig, I., Mefford, H.C., Bayly, M.A., Bellows, S. et al. (2009). Familial and sporadic 15q13.3 microdeletions in idiopathic generalized epilepsy: Precedent for disorders with complex inheritance. *Human Molecular Genetics*, 18(19):3626–3631.

[61] Doose, H. , Baier, W.K. (1987). Genetic factors in epilepsies with primarily generalized minor seizures. *Neuropediatrics*, 18(S 1):1–64.

[62] Engel, J., Thompson, P.M., Stern, J.M., Staba, R.J., Bragin, A. , Mody, I. (2013). Connectomics and epilepsy. *Current Opinion in Neurology*, 26(2):186–94.

[63] Ermentrout, G. , Terman, D. (2010). *Mathematical Foundations of Neuroscience*. Springer, Berlin.

[64] Faugeras, O., Touboul, J. , Cessac, B. (2009). A constructive mean-field analysis of multi-population neural networks with random synaptic weights and stochastic inputs. *Frontiers in Computational Neuroscience*, 3:1.

[65] Fisher, R.S., Acevedo, C., Arzimanoglou, A., Bogacz, A., Cross, J.H., Elger, C.E. et al. (2014). A practical clinical definition of epilepsy. *Epilepsia*, 55(4):475–482.

[66] Fisher, R.S., Boas, W.E., Blume, W., Elger, C.E., Genton, P., Lee, P. et al. (2005). Epileptic Seizures and Epilepsy: Definitions Proposed by the International League Against Epilepsy (ILAE) and the International Bureau for Epilepsy (IBE). *Epilepsia*, 46(4):470–472.

[67] FitzHugh, R. (1955). Mathematical models of threshold phenomena in the nerve membrane. *The Bulletin of Mathematical Biophysics*, 17(4):257–278.

[68] Freeman, W. (1975). *Mass Action in the Nervous System*. Academic Press, New York.

[69] Freeman, W.J., Rogers, L.J., Holmes, M.D. , Silbergeld, D.L. (2000). Spatial spectral analysis of human electrocorticograms including the alpha and gamma bands. *Journal of Neuroscience Methods*, 95(2):111–121.

[70] Freestone, D.R., Aram, P., Dewar, M., Scerri, K., Grayden, D.B. , Kadirkamanathan, V. (2011a). A data-driven framework for neural field modeling. *NeuroImage*, 56(3):1043–1058.

[71] Freestone, D.R., Kuhlmann, L., Chong, M., Nesic, D., Grayden, D.B., Aram, P. et al. (2013). Patient-specific neural mass modeling - stochastic and deterministic methods. *Recent Advances in Predicting and Preventing Epileptic Seizures*, pages 63–82.

[72] Freestone, D.R., Kuhlmann, L., Grayden, D.B., Burkitt, A.N., Lai, A., Nelson, T.S. et al. (2011b). Electrical probing of cortical excitability in patients with epilepsy. *Epilepsy and Behavior*, 22(SUPPL. 1):S110–S118.

[73] Freyer, F., Roberts, J.A., Ritter, P. , Breakspear, M. (2012). A Canonical Model of Multistability and Scale-Invariance in Biological Systems. *PLoS Computational Biology*, 8(8):e1002634.

[74] Friedman, M. (1937). Normality Implicit in the Analysis of Variance. *Journal of the American Statistical Association*, 32:675–701.

[75] Friston, K.J., Moran, R. , Seth, A.K. (2013). Analysing connectivity with Granger causality and dynamic causal modelling. *Current Opinion in Neurobiology*, 23(2):172–178.

[76] Galanopoulou, A.S. , Moshé, S.L. (2011). In search of epilepsy biomarkers in the immature brain: goals, challenges and strategies. *Biomarkers in medicine*, 5(5):615–628.

[77] Gerken, H. , Doose, H. (1973). On the genetics of EEG-anomalies in childhood 3. Spikes and waves. *Neuropädiatrie*, 4(1):88.

[78] Goldensohn, E. , Purpura, D. (1963). Intracellular Potentials of Cortical Neurons during Focal Epileptogenic Discharges. *Science*, 139(2):2–4.

[79] Goodfellow, M. , Glendinning, P. (2013). Mechanisms of Intermittent State Transitions in a Coupled Heterogeneous Oscillator Model of Epilepsy. *Journal of mathematical neuroscience*, 3(1):17.

[80] Goodfellow, M., Schindler, K.A. , Baier, G. (2011). Intermittent spike-wave dynamics in a heterogeneous, spatially extended neural mass model. *NeuroImage*, 55(3):920–932.

[81] Goodfellow, M., Schindler, K.A. , Baier, G. (2012a). Self-organised transients in a neural mass model of epileptogenic tissue dynamics. *NeuroImage*, 59(3):2644–2660.

[82] Goodfellow, M., Taylor, P.N., Wang, Y., Garry, D.J. , Baier, G. (2012b). Modelling the role of tissue heterogeneity in epileptic rhythms. *European Journal of Neuroscience*, 36(2):2178–2187.

[83] Gottesman, I.I. , Gould, T.D. (2003). The Endophenotype Concept in Psychiatry: Etymology and Strategic Intentions. *Amercian Journal of Psychiatry*, 160(April):636–645.

[84] Gregory, R.P., Oates, T. , Merry, R.T.G. (1993). Electroencephalogram epileptiform abnormalities in candidates for aircrew training. *Electroencephalography and Clinical Neurophysiology*, 86(1):75–77.

[85] Grimbert, F. , Faugeras, O. (2006). Bifurcation Analysis of Jansen's Neural Mass Model. *Neural computation*, 18(12):3052–3068.

[86] Guevara, R., Velazquez, J., Nenadovic, V., Wennberg, R., Senjanovic, G. , Domingues, L. (2005). Phase Synchronization Measurements Using Electroencephaologographic Recordings. *Neuroinformatics*, 3(1):11–34.

[87] Hall, D. , Kuhlmann, L. (2013). Mechanisms of Seizure Propagation in 2-Dimensional Centre-Surround Recurrent Networks. *PLoS ONE*, 8(8).

[88] Hastie, T., Tibshirani, R. , Friedman, J.H. (2011). *The elements of statistical learning: data mining, inference, and prediction*. Springer.

[89] Haut, S.R., Hall, C.B., Masur, J. , Lipton, R.B. (2007). Seizure occurrence: Precipitants and prediction. *Neurology*, 69(20):1905–1910.

[90] Helbig, I., Mefford, H.C., Sharp, A.J., Guipponi, M., Fichera, M., Franke, A. et al. (2009). 15Q13.3 Microdeletions Increase Risk of Idiopathic Generalized Epilepsy. *Nature genetics*, 41(2):160–162.

[91] Helbig, I., Scheffer, I.E., Mulley, J.C. , Berkovic, S.F. (2008). Navigating the channels and beyond: unravelling the genetics of the epilepsies. *The Lancet Neurology*, 7(3):231–245.

[92] Hindriks, R., Meijer, H.G.E., van Gils, S.A. , van Putten, M.J.A.M. (2013). Phase-locking of epileptic spikes to ongoing delta oscillations in non-convulsive status epilepticus. *Frontiers in Systems Neuroscience*, 7(December):111.

[93] Hodgkin, A.L. , Huxley, A.F. (1952). A quantitative description of membrane current and its application to conduction and excitation in nerve. *Bulletin of Mathematical Biology*, 52(1-2):25–71.

[94] Howard, P., Twycross, R., Shuster, J., Mihalyo, M., Remi, J. , Wilcock, A. (2011). Anti-epileptic Drugs. *Journal of Pain and Symptom Management*, 42(5):788–804.

[95] Huberfeld, G., Menendez de la Prida, L., Pallud, J., Cohen, I., Le Van Quyen, M., Adam, C. et al. (2011). Distinct mechanisms mediate interictal and pre-ictal discharges in human temporal lobe epilepsy. *Epilepsy Currents*, 11(6):200–202.

[96] Hutchings, F., Han, C.E., Keller, S.S., Weber, B., Taylor, P.N. , Kaiser, M. (2015). Predicting Surgery Targets in Temporal Lobe Epilepsy through Structural Connectome Based Simulations. *PLoS Computational Biology*, 11(12):1–24.

[97] Iannotti, G., Grouiller, F., Centeno, M., Carmichael, D.W., Abela, E., Wiest, R. et al. (2016). Epileptic networks are strongly connected with and without the effects of interictal discharges d e. *Epilepsia*, 10.1111/ep:1–11.

[98] Izhikevich, E. (2000). Neural Excitability, Spiking and Bursting. *International Journal of Bifurcation and Chaos*, 10(6):1171–1266.

[99] Izhikevich, E. (2007). *Dynamical Systems in Neuroscience: The Geometry of Excitability and Bursting*. MIT Press, Cambridge.

[100] Jallon, P. , Latour, P. (2005). Epidemiology of idiopathic generalized epilepsies. *Epilepsia*, 46(SUPPL. 9):10–14.

[101] Jansen, B.H. , Rit, V.G. (1995). Electroencephalogram and visual evoked potential generation in a mathematical model of coupled cortical columns. *Biological Cybernetics*, 73(4):357–366.

[102] Jayalakshmi, S.S., Mohandas, S., Sailaja, S. , Borgohain, R. (2006). Clinical and electroencephalographic study of first-degree relatives and probands with juvenile myoclonic epilepsy. *Seizure*, 15(3):177–183.

[103] Jirsa, V.K. , Haken, H. (1997). A derivation of a macroscopic field theory of the brain from the quasi-microscopic neural dynamics. *Physica D: Nonlinear Phenomena*, 99(4):503–526.

[104] Jirsa, V.K., Jantzen, K.J., Fuchs, A. , Kelso, J.A.S. (2002). Spatiotemporal forward solution of the EEG and MEG using network modeling. *IEEE Transactions on Medical Imaging*, 21(5):493–504.

[105] Jirsa, V.K., Stacey, W.C., Quilichini, P.P., Ivanov, A.I. , Bernard, C. (2014). On the nature of seizure dynamics. *Brain*, 137(8):2210–2230.

[106] Jiruska, P., de Curtis, M., Jefferys, J.G.R., Schevon, C.A., Schiff, S.J. , Schindler, K.A. (2013). Synchronization and desynchronization in epilepsy: controversies and hypotheses. *The Journal of Physiology*, 591(Pt 4):787–97.

[107] Joels, M. (2009). Stress, the hippocampus, and epilepsy. *Epilepsia*, 50(4):586–597.

[108] J.S., E. , T.A., P. (2003). *Current Practice of Clinical Electroencephalography*. LWW medical book collection. Lippincott Williams and Wilkins.

[109] Juarez-Garcia, A., Stokes, T., Shaw, B., Camosso-stefinovic, J. , Baker, R. (2006). The costs of epilepsy misdiagnosis in England and Wales. *Seizure*, 15:598–605.

[110] Kalamangalam, G.P., Tandon, N. , Slater, J.D. (2014). Dynamic mechanisms underlying afterdischarge: A human subdural recording study. *Clinical Neurophysiology*, 125(7):1324–1338.

[111] Kalitzin, S., Koppert, M., Petkov, G., Velis, D.N. , Lopes Da Silva, F.H. (2011). Computational model prospective on the observation of proictal states in epileptic neuronal systems. *Epilepsy and Behavior*, 22(SUPPL. 1):S102–S109.

[112] Kalitzin, S., Velis, D.N. , Lopes Da Silva, F.H. (2010). Stimulation-based anticipation and control of state transitions in the epileptic brain. *Epilepsy and Behavior*, 17(3):310–323.

[113] Kandel, E., Schwartz, J. , Jessel, T. (1991). *Principles of Neural Science*. Elsevier, New York.

[114] Karoly, P.J., Freestone, D.R., Boston, R., Grayden, D.B., Himes, D., Leyde, K. et al. (2016). Interictal spikes and epileptic seizures: their relationship and underlying rhythmicity. *Brain*, page aww019.

[115] Kasteleijn-Nolst Trenite, D. , Vermeiren, R. (2005). The impact of subclinical epileptiform discharges on complex tasks and cognition: relevance for aircrew and air traffic controllers. *Epilepsy and Behavior*, 6(1):31–34.

[116] Kellaway, P., Frost, J.D. , Crawley, J.W. (1980). Time modulation of spike-and-wave activity in generalized epilepsy. *Annals of Neurology*, 8(5):491–500.

[117] Kuramoto, Y. (1984). *Chemical Oscillations, Waves and Turbulence*. Springer, Berlin.

[118] Lachaux, J.p., Rodriguez, E., Martinerie, J. , Varela, F.J. (1999). Measuring phase synchrony in brain signals. *Human Brain Mapping*, 8(4):194–208.

[119] Larsson, G. , Kostov, H. (2005). Lower frequency variability in the alpha activity in EEG among patients with epilepsy. *Clinical Neurophysiology*, 116:2701–2706.

[120] Lehnertz, K. (2008). Epilepsy and Nonlinear Dynamics. *Journal of Biological Physics*, 34(3-4 SPEC. ISS.):253–266.

[121] Lehnertz, K., Ansmann, G., Bialonski, S., Dickten, H., Geier, C. , Porz, S. (2014). Evolving networks in the human epileptic brain. *Physica D: Nonlinear Phenomena*, 267:7–15.

[122] Liao, W., Zhang, Z., Mantini, D., Xu, Q., Ji, G.J., Zhang, H. et al. (2013). Dynamical intrinsic functional architecture of the brain during absence seizures. *Brain structure & function*, 219(6):2001–2015.

[123] Liley, D.T.J. , Bojak, I. (2005). Understanding the transition to seizure by modeling the epileptiform activity of general anesthetic agents. *Journal of Clinical Neurophysiology*, 22(5):300–313.

[124] Liley, D.T.J., Cadusch, P.J. , Dafilis, M.P. (2002). A spatially continuous mean field theory of electrocortical activity. *Network*, 13(1):67–113.

[125] Lopes Da Silva, F.H., Blanes, W., Kalitzin, S., Parra, J., Suffczynski, P. , Velis, D.N. (2003). Dynamical diseases of brain systems: different routes to epileptic seizures. *IEEE Transactions on Biomedical Engineering*, 50(5):540–548.

[126] Lytton, W.W. (2008). Computer modelling of epilepsy. *Nature Reviews Neuroscience*, 9(8):626–637.

[127] Maneshi, M., Moeller, F., Fahoum, F., Gotman, J. , Grova, C. (2012). Resting-State Connectivity of the Sustained Attention Network Correlates with Disease Duration in Idiopathic Generalized Epilepsy. *PLoS ONE*, 7(12).

[128] Markram, H. (2006). The Blue Brain Project. *Nature Reviews Neuroscience*, 7(2):153–160.

[129] Marson, A., Jacoby, A., Johnson, A., Kim, L., Gamble, C. , Chadwick, D. (2005). Immediate versus deferred antiepileptic drug treatment for early epilepsy and single seizures: A randomised controlled trial. *Lancet*, 365(9476):2007–2013.

[130] Marten, F., Rodrigues, S., Benjamin, O., Richardson, M.P. , Terry, J.R. (2009a). Onset of polyspike complexes in a mean-field model of human electroencephalography and its application to absence epilepsy. *Philosophical transactions. Series A, Mathematical, physical, and engineering sciences*, 367(1891):1145–61.

[131] Marten, F., Rodrigues, S., Suffczynski, P., Richardson, M.P. , Terry, J.R. (2009b). Derivation and analysis of an ordinary differential equation mean-field model for studying clinically recorded epilepsy dynamics. *Physical Review E*, 79(2):1–7.

[132] Marvel, S.A. , Strogatz, S.H. (2009). Invariant submanifold for series arrays of Josephson junctions. *Chaos*, 19:013132.

[133] Mattson, R.H. (2003). Overview: Idiopathic Generalized Epilepsies. *Epilepsia*, 44 Suppl 2:2–6.

[134] McCormick, D.A. , Contreras, D. (2001). On The Cellular and Network Bases of Epileptic Seizures. *Annual Reviews Physiology*, 63:815–846.

[135] Meeren, H.K.M., Pijn, J.P.M., van Luijtelaar, E.L.J.M., Coenen, A.M.L. , Lopes Da Silva, F.H. (2002). Cortical focus drives widespread corticothalamic networks during spontaneous absence seizures in rats. *The Journal of Neuroscience*, 22(4):1480–1495.

[136] Meeren, H.K.M., van Luijtelaar, E.L.J.M., Lopes Da Silva, F.H. , Coenen, A.M.L. (2005). Evolving concepts on the pathophysiology of absence seizures: the cortical focus theory. *Archives of Neurology*, 62(3):371–6.

[137] Meisel, C., Schulze-Bonhage, A., Freestone, D., Cook, M.J., Achermann, P. , Plenz, D. (2015). Intrinsic excitability measures track antiepileptic drug action and uncover increasing/decreasing excitability over the wake/sleep cycle. *Proceedings of the National Academy of Sciences*, 112(47):14694–14699.

[138] Meisel, C., Storch, A., Hallmeyer-Elgner, S., Bullmore, E. , Gross, T. (2012). Failure of adaptive self-organized criticality during epileptic seizure attacks. *PLoS Computational Biology*, 8(1).

[139] Milton, J.G. (2010). Epilepsy as a dynamic disease: A tutorial of the past with an eye to the future. *Epilepsy and Behavior*, 18(1-2):33–44.

[140] Molaee-Ardekani, B., Benquet, P., Bartolomei, F. , Wendling, F. (2010). Computational modeling of high-frequency oscillations at the onset of neocortical partial seizures: From 'altered structure' to 'dysfunction'. *NeuroImage*, 52(3):1109–1122.

[141] Moran, R., Pinotsis, D.A. , Friston, K.J. (2013). Neural masses and fields in dynamic causal modeling. *Frontiers in Computational Neuroscience*, 7(May):57.

[142] Mormann, F., Andrzejak, R.G., Elger, C.E. , Lehnertz, K. (2007). Seizure prediction: The long and winding road. *Brain*, 130(2):314–333.

[143] Morris, C. , Lecar, H. (1981). Voltage oscillations in the barnacle giant muscle fiber. *Biophysical Journal*, 35(1):193–213.

[144] Motelow, J. , Blumenfeld, H. (2009). Functional Neuroimaging of Spike-Wave Seizures. *Methods Molecular Biology*, 489(3):81–91.

[145] Mountcastle, V.B. (1997). The columnar organization of the neocortex. *Brain*, 120(4):701–722.

[146] Murta, T., Leal, A., Garrido, M.I. , Figueiredo, P. (2012). Dynamic Causal Modelling of epileptic seizure propagation pathways: A combined EEG-fMRI study. *NeuroImage*, 62(3):1634–1642.

[147] Naylor, S. (2005). Overview of biomarkers in disease , drug discovery. *Drug Discovery World*, Spring:21–29.

[148] Nevado-Holgado, A.J., Marten, F., Richardson, M.P. , Terry, J.R. (2011). Characterising the dynamics of EEG waveforms as the path through parameter space of a neural mass model: Application to epilepsy seizure evolution. *NeuroImage*, 59(3):2374–2392.

[149] NICE (2012). NICE guidelines: Epilepsies: diagnosis and management [CG137]. Available via NICE: https://www.nice.org.uk/guidance/CG137.

[150] NICE (2016). NICE Pathways: Diagnosing epilepsy and supporting investigations. Available via NICE: http://pathways.nice.org.uk/pathways/epilepsy.

[151] Niedermeyer, E. , Lopes da Silva, F. (2005). *Electroencephalography: Basic Principles, Clinical Applications, and Related Fields*. Lippincott Williams & Wilkins.

[152] Noachtar, S., Binnie, C., Ebersole, J., Mauguière, F., Sakamoto, A. , Westmoreland, B. (1999). A glossary of terms most commonly used by clinical electroencephalographers and proposal for the report form for the EEG findings. *Electroencephalography and Clinical Neurophysiology. Supplement*, 52:21–41.

[153] Nunez, P. , Srinivasan, R. (2006). *Electric Fields of the Brain: The Neurophysics of EEG, 2nd Edition*. Oxford University Press, New York.

[154] Obrist, W. (1954). The electroencephalogram of normal aged adults. *EEG Clinical Neurophysiology*, 6:235–244.

[155] O'Hagan, A. (2006). Bayesian analysis of computer code outputs: A tutorial. *Reliability Engineering and System Safety*, 91(10-11):1290–1300.

[156] Okubo, Y., Asai, K. , Toru, M. (1993). A Follow-Up Study of Healthy Children with Epileptiform EEG Discharges. *Journal of Epilepsy*, 6:250–256.

[157] Okubo, Y., Matsuura, M., Asai, T., Asai, K., Kato, M., Kojima, T. et al. (1994). Epileptiform EEG Discharges in Healthy-Children: Prevalence, Emotional and Behavioral-Correlates, and Genetic Influences. *Epilepsia*, 35(4):832–841.

[158] O'Muircheartaigh, J., Vollmar, C. , Barker, G. (2011). Focal structural changes and cognitive dysfunction in juvenile myoclonic epilepsy. *Neurology*.

[159] Organization, W.H. (2012). Fact Sheet 999 Epilepsy. Available via World Health Organization: http://www.who.int/mediacentre/factsheets/fs999/en/.

[160] Osorio, I., Frei, M.G., Sornette, D., Milton, J.G. , Lai, Y.C. (2010). Epileptic seizures: Quakes of the brain? *Physical Review E*, 82(2):1–13.

[161] Ott, E. , Antonsen, T.M. (2008). Low dimensional behavior of large systems of globally coupled oscillators. *Chaos*, 18:037113.

[162] Ott, E., Antonsen, T.M., Ott, E. , Antonsen, T.M. (2009). Long time evolution of phase oscillator systems. *Chaos*, 19:023117.

[163] Owen, J.A., Barreto, E. , Cressman, J.R. (2013). Controlling Seizure-Like Events by Perturbing Ion Concentration Dynamics with Periodic Stimulation. *PLoS ONE*, 8(9).

[164] Pal, D.K., Strug, L.J. , Greenberg, D.A. (2008). Evaluating candidate genes in common epilepsies and the nature of evidence. *Epilepsia*, 49(3):386–392.

[165] Pavlova, M.K., Shea, S.A., Scheer, F.A.J.L. , Bromfield, E.B. (2009). Is there a circadian variation of epileptiform abnormalities in idiopathic generalized epilepsy? *Epilepsy and Behavior*, 16(3):461–467.

[166] Pellegrini, A., Musgrave, J. , Gloor, P. (1979). Role of afferent input of subcortical origin in the genesis of bilaterally synchronous epileptic discharges of feline generalized penicillin epilepsy. *Experimental Neurology*, 64(1):155–173.

[167] Peraza, L.R., Asghar, A.U.R., Green, G. , Halliday, D.M. (2012). Volume conduction effects in brain network inference from electroencephalographic recordings using phase lag index. *Journal of Neuroscience Methods*, 207(2):189–199.

[168] Pereda, E., Quiroga, R.Q. , Bhattacharya, J. (2005). Nonlinear multivariate analysis of neurophysiological signals. *Progress in Neurobiology*, 77(1-2):1–37.

[169] Pesce, L.L., Lee, H.C., Hereld, M., Visser, S., Stevens, R.L. , van Drongelen, W. (2013). Scaling Properties of Two Parallel Neuronal Network Simulation Algorithms. *Computational and Mathematical Methods in Medicine*, 2013.

[170] Petkov, G., Goodfellow, M., Richardson, M.P. , Terry, J.R. (2014). A critical role for network structure in seizure onset: A computational modeling approach. *Frontiers in Neurology*, 5(Dec):1–7.

[171] Pillai, J. , Sperling, M.R. (2006). Interictal EEG and the diagnosis of epilepsy. *Epilepsia*, 47(SUPPL. 1):14–22.

[172] Pittau, F., Mégevand, P., Sheybani, L., Abela, E., Grouiller, F., Spinelli, L. et al. (2014). Mapping epileptic activity: sources or networks for the clinicians? *Frontiers in Neurology*, 5(November):1–21.

[173] Ponten, S.C., Douw, L., Bartolomei, F., Reijneveld, J.C. , Stam, C.J. (2009). Indications for network regularization during absence seizures: Weighted and unweighted graph theoretical analyses. *Experimental Neurology*, 217(1):197–204.

[174] Power, J.D., Fair, D.A., Schlaggar, B.L. , Petersen, S.E. (2010). The Development of Human Functional Brain Networks. *Neuron*, 67(5):735–748.

[175] Prince, D. (1982). Mechanisms of epileptogenesis in brain-slice model systems. *Research publications-Association for Research in Nervous and Mental Disease*, 61:29–52.

[176] Purves, D., Augustine, G., Fitzpatrick, D., Hall, W., LaMantia, A.S. , White, L. (2012). *Neuroscience, 5th Edition*. Sinauer Associates, Sunderland, MA.

[177] Quraan, M.A., McCormick, C., Cohn, M., Valiante, T.A. , McAndrews, M.P. (2013). Altered Resting State Brain Dynamics in Temporal Lobe Epilepsy Can Be Observed in Spectral Power, Functional Connectivity and Graph Theory Metrics. *PLoS ONE*, 8(7).

[178] Richardson, M.P. (2010). Current themes in neuroimaging of epilepsy: Brain networks, dynamic phenomena, and clinical relevance. *Clinical Neurophysiology*, 121(8):1153–1175.

[179] Richardson, M.P. (2011). New observations may inform seizure models: Very fast and very slow oscillations. *Progress in Biophysics and Molecular Biology*, 105(1-2):5–13.

[180] Richardson, M.P. (2012). Large scale brain models of epilepsy: dynamics meets connectomics. *Journal of Neurology, Neurosurgery, and Psychiatry*, 83(12):1238–48.

[181] Robinson, P.A., Rennie, C.J. , Rowe, D.L. (2002). Dynamics of large-scale brain activity in normal arousal states and epileptic seizures. *Physical Review E*, 65(4):1–9.

[182] Robinson, P.A., Rennie, C.J. , Wright, J. (1997). Propagation and stability of waves of electrical activity in the cerebral cortex. *Physical Review E*, 56(1):826–840.

[183] Rodrigues, S., Barton, D., Marten, F., Kibuuka, M., Alarcon, G., Richardson, M.P. et al. (2010a). A method for detecting false bifurcations in dynamical systems: Application to neural-field models. *Biological Cybernetics*, 102(2):145–154.

[184] Rodrigues, S., Barton, D., Szalai, R., Benjamin, O., Richardson, M.P. , Terry, J.R. (2009). Transitions to spike-wave oscillations and epileptic

dynamics in a human cortico-thalamic mean-field model. *Journal of Computational Neuroscience*, 27(3):507–526.

[185] Rodrigues, S., Chizhov, A.V., Marten, F. , Terry, J.R. (2010b). Mappings between a macroscopic neural-mass model and a reduced conductance-based model. *Biological Cybernetics*, 102(5):361–371.

[186] Rogawski, M.A. , Loscher, W. (2004). The neurobiology of antiepileptic drugs. *Nature Reviews Neuroscience*, 5(7):553–564.

[187] Rubinov, M. , Sporns, O. (2010). Complex network measures of brain connectivity: Uses and interpretations. *NeuroImage*, 52(3):1059–1069.

[188] Schelter, B., Timmer, J. , Schulze-Bonhagel, A. (2008). *Seizure Prediction in Epilepsy*. Wiley, Weinheim.

[189] Schiff, S. (2011). *Neural control engineering: The emerging intersection between control theory and neuroscience*. MIT Press, Cambridge.

[190] Schindler, K.A., Bialonski, S., Horstmann, M.T., Elger, C.E. , Lehnertz, K. (2008). Evolving functional network properties and synchronizability during human epileptic seizures. *Chaos*, 18(3).

[191] Schmidt, H., Petkov, G., Richardson, M.P. , Terry, J.R. (2014). Dynamics on Networks : The Role of Local Dynamics and Global Networks on the Emergence of Hypersynchronous Neural Activity. *PLoS Computational Biology*, 10(11).

[192] Seneviratne, U., Cook, M. , D'Souza, W. (2015). Epileptiform K-complexes and sleep spindles: an underreported phenomenon in genetic generalized epilepsy. *Journal of clinical neurophysiology*, 33(2):156–161.

[193] Seneviratne, U., Cook, M.J. , D'Souza, W. (2012). The electroencephalogram of idiopathic generalized epilepsy. *Epilepsia*, 53(2):234–248.

[194] Seneviratne, U., Cook, M.J. , D'Souza, W. (2016a). Consistent topography and amplitude symmetry are more typical than morphology of epileptiform discharges in genetic generalized epilepsy. *Clinical Neurophysiology*, 127(2):1138–1146.

[195] Seneviratne, U., Hepworth, G., Cook, M.J. , D'Souza, W. (2016b). Atypical EEG abnormalities in genetic generalized epilepsies. *Clinical Neurophysiology*, 127(1):214–220.

[196] Seth, A.K. (2010). A MATLAB toolbox for Granger causal connectivity analysis. *Journal of Neuroscience Methods*, 186(2):262–273.

[197] Shackman, A., McMenamin, B., Maxwell, J., Greischar, L. , Davidson, R. (2010). Identifying Robust and Sensitive Frequency Bands for Interrogating Neural Oscillations. *Neuroimage*, 51(4):1319–1333.

[198] Skardal, P.S. , Restrepo, J.G. (2012). Hierarchical synchrony of phase oscillators in modular networks. *Physical Review E*, 85:016208.

[199] Smit, D.J.A., Boersma, M., van Beijsterveldt, C.E.M., Posthuma, D., Boomsma, D.I., Stam, C.J. et al. (2010). Endophenotypes in a dynamically connected brain. *Behavior Genetics*, 40(2):167–177.

[200] Smit, D.J.A., Stam, C.J., Posthuma, D., Boomsma, D.I. , de Geus, E.J.C. (2008). Heritability of "small-world" networks in the brain: A graph theoretical analysis of resting-state EEG functional connectivity. *Human Brain Mapping*, 29(12):1368–1378.

[201] Smith, D., Defalla, B.A. , Chadwick, D.W. (1999). The misdiagnosis of epilepsy and the management of refractory epilepsy in a specialist clinic. *Quarterly Journal of Medicine*, 92:15–23.

[202] Smith, S.J.M. (2005). EEG in the diagnosis, classification, and management of patients with epilepsy. *Journal of Neurology, Neurosurgery, and Psychiatry*, 76(Suppl II):ii2–ii7.

[203] So, E.L. (2010). Interictal epileptiform discharges in persons without a history of seizures: what do they mean? *Journal of Clinical Neurophysiology*, 27(4):229–238.

[204] Soltesz, I. , Staley, K. (2008). *Computational Neuroscience in Epilepsy*. Academic Press, San Diego.

[205] Sporns, O., Tononi, G. , Kötter, R. (2005). The human connectome: A structural description of the human brain. *PLoS Computational Biology*, 1(4):0245–0251.

[206] Stam, C.J., de Haan, W., Daffertshofer, A., Jones, B.F., Manshanden, I., van Cappellen Van Walsum, A.M. et al. (2009). Graph theoretical analysis of magnetoencephalographic functional connectivity in Alzheimer's disease. *Brain*, 132(1):213–224.

[207] Stam, C.J., Jones, B.F., Nolte, G., Breakspear, M. , Scheltens, P. (2007). Small-world networks and functional connectivity in Alzheimer's disease. *Cerebral Cortex*, 17(1):92–99.

[208] Stead, M., Bower, M., Brinkmann, B.H., Lee, K., Marsh, W.R., Meyer, F.B. et al. (2010). Microseizures and the spatiotemporal scales of human partial epilepsy. *Brain*, 133(9):2789–2797.

[209] Stefanescu, R.A., Shivakeshavan, R.G. , Talathi, S.S. (2012). Computational models of epilepsy. *Seizure*, 21(10):748–759.

[210] Strogatz, S.H. (2000). From Kuramoto to Crawford : exploring the onset of synchronization in populations of coupled oscillators. *Physica D*, 143:1–20.

[211] Suffczynski, P., Kalitzin, S. , Lopes Da Silva, F.H. (2004). Dynamics of non-convulsive epileptic phenomena modeled by a bistable neuronal network. *Neuroscience*, 126(2):467–484.

[212] Suffczynski, P., Lopes Da Silva, F.H., Parra, J., Velis, D.N., Bouwman, B.M., van Rijn, C.M. et al. (2006). Dynamics of epileptic phenomena determined from statistics of ictal transitions. *IEEE Transactions on Biomedical Engineering*, 53(3):524–532.

[213] Tao, J.X., Baldwin, M., Hawes-Ebersole, S. , Ebersole, J.S. (2007). Cortical Substrates of Scalp EEG Epileptiform Discharges. *Journal of Clinical Neurophysiology*, 24(2):96–100.

[214] Tao, J.X., Ray, A., Hawes-Ebersole, S. , Ebersole, J.S. (2005). Intracranial EEG Substrates of Scalp EEG Interictal Spikes. *Epilepsia*, 46(5):669–676.

[215] Tass, P., Rosenblum, M.G., Weule, J., Kurths, J., Pikovsky, A., Volkmann, J. et al. (1998). Detection of n:m Phase Locking from Noisy Data: Application to Magnetoencephalography. *Physical Review Letters*, 81(15):3291–3294.

[216] Taylor, P.N. , Baier, G. (2011). A spatially extended model for macroscopic spike-wave discharges. *Journal of Computational Neuroscience*, 31(3):679–684.

[217] Tejada, J., Costa, K.M., Bertti, P. , Garcia-Cairasco, N. (2013). The epilepsies: Complex challenges needing complex solutions. *Epilepsy and Behavior*, 26(3):212–228.

[218] Terry, J.R., Benjamin, O. , Richardson, M.P. (2012). Seizure generation: The role of nodes and networks. *Epilepsia*, 53(9):1–4.

[219] Traub, R.D., Whittington, M.A., Buhl, E.H., LeBeau, F.E.N., Bibbig, A., Boyd, S. et al. (2001). A possible role for gap junctions in generation of very fast EEG oscillations preceding the onset of, and perhaps initiating, seizures. *Epilepsia*, 42(2):153–170.

[220] Tuunainen, A., Nousiainen, U., Pilke, A., Mervaala, E., Partanen, J. , Riekkinen, P. (1995). Spectral EEG During Short-Term Discontinuation of Antiepileptic Medication in Partial Epilepsy. *Epilepsia*, 36(8):817–823.

[221] Valentin, A., Alarcon, G., Garcia-Seoane, J., Lacruz, M., Nayak, S., Honavar, M. et al. (2005). Single-pulse electrical stimulation identifies epileptogenic frontal cortex in the human brain. *Neurology*, 65(3):426–435.

[222] van Donselaar, C.A., Stroink, H. , Arts, W.F. (2006). How confident are we of the diagnosis of epilepsy? *Epilepsia*, 47(Suppl. 1):9–13.

[223] van Drongelen, W. (2010). *Signal Processing for Neuroscientists, A Companion Volume, 1st Edition*. Elsevier.

[224] van Drongelen, W., Lee, H.C., Hereld, M., Chen, Z., Elsen, F.P. , Stevens, R.L. (2005). Emergent epileptiform activity in neural networks with weak excitatory synapses. *IEEE Transactions on Neural Systems and Rehabilitation Engineering*, 13(2):236–241.

[225] van Gils, S.A., Janssens, S.G., Kuznetsov, Y.A. , Visser, S. (2013). On local bifurcations in neural field models with transmission delays. *Journal of Mathematical Biology*, 66(4-5):837–887.

[226] van Putten, M. (2009). *Essentials of Neurophysiology: Basic Concepts and Clinical Applications for Scientists and Engineers, Book. Series: Series in Biomedical Engineering*. Springer Berlin.

[227] van Vreeswijk, C., Abbott, L.F. , Ermentrout, G. (1994). When inhibition not excitation synchronizes neural firing. *Journal of Computational Neuroscience*, 1(4):313–321.

[228] van Wijk, B.C.M., Stam, C.J. , Daffertshofer, A. (2010). Comparing brain networks of different size and connectivity density using graph theory. *PLoS ONE*, 5(10).

[229] Varela, F.J., Lachaux, J.p., Rodriguez, E. , Martinerie, J. (2001). The Brainweb : Phase synchronization and large-sale integration. *Nature Reviews Neuroscience*, 2(April).

[230] Vincent, R.D., Courville, A. , Pineau, J. (2011). A bistable computational model of recurring epileptiform activity as observed in rodent slice preparations. *Neural Networks*, 24(6):526–537.

[231] Visser, S., Meijer, H.G.E., Lee, H.C., van Drongelen, W., van Putten, M.J.A.M. , van Gils, S.A. (2010). Comparing epileptiform behavior of mesoscale detailed models and population models of neocortex. *Journal of Clinical Neurophysiology*, 27(6):471–8.

[232] Visser, S., Meijer, H.G.E., van Putten, M.J.A.M. , van Gils, S.A. (2012). Analysis of stability and bifurcations of fixed points and periodic solutions

of a lumped model of neocortex with two delays. *Journal of Mathematical Neuroscience*, 2(1):8.

[233] Vogels, T.P., Abbott, L.F. , Rajan, K. (2005). Neural Network Dynamics. *Annual Reviews Neuroscience*, 28:357–376.

[234] Volman, V., Perc, M. , Bazhenov, M. (2011). Gap junctions and epileptic seizures - two sides of the same coin? *PLoS ONE*, 6(5).

[235] Wang, H.E., Bénar, C.G., Quilichini, P.P., Friston, K.J., Jirsa, V.K. , Bernard, C. (2014). A systematic framework for functional connectivity measures. *Frontiers in Neuroscience*, 8(December):1–22.

[236] Wang, Y., Goodfellow, M., Taylor, P.N. , Baier, G. (2012). Phase space approach for modeling of epileptic dynamics. *Physical Review E*, 85(6):061918.

[237] Wendling, F. (2005). Neurocomputational models in the study of epileptic phenomena. *Journal of Clinical Neurophysiology*, 22(5):285.

[238] Wendling, F. (2008). Computational models of epileptic activity: a bridge between observation and pathophysiological interpretation. *Expert Review of Neurotherapeutics*, 8(6):889–896.

[239] Wendling, F., Bartolomei, F., Bellanger, J.J. , Chauvel, P. (2001). Interpretation of interdependencies in epileptic signals using a macroscopic physiological model of the EEG. *Clinical Neurophysiology*, 112(7):1201–1218.

[240] Wendling, F., Bartolomei, F., Mina, F., Huneau, C. , Benquet, P. (2012). Interictal spikes, fast ripples and seizures in partial epilepsies - combining multi-level computational models with experimental data. *European Journal of Neuroscience*, 36(2):2164–2177.

[241] Wendling, F., Bartolomei, F. , Senhadji, L. (2009). Spatial analysis of intracerebral EEG in the time and frequency domain : identification of epileptogenic networks in partial epilepsy. *Philosophical transactions. Series A, Mathematical, physical, and engineering sciences*, 367(1887):297–316.

[242] Whiston, S., Coyle, B. , Chappel, D. (2009). *Health needs assessment for long term neurological conditions in North East England.* North East Public Health Observatory.

[243] Wilson, H.R. , Cowan, J.D. (1972). Excitatory and inhibitory interactions in localized populations of model neurons. *Biophysical Journal*, 12(1):1–24.

[244] Wilson, H.R. , Cowan, J.D. (1973). A mathematical theory of the functional dynamics of cortical and thalamic nervous tissue. *Kybernetik*, 13(2):55–80.

[245] Worrell, G. , Gotman, J. (2011). High-frequency oscillations and other electrophysiological biomarkers of epilepsy: clinical studies. *Biomarkers in medicine*, 5(5):557–566.

[246] Worrell, G.A., Cranstoun, S.D., Echauz, J. , Litt, B. (2002). Evidence for self-organized criticality in human epileptic hippocampus. *Neuroreport*, 13(16):2017–2021.

[247] Wyllie, E., Comair, Y.G., Kotagal, P., Bulacio, J., Bingaman, W. , Ruggieri, P. (1998). Seizure outcome after epilepsy surgery in children and adolescents. *Annals of Neurology*, 44(5):740–748.

[248] Xue, K., Luo, C., Zhang, D., Yang, T., Li, J., Gong, D. et al. (2014). Diffusion tensor tractography reveals disrupted structural connectivity in childhood absence epilepsy. *Epilepsy Research*, 108(1):125–138.

[249] Yan, B. , Li, P. (2013). The emergence of abnormal hypersynchronization in the anatomical structural network of human brain. *NeuroImage*, 65:34–51.

[250] Zhang, Z., Liao, W., Chen, H., Mantini, D., Ding, J.R., Xu, Q. et al. (2011). Altered functional-structural coupling of large-scale brain networks in idiopathic generalized epilepsy. *Brain*, 134(10):2912–2928.

[251] Žiburkus, J., Cressman, J.R. , Schiff, S.J. (2013). Seizures as imbalanced up states: excitatory and inhibitory conductances during seizure-like events. *Journal of Neurophysiology*, 109(5):1296–306.

[252] Zijlmans, M., Jiruska, P., Zelmann, R., Leijten, F.S.S., Jefferys, J.G.R. , Gotman, J. (2012). High-Frequency Oscillations as a New Biomarker in Epilepsy. *Annals of Neurology*, 71(2):169–178.